UNIVERSITY OF CALIFORNIA
RIVERSIDE

Through-Bond Correlation Methods for Assigning Protein Resonances with Solid-State NMR Spectroscopy

A Dissertation submitted in partial satisfaction
of the requirements for the degree of

Doctor of Philosophy

in

Chemistry

by

Lingling Chen

December 2008

Dissertation Committee:

Dr. Leonard J. Mueller, Chairperson
Dr. Jingsong Zhang
Dr. Eric Chronister

The Dissertation of Lingling Chen is approved:

Committee Chairperson

University of California, Riverside

ACKNOWLEDGEMENTS

The Text of this thesis, in part or in full, is a reprint of the material as it appears in:

1. *Journal of the American Chemical Society*, 2006, 128(31): 9992
2. *Journal of the American Chemical Society*, 2007; 129(35): 10650
3. *Magnetic Resonance in Chemistry*, 2007; 45: S84-S92

The co-author L.J. Mueller listed in these publications directed and supervised the research which forms the basis for this thesis.

J.M. Kaiser designed and built the probe for doing NMR experiment.

J. Lai performed most of the calculations for theoretical scalar couplings.

T. Polenova and her student J. Yang performed several of the solid state experiments in chapter III and IV.

C.M. Rienstra and his students J.M. Boettcher and D. Zhou generously provided the sample of GB1 and their valuable suggestions on experiments.

From a more global perspective I would like to thank my research adviser Professor Leonard Mueller. Without his support, I would have never made it through to the end of this journey. He is not only a good teacher but also a life mentor who teaches the most two important things in my life: “Never look down on yourself” and “Do not be afraid to fight for what you want”. Also, this research would have been impossible without his guidance, patience and motivation.

I would also like to thank all of my lab mates who made the journey more enjoyable and were there to assist me with whatever problem I encountered.

ABSTRACT OF THE DISSERTATION

Through-Bond Correlation Methods for Assigning Protein Resonances with Solid-State NMR Spectroscopy

by

Lingling Chen

Doctor of Philosophy, Graduate Program in Chemistry
University of California, Riverside, December, 2008
Dr. Leonard J. Mueller, Chairperson

Solid state NMR Spectroscopy is emerging as a mainstream tool in structural biology. Resonance assignments are an essential first step in structural studies, and in the majority of studies to date, these have employed through-space, dipolar correlation spectroscopy. In NMR, it is the scalar or J-coupling interaction that signifies covalent through-bong contact, while the dipolar coupling provides through-space distance constraints. This research involves developing new correlation methods based on scalar-couplings for solid state NMR of proteins.

CTUC COSY, a new scalar-coupling-driven correlation method is introduced which is robust for chemical shift correlation in solids by combining the indirect evolution and transfer periods into a single constant time interval. Both theory and experiment point to distinct advantages of this protocol which was originally motivated by the challenge of obtaining through-bond connectivity in dynamic solids, where global molecular motion renders dipolar-driven correlation methods ineffective, and where liquid-state methodologies proved inapplicable. In this work, it was shown that this new J-MAS method provides substantially increased spectral resolution without compromising sensitivity, which we find to be comparable to or better than the sensitivity of dipolar methods. The results demonstrated that scalar-based methods are sufficiently well developed to serve as a complementary tool to dipolar methods, which will be especially useful for the assignment of large proteins, where resonance overlap presents a major challenge to solid-state NMR.

TABLE OF CONTENTS

LIST OF FIGURES

CHAPTER I

CHAPTER II

CHAPTER III

CHAPTER IV

LIST OF TABLES

CHAPTER I

INTRODUCTION

Over five decades since its discovery, high-resolution nuclear magnetic resonance (NMR) spectroscopy has been widely accepted as an essential tool to analyze the structure and dynamics of isolated molecules in pure and applied sciences and a variety of complex molecular systems[1]. Solution NMR approach has been extensively explored to this end, because complicated spectral feature of solid state NMR[2-7] arising from inherent dipolar interactions with neighboring nuclei and chemical shift anisotropy (CSA) is substantially simplified in solution NMR due to time-averaging caused by rapid tumbling motion. Alternatively, high-resolution solid state NMR can be achieved if such interactions were successfully removed by specific manipulations of spin system, although a wealth of very important structural data such as interatomic distance, orientation to the applied magnetic field, etc. are naturally lost by this procedure. Resonance assignments are an essential first step in structural studies, and in the majority of studies to date, these have employed through-space, dipolar driven correlation spectroscopy. In NMR, it is the scalar or *J*-coupling interaction that signifies covalent through-bond contact, while the dipolar coupling provides through-space distance constraints. This work focuses on the development of new correlation methods based on

scalar-couplings for solid state NMR of proteins. Before tackling these foci, a short introduction to the field of NMR with a focus on solid-state is given.

1.1 Basic Solid State NMR (SSNMR) Parameters

Chemists are familiar with the narrow Lorentzian lines in liquid-state NMR, but static solid-state NMR on a non-crystalline sample has a very different profile. The similarities between the liquid and solid-state powder spectra of glycine (Figure 1.1) all but end with there being two peaks of different chemical shift.

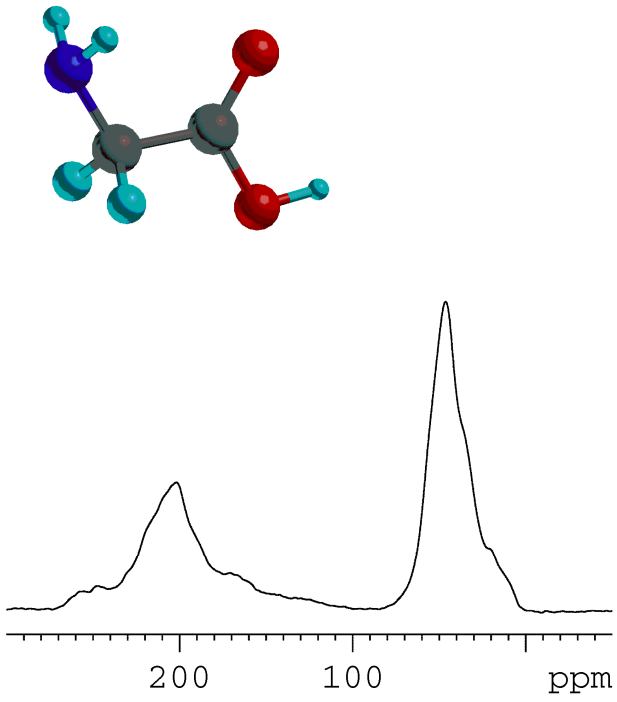

Figure 1.1 ^{13}C Pulse-Acquired ^{1}H Decoupled Spectrum of Static Powdered Glycine

The ^{13}C pulse-acquire of natural abundance powdered glycine acquired on a 9.5 T Bruker DSX spectrometer (^{1}H frequency 400.13 MHz) equipped with triple-resonance 4mm MAS probe that was not spinning. The initial pulse on the ^{13}C channel was due to ramped cross-polarization from the protons, which where then decoupled at 80 kHz. 4096 points were acquired with a spectral width of 50 kHz.

The substantial loss of resolution and sensitivity of the static solid powder versus the liquid NMR arises from the field-orientation dependence of the Hamiltonian. In a liquid sample the molecules are in isotropic motion, which leads to an averaging of the molecules' Hamiltonians. In a solid powdered sample the molecules are not allowed to freely reorient themselves and so the entire Hamiltonian is expressed across a powdered sample. A solid crystal NMR spectrum looks much like the liquid spectrum in that there are two sharp peaks, but these peaks are not just the isotropic peaks, they are specific orientation dependent members as the total powder shape shown in Figure 1.1.

1.1.1 The SSNMR Hamiltonian

To fully explain the line shapes found in the NMR of static powder samples, one must first look at the SSNMR Hamiltonian. The SSNMR phenomenological Hamiltonian can be thought of as being made up of the sum of several single rank two tensor interactions. Chief amongst these single rank two tensor interactions for spin -1/2

SSNMR are the chemical shift anisotropy, through-space dipolar interaction, and through-bond dipolar interaction. These tensors govern the interaction of the nuclear spin vector ($\underline{I}$) with another vector ($\underline{S}$) as:

$$H^{\lambda} = C^{\lambda}\, \underline{I} \cdot \underline{\underline{M}} \cdot \underline{S}$$

Where λ indicates the particular interaction and so C^{λ} is a constant associated with that interaction and $\underline{\underline{M}}$ is the rank two interaction tensor.

The chemical shift anisotropy and the direct dipolar coupling tensors are generally considered symmetric since anti-symmetric terms only contribute to second order energy corrections. A symmetric tensor can always be diagonalized using a complete set of Euler rotations ($\underline{\underline{R}} \cdot \underline{\underline{\mathrm{M}}} \cdot \underline{\underline{R}}^{-1} = \underline{\underline{\Lambda}}$), the frame in which a tensor is diagonalized is called that tensor's principle axis system. A diagonalized tensor has its eigenvalues as its diagonal elements, which when ordered $\underline{\underline{\Lambda}}_{33} = |\lambda_3 - \Lambda| \geq |\lambda_1 - \Lambda| \geq |\lambda_2 - \Lambda|$ (where Λ is the isotropic value $\Lambda = (\lambda_1 + \lambda_2 + \lambda_3)/3$) are also called the principle axis values.

1.1.2 Chemical Shift Anisotropy (CSA)

This component of Hamiltonian is associated with the shielding effect provided to a nucleus from applied magnetic fields due to the electronic environment[8]. The acquisition of a CSA line shape can be easily accomplished on a rare spin by using a pulse-acquire experiment while decoupling other nuclei in the system. This broad featured shape can be

shown to be for $\omega_1<\omega_2<\omega_3$ (see Appendix A):

$$I(\omega) = \mathrm{Re}\left\{ \frac{(-1)^{If[\omega>\omega_2,1,0]}}{\pi\left[(\omega_1-\omega)(\omega_3-\omega_2)\right]^{1/2}} K\left[\sqrt{-\frac{(\omega_3-\omega_1)(\omega-\omega_2)}{(\omega_1-\omega)(\omega_3-\omega_2)}} \right] \right\}$$

Where $K[\varphi]$ is the complete elliptic integral of the first kind, ω_1, ω_2 and ω_3 are the principle axis values, and the $I(\omega)$ is zero otherwise. This result with Lorentzian relaxation produced the gray fit line in Figure 1.2.

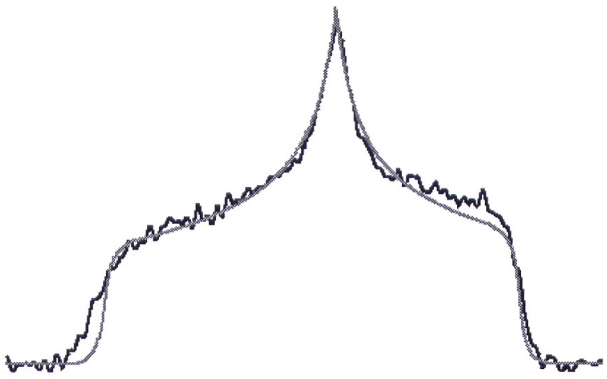

Figure 1.2 Static ^{15}N spectrum of [3-^{15}N] uracil and fit

The ^{15}N pulse-acquire of powdered [3-^{15}N] uracil acquired on a 9.5 T Bruker DSX spectrometer (^1H frequency 400.13 MHz) equipped with triple-resonance 4 mm MAS probe that was not spinning. The initial pulse on the ^{15}N channel was due to ramped cross-polarization from the protons, which where then decoupled at 80 kHz using TPPM. 4096 points were acquired with a spectral width of 50 kHz.

1.1.3 Through-Space Dipolar Interaction

This large term in the solid-state Hamiltonian is due to the through-space or direct spin-spin interactions by their magnetic dipoles. The dipolar tensor is known to be traceless and axially symmetric[8], which allows for two solutions to the PAS associated with the sign of the largest component (that is, it is bilinear in spin). The physical interpretation of this characteristic is that for one of the spins in a given orientation there are two possible orientations of the second spin each contributing a fundamental lineshape (shown in gray) to the overall lineshape as shown in Figure 1.3.

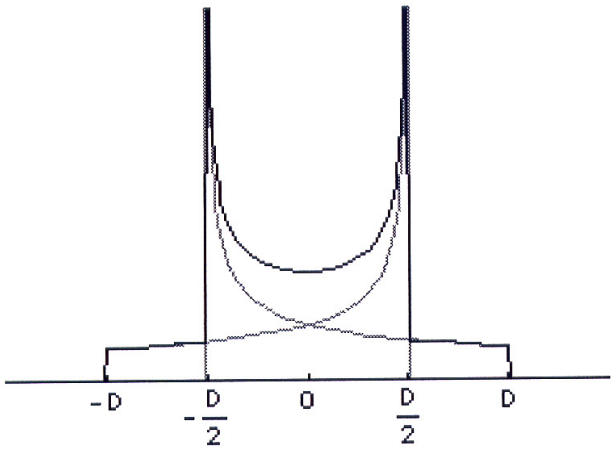

Figure 1.3 Dipolar Pake Pattern Simulation

The dipolar interaction is an important tool in SSNMR for determining structure because of its dependence on the inverse of the cube of the distance between the spins.

But due to the low resolution and sensitivity of static powder SSNMR more sophisticated techniques involving either single crystal samples or partial removal of the coupling have been developed.

1.1.4 Through-Bond Dipolar Interaction

Also called the indirect dipolar interaction and more commonly the scalar coupling, this is generally a much smaller term than either the chemical shift or direct dipolar coupling. The term is so small in fact that the indirect spin-spin coupling tensor is not only considered symmetric, it is considered to be only isotropic.

$$H^J = \underline{I} \cdot \underline{\underline{J}} \cdot \underline{S} = J\, \underline{I} \cdot \underline{S}$$

The spectroscopic effect of scalar coupling is the replication of spectra due to the other terms in the Hamiltonian offset by the coupling J with intensities following the binominal coefficients. In liquid-state NMR the term is much more significant due to the narrow Lorentzian lines, but in solid-state NMR the term is often neglected as it is generally smaller than the linewidth.

1.2 NMR Techniques

Sixty years ago Purcell[9] and Bloch[10] demonstrated the first bulk condensed phase nuclear magnetic resonance experiments. They were motivated to extend the molecular

beam technique of Rabi[11], which was a variation of the original work by Stern and Gerlach[12, 13]. In twenty five years separating Stern and Gerlach from Bloch and Purcell, the physics of an intrinsic angular momentum called spin was developed. Spin is a quantized integer or half-integer constructed with no classical analog, the rules and conventions of which used to describe it make up much of the vocabulary of NMR.

Two years after Purcell's announcement, Pake used the dipolar coupling information in NMR to study the structure of hydrated crystals[14]. Using the r^{-3} (where r is the through-space distance between the spins) character of the dipolar coupling, Pake was able to determine distances to ±2%. Nevertheless, the phenomenon of NMR was of little interest to chemists until Proctor[15] demonstrated that the resonant frequency of a nucleus depended not only on isotope but also on the chemical environment of the nucleus. This small deviation became known as the chemical shift, and it is a primary tool for structure work in NMR. Soon thereafter Gutowsky observed and explained the splitting of resonances by an indirect dipolar coupling[16]. This indirect dipolar coupling was shown to be a transfer through an electron density between two nuclei and can then be used to answer questions of through-bond structure.

For spin-1/2 nuclei such as ^{13}C or ^{15}N, solid state NMR spectra of biopolymers, including fibrous, globular, and membrane proteins, biomembranes, polysaccharides, etc. yield enormously broadened signals with line widths in the order of 20 kHz. A wealth of

structural data in relation to interatomic distances and nuclear orientation to the applied magnetic field is contained in such broadened NMR signals in the crystalline or noncrystalline state, and should be carefully analyzed in a site-specific manner using site-specific isotope labeling. Nevertheless, such broadened NMR signals are usually not easy to interpret in terms of chemical or biological significance, unless otherwise an attempt is made to narrow line widths to give rise to high resolution solid state NMR signals, as encountered in solution NMR.

1.2.1 Dipolar Decoupling

From a classical viewpoint, the component of local magnetic field at spin *I*, caused by magnetic moment μ from neighboring nucleus *S* (in many cases, proton), parallel to the applied static magnetic field B_0 is

$$B_L = \pm \mu r^{-3} (3\cos^2 \theta - 1),$$

Where *r* is the distance between two nuclei and θ is the angle between B_0 and *r* (Figure 1.4), leading to splitting of peak to doublet. This equation can be rewritten using quantum mechanical formalism as

$$H_D = -\gamma_I \gamma_S \hbar^2 r^{-3} (3\cos^2 \theta - 1) I_z S_z,$$

Where *I* and *S* are nuclear spin numbers for nuclei *I* and *S*, γ_I and γ_S are gyromagnetic ratios for *I* and *S* spin, respectively, and $\hbar$ is Planck's constant (*h*)

divided by 2π. NMR signals of rare spins of spin number ½ such as ^{13}C and ^{15}N nuclei are mainly broadened by dipolar interactions with neighboring proton nuclei, because homonuclear ^{13}C-^{13}C and ^{15}N-^{15}N dipolar interactions are very weak under the condition of natural abundance, and hence negligible in most cases. Therefore, such dipolar couplings can be effectively removed by irradiation of strong radio-frequency (rf) at proton resonance frequency (dipolar decoupling) to result in time-averaged magnetic dipolar field to zero ($\langle \mu \rangle = 0$), as in similar manner to proton decoupling in solution NMR to remove scalar C-H spin coupling, it is required to use decoupling fields of 40 kHz or more to reduce the stronger dipolar couplings of 20 kHz.

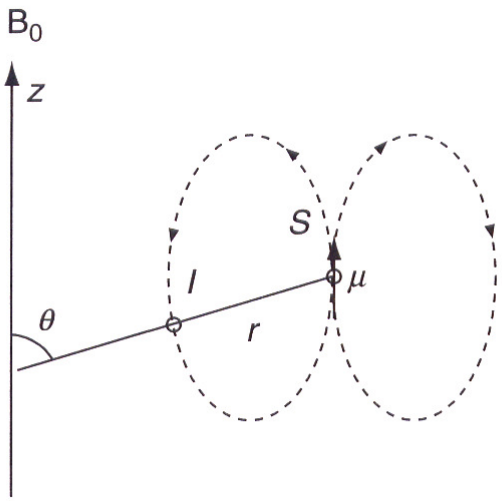

Figure 1.4 Dipolar field at the spin *I* caused by the neighboring spin *S*

1.2.2 Magic Angle Spinning

Magic angle spinning is a SSNMR technique, introduced by Andrew[17] and Lowe[18], where the sample is mechanically spun about a carefully chosen axis which averages out second rank interactions. The method is best visualized as adding a zero average time-dependent component to the Hamiltonian to everything lying off the axis of rotation. Then by examining the elements of the Wigner rotation $D^{'}_{m'm}(\Omega_{RL} = \{\alpha, \theta_M, \omega_R t\}$ we find that for I = {0, 1, 2} the only time independent terms are $D^0_{00}(\Omega_{RL}) = 1$ and $D^2_{00}(\Omega_{RL}) = \frac{1}{2}(3\cos^2\theta_M - 1)$, the latter of which can be made zero by choosing the axis of rotation to be $\theta_M = \cos^{-1}\frac{1}{\sqrt{3}} \approx 54.74^\circ$. .

When the axis of rotation is chosen at the "magic angle" of $\theta_M \approx 54.74^\circ$, the second rank interactions can then be averaged to zero assuming the spinning rate is greater than or equal to the line width. If the spinning rate is less than the line width a series of spinning side bands is produced at the spinning frequency. These sidebands have been thoroughly described elsewhere[19, 20] and can provide valuable orientation information. Frequently however the goal is to spin fast enough to completely average the second order interactions, which requires spinning at least twice $\underline{\underline{\Lambda}}_{33}$.

Spectroscopically, fast MAS condense the magnetization in the powder line shape into a liquid-like line shape. In other words, a series Lorentzian lines at the isotropic values of the Hamiltonian tensors (which transforms as $D^0_{00}(\Omega_{RL})$). Frequently in

SSNMR on rare spins only a single line at the isotropic value of the chemical shift tensor survives). Therefore, MAS can improve the resolution and sensitivity of SSNMR spectra at the expense of removing the information provided by the second rank interactions (like the dipolar couplings and the "shape" of the electronic environment around the nucleus provided by the full chemical shift tensor).

1.2.3 Cross Polarization

This technique relies on polarization transfer from the abundant *I* spin such as ^{1}H to the rare spin *S* such as ^{13}C through matched H_1 fields for both the ^{1}H and ^{13}C, known as the Hartmann-Hahn condition:

$$\gamma_I B_{1I} = \omega_I = \omega_S = \gamma_S B_{1S} \qquad (1.1)$$

where γ_I and γ_S are the gyromagnetic ratios, and ω_I and ω_S are radio frequencies, B_{1I} and B_{1S} are the frequency strength for abundant *I* and rare *S* nuclei, respectively. This procedure starts when a 90º rf pulse B_{1I} in the *x*-direction brings the magnetization along the *y*-direction. This magnetization M_I is then "spin-locked" along with B_{1I} when the phase of the rf field is shifted by 90º from the *x* to the *y* directions, as far as it is greater than any local dipolar fields and there is no static magnetic field in the *z*-direction as viewed from the rotating frame[21], which is rotating at Lamore frequency $\omega_0 = \gamma_I B_0$, as illustrated in Figure 1.5 and Figure 1.6.

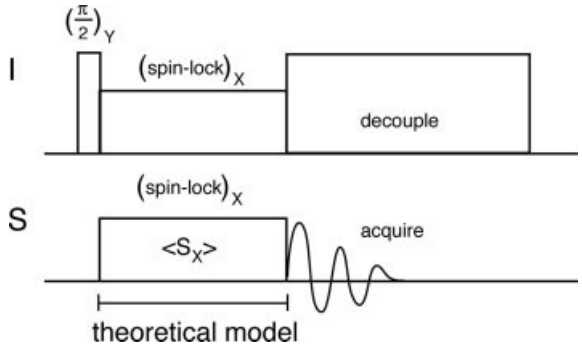

Figure 1.5 Pulse sequence for cross polarization.

After 90º rf pulse, B_{1I} pulse is applied in the *x* direction, the *I* magnetization at *y* axis is spin locked along with B_{1I} when the phase of the rf field is shifted by 90º from the *x* to the *y* axis. The *I* spins transfer polarization to *S* spins during the contact time. The *S* signal is then acquired.

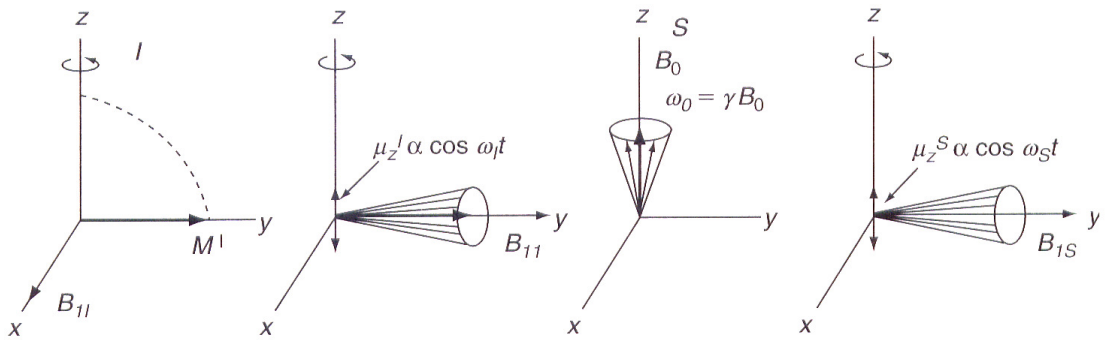

Figure 1.6 Spin-lock in the rotating frame and cross polarization

The μ_{zI}, the z-component of M_I, oscillates as

$$\mu_{zI} \propto \cos \omega_I t \qquad (1.2)$$

and its time-averaged value

$$\langle \mu_{zI} \rangle = 0 \qquad (1.3)$$

consistent with the explanation already described. In the presence of B_{1I}, the rare spins S (^{13}C or ^{15}N) are naturally dipolar decoupled and their magnetization M_S is exactly aligned with their applied rf field B_{1S} in the y-axis, while individual S spin process about the rf field B_{1S} in the y-axis, as views from the Cartesian coordinates in the rotating frame, instead of the z-axis in the laboratory frame. The μ_{zS}, the z-component of M_S, also oscillates as

$$\mu_{zS} \propto \cos \omega_S t \qquad (1.4)$$

The z-axis components of the I and S spins, μ_{zI} and μ_{zS}, have the same time-dependence in Eq.(1.2) and (1.4), when the Hartmann-Hahn condition is satisfied as demonstrated in Eq.(1.1). Therefore, in a doubly rotating coordinate system, efficient CP transfer occurs from the abundant spin I to rare spin S through cross relaxation by dipolar coupling between I and S spins, in view of the same time dependence ($\omega_I = \omega_S$) in μ_{zI} and μ_{zS} in Eq.(1.2) and (1.4). In the laboratory reference frame, this interaction can be expressed as[22, 23]

$$H_{IS} = \gamma_I \gamma_S \hbar^2 \sum \sum r_{im}^{-3} (3\cos^2 \theta_{im} - 1) I_{iz} I_{mz} \qquad (1.5)$$

where r_{im} is the distance between i(I) and m(S) spins and θ_{im} is the angle between the vector r_{im} and B_0. In the doubly rotating reference frame, the interaction B_{IS} transforms approximately to

$$H_P \sim \sin\theta \sum r_{im}^{-3}(3\cos^2\theta_{im} - 1) I_{ix} I_{mx} \qquad (1.6)$$

$$\theta = \tan^{-1}(B_{1I} / B_L)$$

The spin operator part of this interaction involves $I_x S_x$ and so $I_{\pm} S_{\mp}$. Therefore, the spin-lock CP transfer results from a mutual spin flip between S spins (carbons and nitrogens) and I spins (protons) by the combination of spin-raising and spin-lowering operators in Eq (1.6). The requirement of a CP transfer for a strong static interaction is contained in $r_{im}^{-3}(3\cos^2\theta_{im} - 1)$ and this term averages to 0 in the presence of rapid, isotropic molecular motions. In the absence of such motions, therefore, the optimum magnetization achieved by CP-MAS NMR, following a single spin-lock CP transfer, is B_{1S} / B_{1I} (or $\gamma_I / \gamma_S = 4$ for carbons) greater than the magnetization that would be observed in a fully relaxed Fourier transform (FT) experiment. This is the major advantage to record CP-MAS NMR spectra, as viewed from gaining sensitivity as well as feasibility of spectral accumulation with shorter repetition times for abundant spins such as proton, as described above.

1.3 NMR Pulse Diagram

A pulse diagram is really nothing more than a plot of radio-frequency (rf) power versus time. It is rarely shown with axes as the power axis is a relative scale, and the time axis is dilated or contracted to emphasize the more "interesting" parts. An example of a pulse diagram which contains all the elements necessary for this work is shown in Figure 1.7.

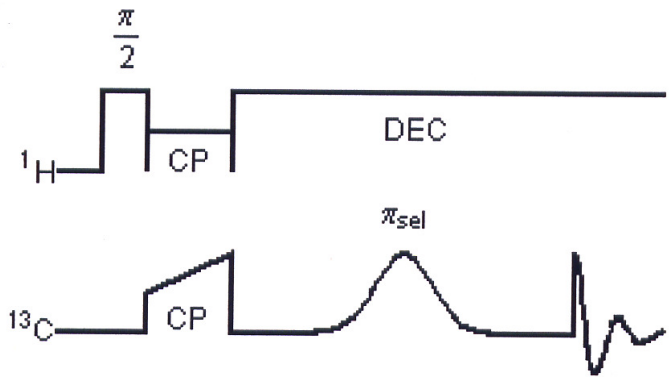

Figure 1.7 Selective echo pulse diagram

The channel (nucleus) receiving pulses is shown to the left of the profile it is given, here ^{1}H and ^{13}C. Following the ^{1}H profile, the first event in time is the radio-frequency pulse with a label of $\pi/2$, which is the flip angle. The flip angle is the radio frequency of the pulse multiplied by its duration which is $\pi/2$ here ($2 \pi \upsilon_{rf} t_{rf} = \pi/2$); in other words, the

magnetization is rotated by the rf through an angle of π/2. Sometimes the flip angle is labeled with a subscript to indicate the phase of the rf pulse. Typically, such a π/2 pulse will be 3 μs in duration meaning an 83kHz frequency. The next element in the ^{1}H profile is a reduced power pulse labeled CP for Cross-Polarization (see section 1.2.3). The Cross-Polarization technique, introduced by Pines[24] and developed as shown by Smith[25], is used to enhance the signal from rare spins (like natural abundant ^{13}C) by transferring magnetization (usually through the dipolar coupling) from the abundant protons to the rare spins. Typically, in CP the rf is applied to both channels for 1ms, disproportionately longer than the π/2 pulse but it is given little more consideration on the time axis as it is not significantly more "interesting". The net effect of CP step is a reduction in ^{1}H magnetization and a gain in ^{13}C magnetization that appears similar to a π/2 pulse on ^{13}C. The final component of the ^{1}H profile is what would appear to be a long pulse at the same power as the π/2 pulse labeled "DEC", this is really a placeholder for a decoupling pulse sequence which uses the same power as the π/2 pulse. Sometimes the decoupling scheme is explicitly indicated (for example instead of the generic DEC perhaps TPPM would be indicated) but regardless the intent is to convey that couplings to the protons have been eliminated (or scaled). Looking now to the ^{13}C profile, the CP step has produced magnetization in the transverse plane and then there is a delay where the magnetization is allowed to freely evolve in the static field. Following this period of free evolution, which

could be tens of milliseconds, a Gaussian shaped pulse is given which is labeled as having a flip angle of π. The Gaussian pulse is a selective pulse which trades time domain footprint for frequency domain specificity; it often takes a few hundred microseconds. Using a selective pulse allows the spectroscopist to choose which resonances of the channel are affected by the pulse. In this case, those resonances which are chosen to lie within the excitation profile of the selective pulse will be the only resonances observed after the delay following the pulse. The exponentially decaying sinusoid at the very end of the ^{13}C profile indicates which channel is being observed.

1.3.1 The spin Echo Experiment

Around the same time as the discovery of the chemical shift, Hahn reported the case of the first spin echo[26] and a few years later Purcell explained and expanded the phenomenon[27]. The basic pulse sequence is shown in Figure 1.8.

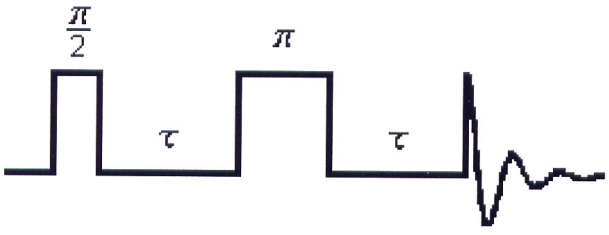

Figure 1.8 Carr-Purcell Pulse-Echo Pulse Diagram

The transverse magnetization produced after the initial π/2 pulse is allowed to freely evolve in the static magnetic field for a time τ, it is then given a π pulse, allowed to freely evolve for another time τ, and is then detected. The surprise is that the detected signal is generally not significantly less intense than the signal that would be observed immediately after detection. The character second free induction signal is to this day a topic of interest in the field[28].

Following Slichter[29] and Ernst[30], a directly observed free induction decays at with a relaxation rate of T_2*, which is the reduced sum of the natural relaxation rate T_2' and the inhomogeneous rate $T_2^{\dagger}$. The spin echo experiment evolves solely under the natural relaxation rate during the echo because the inhomogeneity of the static field across the sample averages to zero resulted from the change of handedness granted by the π pulse. The fact that echoes relax under only natural relaxation rate is the slowest is crucial to through-bond developments in later chapters.

The spin-echo signal is not however just a scaled down copy of the directly detected signal. The most significant difference is that (homonuclear) coupling terms are not fully refocused by a spin-echo without careful design of the refocusing time τ[31]. This is another feature that is crucial to later developments, that the pulse sequence must be engineered to maximize its signal power.

1.3.2 Phase Cycling

The art of phase cycling is thoroughly explored by Keeler[32] in his lectures, which are available online. The goal of phase cycling is alter the phase of the rf pulses used in a sequence to allow desired terms to constructively add together and unwanted terms to destructively add together over the course of the full cycle. A classic example, which is used in every sequence in later chapters, is the double quantum filter. A double quantum filter is a phase cycle that only permits bilinear terms of coherence order two, that is terms like I_+S_+ and I_-S_-, to constructively add. Keeler also discusses coherence diagrams, which are a series of lines generally drawn over the pulse diagram (Figure 1.9), which map out the effect of the phase cycling by tracing the coherences that are being constructively added.

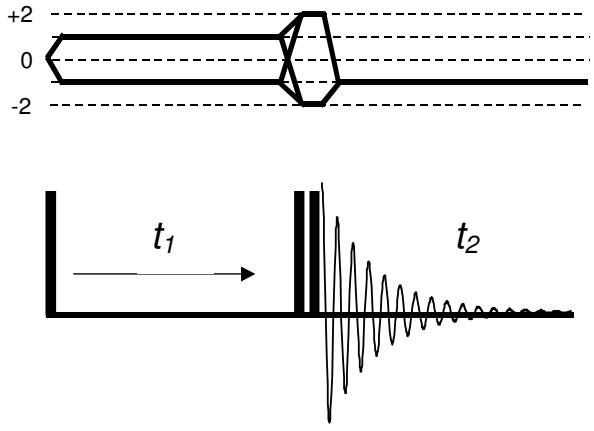

Figure 1.9 Pulse Sequence of the 2QFCOSY

1.4 Two-Dimensional NMR Spectroscopy

Jeener first proposed the idea of placing an incrementally changed period of free evolution in a sequence and then taking a two-dimensional Fourier transform to improve resolution[33]. The concept really has not changed much since it expanded. The overall idea is that coupling terms transfer magnetization from one spin to another, and that by giving the system time to undergo these transfer and collecting the signals at different times the observed signal will be modulated by the couplings. Then taking a Fourier transform across the different times, the modulation from the couplings will separate the directly observed peaks along the second dimension. Better yet, since the coupling is bilinear in spin, the peak is encoded with the resonance frequencies of both members of the coupling, so the two-dimensional plot can be viewed as a map of "what is coupled to what". Therefore, if the experiment is engineered to use indirect dipolar coupling it can answer "what is bonded to what" and if the experiment is engineered to use the direct dipolar coupling it can answer "what is spatially close to what".

An important point should be made which is that two-dimensional (or higher) spectroscopy does not contain more information than one-dimensional spectroscopy. The advantage of two-dimensional spectroscopy is that separating the information contained in the one-dimensional spectrum and increases the resolution of the experiment. Figure 1.10 is an example of a two-dimensional indirect dipolar coupling experiment shown as a

contour plot of [U-^{13}C, ^{15}N] tyrosine.

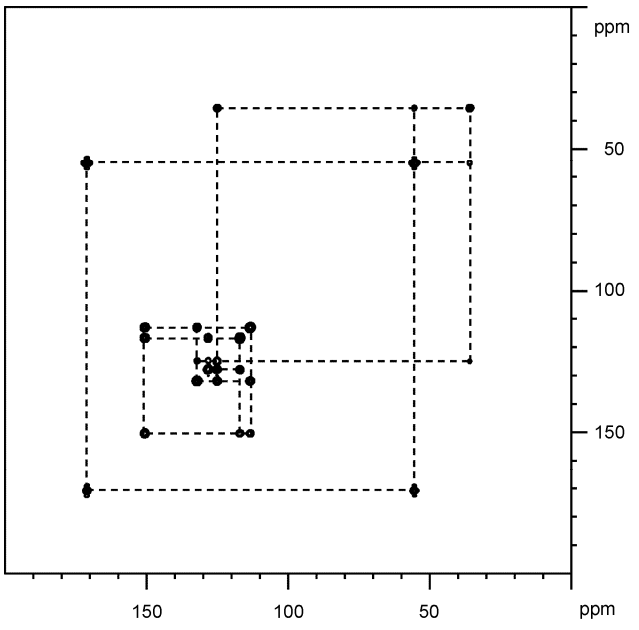

Figure 1.10 UC2QFCOSY of [U-^{13}C, ^{15}N] Tyrosine

The spectra is of ^{13}C chemical shift versus ^{13}C chemical shift of [U-^{13}C, ^{15}N] tyrosine (diluted to 50% in unlabeled tyrosine) acquired on a 9.4 T Bruker DSX Spectrometer (^{1}H frequency 400.13 MHz) equipped with a double-resonance 2.5 mm MAS probe spinning at 30 kHz. 50 kHz ^{13}C pulse were used throughout, along with 80 kHz TPPM ^{1}H decoupling. 256 points were acquired with a spectral width of 25 kHz in t_1, and 1024 points were acquired in t_2 with a spectral width of 25 kHz.

The pulse sequence used in Figure 1.10 will be explained in later chapter, but a few

comments on the experimental conditions are in order. First, the labeled sample is diluted in natural abundance material to lessen inter-molecule interactions. Next the spectrometer is characterized by its static field of 9.4 T and its manufacturer Bruker. The probe is a tuned and matched LC circuit that also carries the sample, which in this case is packed in a 2.5 mm rotor and is being spun about the magic angle at 30 kHz (see section). The pulse sequence uses ^{13}C and ^{1}H pulse, the ^{13}C pulses are 50 kHz (5 μs) and the ^{1}H pulse are 80 kHz (3 μs) pulses. The amount of data collected is a block of 256×1024 as 256 time steps from the free evolution period inside the pulse sequence (called t_1) and 1024 directly detected points at the end of each sequence (called t_2) for each step of t_1. The final parameters given indicate how far separated the t_1 points are from each other and how far the t_2 points are separated from each other. One can convert between the spectral width and the time separation of points using the properties of the Fast Fourier Transform (FFT) [34], in this case the points are separated by 20 μs in both dimensions and the resolution is four times better in directly detected (t_2) dimension because it has four times as many points over the same spectral width.

1.5 SSNMR for Protein Structure Determination

Over the past few years, there have been remarkable advances in solid-state NMR (SSNMR) experiments for the characterization of protein structure and function. A recent

review [35] illustrates the broad range of biological problems for which SSNMR has usefully been applied. For a wide variety of proteins, insolubility may make X-ray crystallography or solution NMR unsuitable; SSNMR, however, can address structural issues in these cases. For example, the contribution of SSNMR to the specific problem of fibril formation, particularly in connection with Alzheimer's disease, has also been recently reviewed [36]. This review highlights emerging methods that facilitate the efficient biophysical and structural characterization of solid amorphous biological systems, and that further widen the scope of problems uniquely addressed by SSNMR.

The determination of high-resolution structures of macromolecules relies on the availability of numerous structural constraints distributed throughout the system: accordingly, assignment of the spectra is a central objective in NMR-based structure determination. Based on the assigned spectra, it is possible not only to solve three dimensional structures, but also to probe such issues as conformational dynamics and ligand binding, as well as to obtain valuable spectroscopic parameters unavailable from other methods, such as shielding anisotropies. Significant work by Cole and Torchia illustrated the excellent NMR line-widths that can be obtained for microcrystalline or precipitated hydrated globular systems using magic angle spinning (MAS) methods [37].

These authors also pointed out the similarity between solution and solid-state chemical shifts, and thus presumably the close similarity of structure. Seminal work by

Strauss and Ernst [38] illustrated early on that directional magnetization transfer methods could be implemented in the context of two- and three-dimensional experiments to carry out systematic sequential assignments of biological solids. More recent advances in high-field instrumentation and pulse sequences for chemical shift correlation experiments led to more efficient methods for assigning solid-state spectra for proteins with extensive isotopic enrichment. A rapid succession of studies by a variety of laboratories on small globular proteins has ensued, including partial assignments of BPTI [39], and nearly complete assignments of heteroatoms for many small thermostable proteins with mixed a/b structures: human ubiquitin [40, 41], the SH3 domain of a-spectrin[42], the catabolite repression phosphocarrier protein (Crh)[43], Thioredoxin[44], the immunoglobulin-binding domain B1 of streptococcal protein G (GB1) [45] and mastoparan [46]. It is likely that other systems are also in progress. Many technical issues were surmounted in achieving assignments for these systems. Pulse sequences originally developed for isolated pairs of spins [47] give good performance in uniformly labeled materials with minor modification or without modification, and have been implemented to accomplish multidimensional chemical shift correlation. To achieve acceptable line-widths (1 ppm or less), MAS is used and strong proton decoupling is applied during detection periods. Internuclear homonuclear ^{13}C couplings, both J and D, can have a dominant effect on the line-widths of uniformly enriched materials [48, 49]; constant time detection periods or selective

decoupling pulses are possible remedies for this broadening in indirect dimensions, but have not been extensively used in biophysical applications to date. The work presented in later chapters will be focused on this domain.

1.6 Conclusion

It is a natural consequence to expect solid state NMR as an alternative means to X-ray crystallography and multidimensional solution NMR in revealing the 3D structure of globular proteins, nucleic acids, and peptides in relation to the currently active structural biology. The expected NMR line widths available from achieved high-resolution solid state NMR can be manipulated experimentally and are not any more influenced by motional fluctuation of proteins under consideration as a whole, in contrast to solution NMR. Accordingly, detailed structural information such as mutual orientation of molecules, interatomic distances, torsion angles, etc. is available from NMR parameters contained in solid state NMR, although most of them are lost due to time-averaging in solution NMR.

With an understanding of spin physics, one can design NMR pulse sequences combined with dipolar decoupling, MAS and cross polarization etc. techniques to achieve spectra with better resolution and sensitivity for solid state proteins.

REFERENCES

1. Grant, D.M. and Harries, R.K. *Encylcopedia of Nuclear Magnetic Resonance*, **1996**.

2. Mehring, M. *Principle of High Resolution NMR in Solids*, *Second Edition*, **1983**.

3. Slichter, C.P. *Principle of Magnetic Resonance*, Harper & Row, New York, **1963**; Third Enlarged and Updated Edition, Springer-Verlag, **1989**.

4. Fyfe, C.A. *Solid State NMR for Chemists*, CFC Press, **1983**.

5. Gerstein, B.C. and Dybowski, C.R. *Transient Techniques in NMR of Solids: An Introduction to Theory and Practice*, **1985**.

6. Haeberlen, U. *High Resolution NMR in Solids*: *Selective Averaging*, **1976**.

7. Schmidt-Rohr, K. and Spiess, H.W. *Multidimensional Solid-state NMR and Polymers*, **1994**.

8. Abragam, A. *Principle of Nuclear Magnetism*, Oxford, **1961**.

9. Purcell, E.M.; Torrey, H.C. *Physical Review*, **1946**, *69*, 37-38.

10. Bloch, F.; Hansen, W.W. *Physical Review*, **1946**, *69*, 127.

11. Rabi, I.I.; Zacharias, J.R. *Physical Review*, **1938**, *53*, 318.

12. Stern, O. *Zeitschrift für Physik*, **1921**, *7*, 249-253.

13. Gerlach, W. and Stern, O. *Zeitschrift für Physik*, **1921**, *8*, 110-111.

14. Pake, G.E. *Journal of Chemical Physics*, **1948**, *16*, 327-336.

15. Proctor, W.G. and Yu, F.C. *Physical Review*, **1950**, *77*, 717.

16. Gutowsky, H.S.; McCall, D.W. *Physical Review*, **1951**, *84*, 589-590.

17. Andrew, E.R.; Bradbury, A. *Nature*, **1959**, *183*, 1802-1803.

18. Lowe, I.J. *Physical Review Letters*, **1959**, *2*, 285-287.

19. Herzfeld, J. and Berger, A.E., *Journal of Chemical Physics*, **1980**, *73*, 6021-6030.

20. Maricq, M.M. and Waugh, J.S., *Journal of Chemical Physics*, **1979**, *70*, 3300-3316.

21. Becher, E.D. *High Resolution NMR, Theory and Chemical Applications*. Second Edition, Academic Press, New York, **1980**.

22. Demco, D.E.; Tegenfeldt, H. and Waugh, J.S. *Physical Review*, 1**976**, *B11*, 4133-4155.

23. Schaefer, J. in *Topics in Carbon-13 NMR Spectroscopy*, **1979**, *3*, 283-324.

24. Pines, A. and Gibby, M.G. *Journal of Chemical Physics*, **1973**, *59*, 569-590.

25. Metz, G.; Wu, X.L. *Journal of Magnetic Resonance Series A*, **1994**, *110*, 219-227.

26. Hahn, E.L. *Physical Review*, **1950**, *80*, 580-594.

27. Carr, H.Y. and Purcell, E.M. *Physical Review*, **1954**, *94*, 630-638.

28. Waugh, J. NMR meets Boltzman, does an isolated system go to equilibrium. San Diego, University of California at San Diego: Unpublished.

29. Slichter, C.P. *Principle of Magnetic Resonance*, **1996**.

30. Ernst, R.R. and Bodenhausen, G. *Principles of Nuclear Magnetic Resonance in One and Two Dimensions*, **1987**.

31. Cavanagh, J.; Fairbrother, W.J. *Protein NMR Spectroscopy: Principles and Practice*, **1996**.

32. Keeler, J. *Understanding NMR Spectroscopy*, **2002**

33. Jeener, J.; Lectures, Ampere International Summer School: Unpublished,1971

34. Cooley, J.W. and Tukey, J.W. *Mathematics of Computation*, **1965**, *19*, 297-301

35. Thompson, L.K. *Curr Opin Struct Biol*, **2002**, *12*, 661-669.

36. Tycko, R. *Curr Opin Struct Biol*, **2004**, *14*, 96-103.

37. Cole, H.B.; Sparks, S.W. *Proc Natl Acad Sci*, USA, **1988**, *85*, 6362-6365.

38. Straus, S.K.; Bremi, T.; Ernst, R.R. *J Biomol NMR*, **1998**, *12*, 39-50.

39. McDermott, A.; Polenova, T. *J Biomol NMR*, **2000**, *16*, 209-219.

40. Igumenova, T.I.; McDermott, A.E. *J Am Chem Soc*, **2004**, *126*, 6720-6727.

41. Igumenova, T.; McDermott, A. *J Am Chem Soc*, **2004**,

42. Pauli, J.; Baldus, M.; van Rossum, B. *ChemBioChem*, **2001**, *2*, 272-281.

43. Bockmann, A.; Lange, A.; Galinier, A.; Baldus, M. *J Biomol NMR*, **2003**, *2*, 323-339.

44. Yang, J.; Polenova, T. *Magnetic Resonance in Chemistry, special issue on new techniques in solid-state NMR*, **2007**, *45*, S73-S83.

45. Franks, W.T.; Zhou, D.H. and Rienstra, C. M. *J. Am. Chem. Soc.* **2005**, *127*, 12291-12305.

46. Fujiwara, T.; Todokoro, Y.; Akutsu, H. *J Biomol NMR*, **2004**, *28*, 311-325.

47. Griffin, R.G. *Nat Struct Biol*, **1998**, *5*, 508-512.

48. Straus, S.K.; Bremi, T.; Ernst, R.R. *Chem Phys Lett*, **1996**, *262*, 709-715.

49. Igumenova, T.I.; McDermott, A.E. *J Magn Reson*, **2003**, *164*, 270-285.

CHAPTER II

CONSTANT-TIME THROUGH-BOND ^{13}C CORRELATION SPECTROSCOPY FOR ASSIGNING PROTEIN RESONANCES WITH SOLID-STATE NMR SPECTROSCOPY

ABSTRACT

Even as available magnetic fields for NMR continue to increase, resolution remains one of the most critical limitations in assigning and solving structures of larger biomolecules. Here presents a novel constant-time through-bond correlation spectroscopy for solids that offers superior resolution for ^{13}C chemical shift assignments in proteins. In this experiment, the indirect evolution and transfer periods are combined into a single constant time interval, offering increased resolution while not sacrificing sensitivity. In GB1, this allows us to resolve peaks that are otherwise unresolved and to make assignments in the absence of multi-bond transfers.

2.1 INTRODUCTION

While protein structural folds provide architectural templates for enzymatic function, side-chain conformation and dynamics ultimately determine mechanism. Subtle

differences in structure and activity among closely related molecules often arise from amino acid mutations or changes in chemical environment. NMR spectroscopy provides exquisite insight into this chemistry, including hybridization, protonation state, hydrogen-bond lengths, bond order, and rates of chemical exchange. Solid-state NMR in particular offers unique access to macroscopically disordered states, such as fibrils, integral membrane proteins, and trapped reaction intermediates. In several cases now, complete site-specific assignments of solid-state proteins have been reported using through-space, dipolar-driven correlation spectroscopy.[2-4] In contrast, there have been relatively few reports of ^{13}C scalar coupling driven correlation in solid-state proteins.[4,5] Yet through-bond, scalar-coupling-driven correlation offers several unique features that make it an important complementary tool to through-space methods. In particular, scalar couplings are relatively insensitive to global molecular motion, which can compromise sensitivity in dipolar methods. As well, scalar methods provide a means to delineate through-bond and through-space connectivity, a critical step for establishing structure. Here we show that an important additional benefit is that through-bond correlation in solids can be implemented in an efficient "constant time" manner, with the indirect evolution and transfer periods combined into a single constant time interval.[6] This provides substantially increased spectral resolution without compromising sensitivity, which we find to be comparable to or better than the sensitivity of dipolar methods. In the

β1 immunoglobulin binding domain of protein G (GB1), this allows us to resolve peaks that are otherwise unresolved and to make assignments in the absence of multibond transfers.

2.2 THE CTUC COSY TECHNIQUE

2.2.1 Pulse Sequence and Phase Cycle

Our approach makes use of a constant time, refocused COSY framework (Figure 2.1a,b). This sequence is closely related to the previously introduced UC2QF COSY[7] (Figure 2.1 c). Differences, however, include a modified phase cycle that passes both zero and double quantum coherences, resulting in cross-peaks with twice the intensity compared to that of the original DQ-filtered version (Figure 2.1 d). Although the sequence no longer filters out uncoupled spins, the combined constant-time evolution and mixing period improves resolution through homonuclear decoupling in the indirect dimension (Figure 2.1 e). This further increases sensitivity when the scalar couplings are partially or fully resolved. We refer to this pulse sequence as the *c*onstant-*t*ime *u*niform-sign *c*ross-peak (CTUC) COSY.

(a)

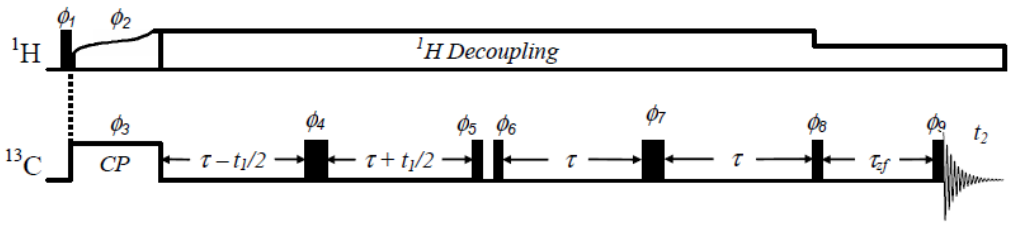

(b)

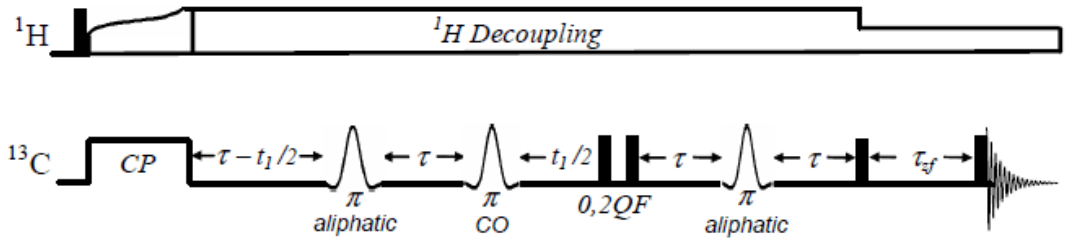

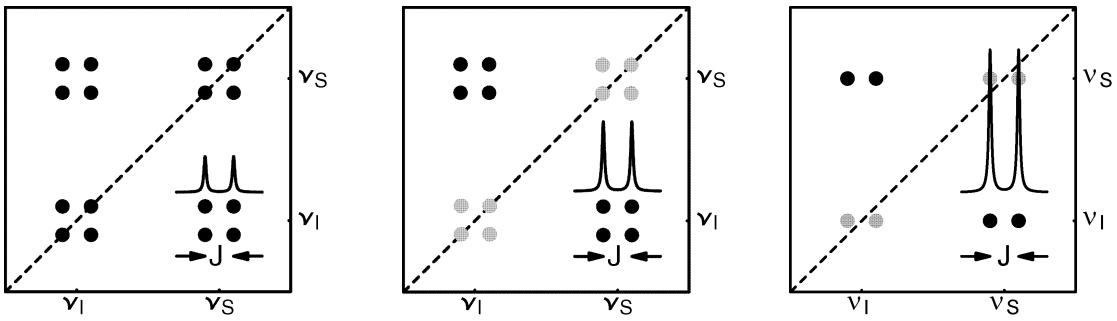

(c) **(d)** **(e)**

Figure 2.1 Pulse sequence for the constant-time uniform-sign cross-peak (CTUC) COSY, shown optimized for (a) CA-CO correlation and (b) aliphatic correlation. Model Spectra of (c) UC2QF COSY, (d) Evolution and (e) CTUC are shown at the bottom.

In these pulse sequences, thin vertical lines indicate π/2 pulses, wide vertical lines indicate π pulses, and selective π pulses are shown as amplitude modulated waveforms. 80 kHz ^{13}C pulses were used throughout for the hard pulses along with 150 kHz SPINAL64 ^{1}H decoupling[10] during the τ constant-time intervals. 100 kHz decoupling was used during the *z*-filter (τ_{zf}, typically 16 ms) and acquisition (t_2). For the selective π

Table 2.1 Complete Phase Cycling for the CTUC COSY

Phase	Cycle
ϕ_1	1
ϕ_2	0
ϕ_3	0, 2
ϕ_4	0, 2, 1, 3, 2, 0, 3, 1
ϕ_5	1, 3
ϕ_6	0
ϕ_7	1, 1, 1, 1, 1, 1, 1, 1, 2, 2, 2, 2, 2, 2, 2, 2, 3, 3, 3, 3, 3, 3, 3, 3, 0, 0, 0, 0, 0, 0, 0, 0
ϕ_8	0
ϕ_9	2
ϕ_{rec}	0, 0, 2, 2, 0, 0, 2, 2, 2, 2, 0, 0, 2, 2, 0, 0, 0, 0, 2, 2, 0, 0, 2, 2, 2, 2, 0, 0, 2, 2, 0, 0

pulses, 180 μs and 420 μs r-SNOB pulses were used for selective aliphatic and carbonyl pulses, respectively. These were centered in the respective spectral regions and rotor

synchronized as described in ref 10. The rotor-synchronized refocusing delay τ was set to 5 ms. The first three ^{13}C pulses (φ3, φ4, φ5) are phase cycled together for zero and double quantum excitation and the two π pulses (highlighted in grey) are independently phase cycled for a coherence order change of ± 2. In table 2.1, the phase of the rf is given as integer multiples of 90 ° (i.e., 0 = "x", 1 = "y", 2 = "-x", 3= "-y") and the list repeats once the end of the line has been reached. If gradients are incorporated for π selection, only the first two steps of the phase cycle would be necessary. Pure phase spectra are obtained using the method of States[1] by incrementing φ 3 by 90°.

2.2.2 CTUC COSY Experiments

The CTUC COSY of GB1 shows superior resolution in both the aliphatic-carbonyl region Figure 2.2 (b) and the aliphatic region Figure 2.2 (c).

Data were acquired on a 9.4 T Bruker DSX spectrometer (^1H frequency 400.13 MHz) equipped with a double resonance 2.5 mm MAS probe spinning at a MAS rate of 25 kHz. 3.5 mg of GB1[6] was center-packed in the rotor, and the drive gas was cooled to 5 °C. For (c), 125 complex-valued t_1 points and 256 complex t_2 points were acquired with a spectral width of 12.5 kHz in each dimension. 128 scans per t_1 increment were co-added with a relaxation delay of 2 s. For (b), 250 complex-valued t_1 points and 512 complex t_2 points were acquired with a spectral width of 25 kHz in both dimensions; 64 scans per t_1

(a) (b)

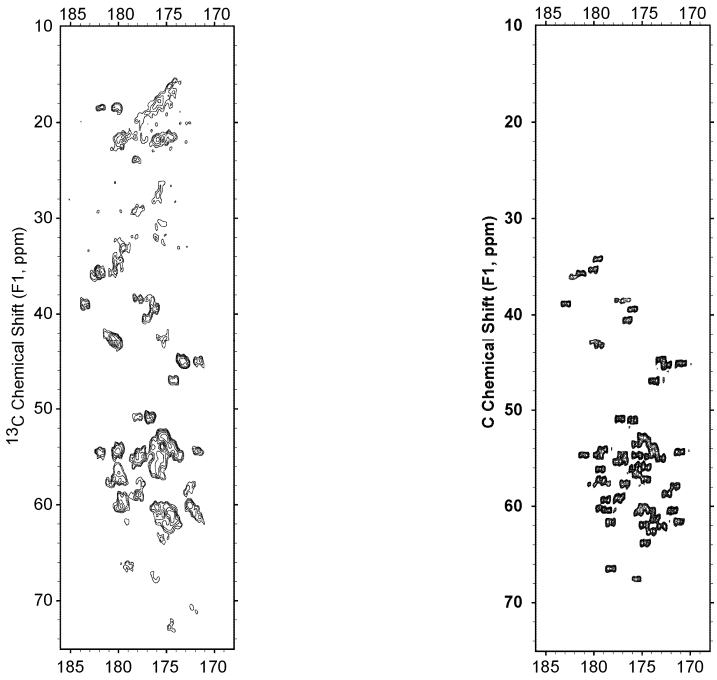

(c)

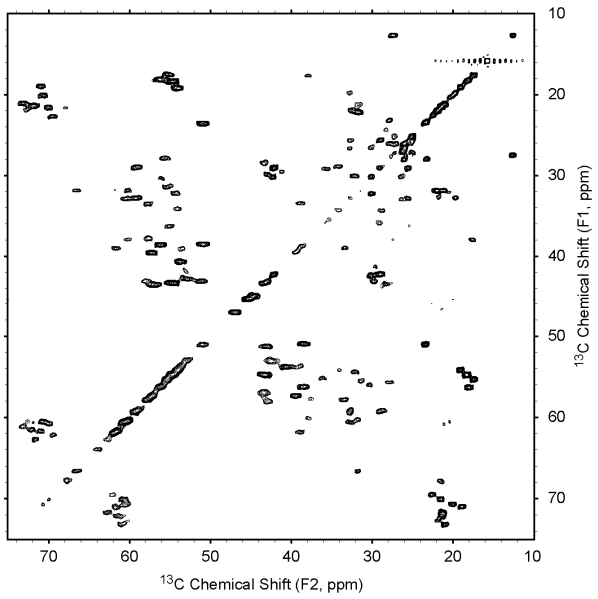

Figure 2.2 CTUC COSY of GB1

increment were co-added with a relaxation delay of 2 s. In (a), the proton-driven spin diffusion spectrum of GB1 is shown for comparison. Acquisition was carried out similar to (b), with 9 kHz MAS (chosen to bracket the aliphatic region between the first- and second-order spinning sidebands of the carbonyl) and a 9 kHz proton spin lock during the 5 ms mixing time. All spectra were linear predicted once in the indirect dimension and zero-filled to 4096 points in both dimensions before Fourier transformation.

Figure 2.2 (c) shows the application of the aliphatic-selective CTUC COSY (Figure 2.1b) to uniformly-^{13}C, ^{15}N-enriched GB1. Based on the previously assigned spectra,[3] all directly bonded carbons are observed in the aliphatic region. Under 25 kHz magic angle spinning (MAS) and 150 kHz proton decoupling (conditions where T_2' is maximized[8] and residual dipolar couplings are suppressed[9]), we find superior side-chain correlation, with sensitivity comparable to or surpassing that of dipolar-driven correlation using spin diffusion. In particular, compared to experiments using dipolar-assisted rotational resonance (DARR) under similar conditions (albeit at necessarily lower MAS rates), we find larger cross-peak intensities (ranging from a factor of 2 to 4) and significantly improved resolution (reduction in line widths in the indirect dimension of 30-50 Hz at primary carbons and 90 Hz at tertiary carbons). The higher resolution is a direct consequence of the removal of homonuclear couplings during the constant-time evolution period and is observed when comparing the CTUC COSY to any directly evolved

(nonconstant-time) single-quantum or double-quantum experiment. Indeed, we have performed such comparisons with the nonconstant-time version of the UC COSY, the refocused INADEQUATE, and DARR (see section 2.4). In addition to the improved sensitivity and resolution, the CTUC COSY diagonal intensity is ideally zero for a two-spin system and, in all cases, is significantly reduced relative to DARR. This allows closer scrutiny, for example, of Leu and Lys Cγ-Cδ side-chain correlations that often arise close to the diagonal. We also note that all cross-peaks are single-bond transfers, except for an extremely weak cross-peak between Val39 Cα-Cγ1. This is in contrast to DARR, where for the intermediate length mixing time of 5 ms, multi-bond transfers are prevalent.

The aliphatic-selective sequence is just one of several variations that can be constructed under the CTUC COSY framework. For example, the aliphatic-carbonyl correlation shown in Figure 2.2 (b) is effected by replacing the aliphatic-selective π pulses with hard π pulse and removing the carbonyl-selective π pulse. The multi-spin dynamics result in strong cross-peaks between the carbonyl and the aliphatic regions, with only correlations not involving alpha carbons in the aliphatic region. Again, the increases in resolution and sensitivity are significant, while the constraint of single-bond transfers diminishes spectral congestion and aids in assignment, especially among Asp and Glu side-chain carboxyl sites, where the protonation state is of great importance to

enzymatic function. The same cross-peak region of the DARR experiment is shown in Figure 2.2a and illustrates the dramatically increased resolution of the CTUC COSY.

2. 3 MULTI-SPIN DYNAMICS

For an I_1-I_2 spin pair, in which each I spin is passively coupled to as many as n_i additional spins, an extension of the product operator calculation from Mueller[13] gives the magnetization transfer during the UC COSY mixing period as

$$T_{12} = \sin^2(\pi J_{12}\tau)\prod_{n_1}\cos(\pi J_{1n_1}\tau)\prod_{n_2}\cos(\pi J_{2n_2}\tau),$$

We consider several specific cases of interest to solid-state ^{13}C correlation in proteins. For concreteness, couplings between sp^3 carbons are assumed to be 35 Hz and those between sp^3 and sp^2 carbons are assumed to be 50 Hz. Below, the nuclei in bold font indicate the cross-peak of interest (the active coupling), while additional spins are indicated by regular type font (the passive couplings).

1. **C'-Cα**

For a single, isolated spin pair, the **C'-Cα** cross-peak intensity $T = \sin^2(\pi J_{C'C_\alpha}\tau)$. This cross-peak has maximum intensity at τ = 5 ms. This case is observed for Gly or amino acids in which the side-chain resonances can be selectively decoupled (see Figure 2.3).

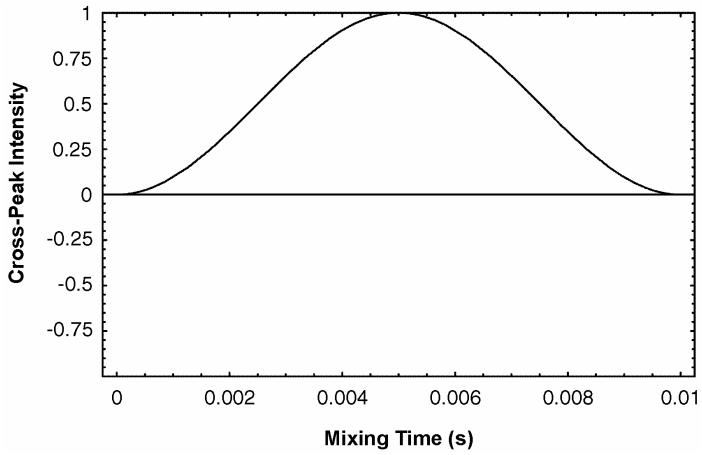

Figure 2.3 Cross peak intensity simulation for **C'-Cα**

2. **C'-C**α-Cβ- …

With a β carbon present, the **C'-C**α cross-peak intensity $T = \sin^2(\pi J_{C'C_\alpha}\tau)\cos(\pi J_{C_\alpha C_\beta}\tau)$. The additional passive coupling between Cα-Cβ shortens the time to the first maximum, which now occurs at slightly less than 5 ms. The maximum intensity is also somewhat diminished (see Figure 2.4).

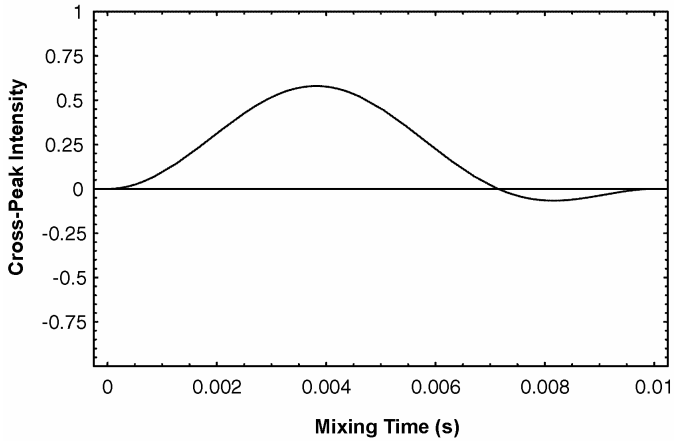

Figure 2.4 Cross peak intensity simulation for **C'-C**α-Cβ- …

3. C'-**C**α-**C**β

The passive C'-Cα coupling greatly attenuates the cross-peak intensity of the **C**α-**C**β carbons at times less than 5 ms. In this case, where $T = \sin^2(\pi J_{C\alpha C\beta}\tau)\cos(\pi J_{C'C\alpha}\tau)$, the cross-peak intensity is zero at 5 ms (see Figure 2.5).

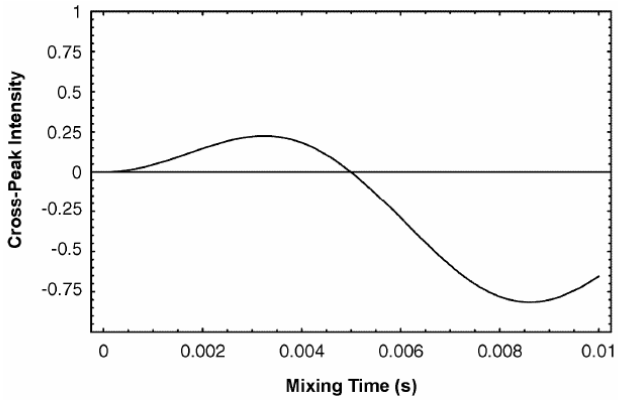

Figure 2.5 Cross peak intensity simulation for C'-**C**α-**C**β

4. **C**α-**C**β

With the C' carbon decoupled, the **C**α-**C**β cross-peak intensity $T = \sin^2(\pi J_{C\alpha C\beta}\tau)$ has a maximum at τ ~ 7 ms with unit intensity (see Figure 2.6).

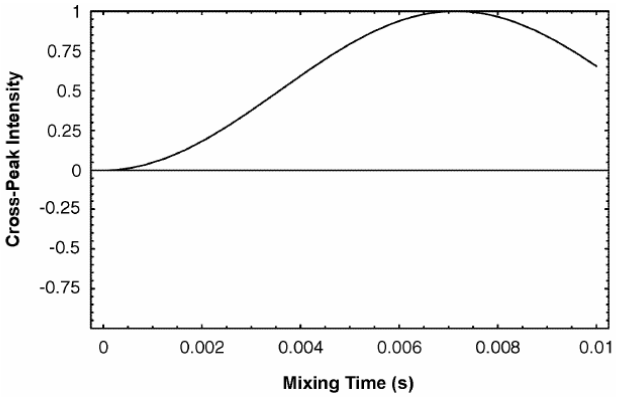

Figure 2.6 Cross peak intensity simulation for **C**α-**C**β

5. **C**α-**C**β-Cγ-...

With the C' carbon decoupled, a cross-peak involving a single passive coupling has intensity $T = \sin^2(\pi J_{C\alpha C\beta}\tau)\cos(\pi J_{C\beta C\gamma}\tau)$ and a maximum at τ ~ 4.5 ms (see Figure 2.7)

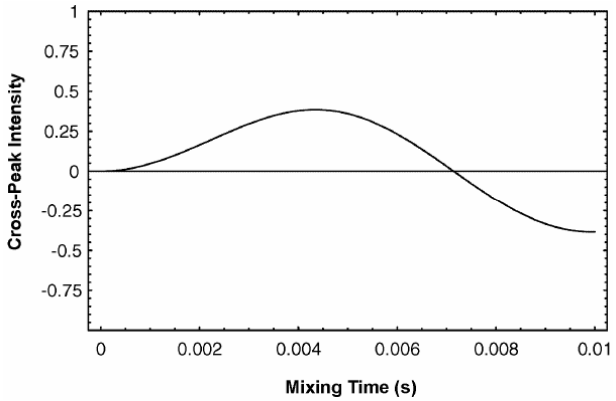

Figure 2.7 Cross peak intensity simulation for **C**α-**C**β-Cγ-...

6. Cα-**C**β-**C**γ-Cδ-...

A cross-peak involving two secondary carbons has intensity $T = \sin^2(\pi J_{C\beta C\gamma}\tau)\cos(\pi J_{C\alpha C\beta}\tau)\cos(\pi J_{C\gamma C\delta}\tau)$. The maximum is closer to zero and has lower intensity than in 5 (see Figure 2.8)

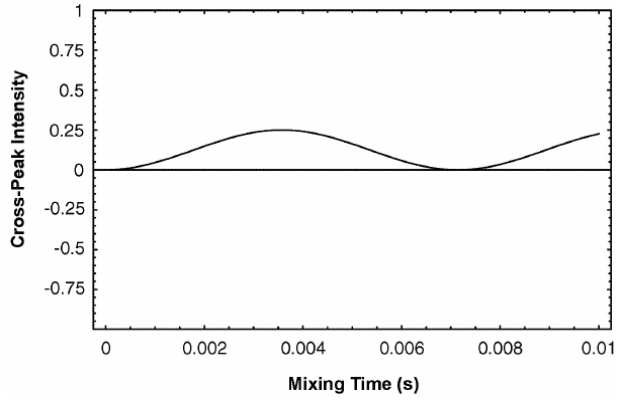

Figure 2.8 Cross peak intensity simulation for Cα-**C**β-**C**γ-Cδ-...

Cδ1
/
7. Cα-**C**β-**C**γ
\
Cδ2

Finally, a cross-peak involving one secondary carbon and one tertiary carbon (three passive couplings) has intensity $T = \sin^2(\pi J_{C\beta C\gamma}\tau)\cos(\pi J_{C\alpha C\beta}\tau)\cos^2(\pi J_{C\gamma C\delta}\tau)$. This situation is observed only for Leu Cβ-Cγ and Ile Cβ-Cγ (see Figure 2.9).

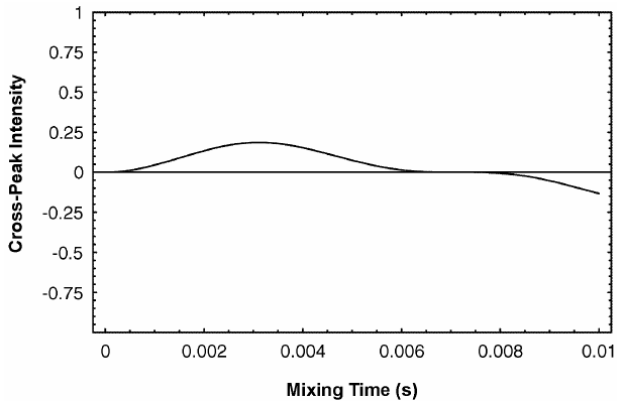

Cδ1
/
Figure 2.9 Cross peak intensity simulation for Cα-**C**β-**C**γ
\
Cδ2

Several points are worth noting. The first is that in order to maximize Cα-Cβ intensity, decoupling the carbonyl carbon is essential, particularly for mixing times close to 5 ms. This is the motivation for the aliphatic selective version of the CTUC COSY

(Figure 2.1 (b)). Second, in a protein, where multiple types of spin systems are present, there is a trade-off between mixing time, resolution, and peak intensities. Our choice of τ = 5 ms favors higher resolution at the expense of some attenuation at Leu and Ile Cβ-Cγ peaks. For a mixing time of 3.5 ms, we find improved cross-peak intensity with only slightly lower resolution.

2.4 COMPARING THE CTUC COSY TO OTHER METHODS

We have compared the CTUC COSY to several other correlation methods in solids. In particular, comparisons were made to the non-constant-time version of the UC COSY (with and without aliphatic selective pulses for excitation), the refocused INADEQUATE experiment (with and without aliphatic selective pulses for excitation), and spin diffusion using DARR (see pulse sequences, Figure 2.10 and Figure 2.11).

In the pulse sequences in Figure 2.10, thin vertical lines indicate $\pi/2$ pulses and wide vertical lines indicate π pulses. 80 kHz ^{13}C pulses were used throughout for the hard pulses along with 150 kHz SPINAL64 1H decoupling during the t_1, τ , and constant-time intervals, and 100 kHz decupling during the z-filter (τ_{zf}, typically 16 ms) and acquisition (t_2). The rotor-synchronized refocusing delay τ was set to 5 ms for the COSY and INADEQUATE experiments and 5 ms mixing time was used in DARR. Data were acquired on a 9.4 T Bruker DSX spectrometer (^{1}H frequency 400.13 MHz) equipped

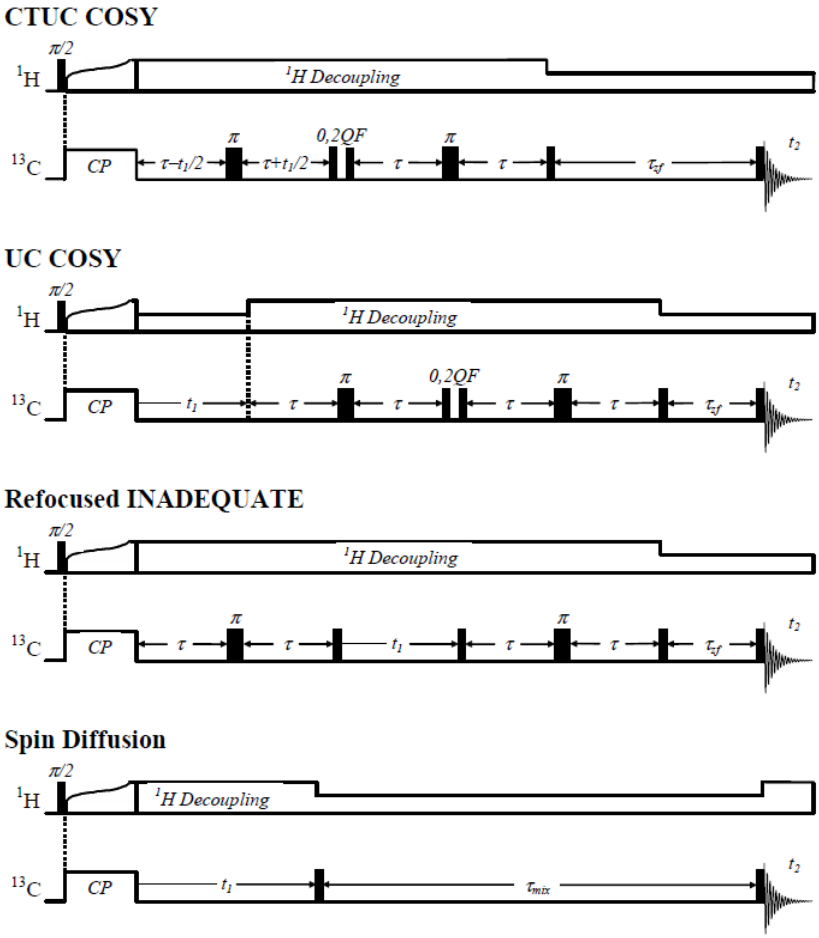

Figure 2.10 Pulse sequences for the CTUC COSY, UC COSY, refocused INADEQUATE, and spin diffusion under DARR.

with a double resonance 2.5 mm MAS probe spinning at a MAS rate of 25 kHz (COSY and INADEQUATE) and 9 kHz (DARR). 250 complex-valued t_1 points and 512 complex t_2 points were acquired with a spectral width of 25 kHz in both dimensions; 64 scans per t_1 increment were co-added with a relaxation delay of 2 s.

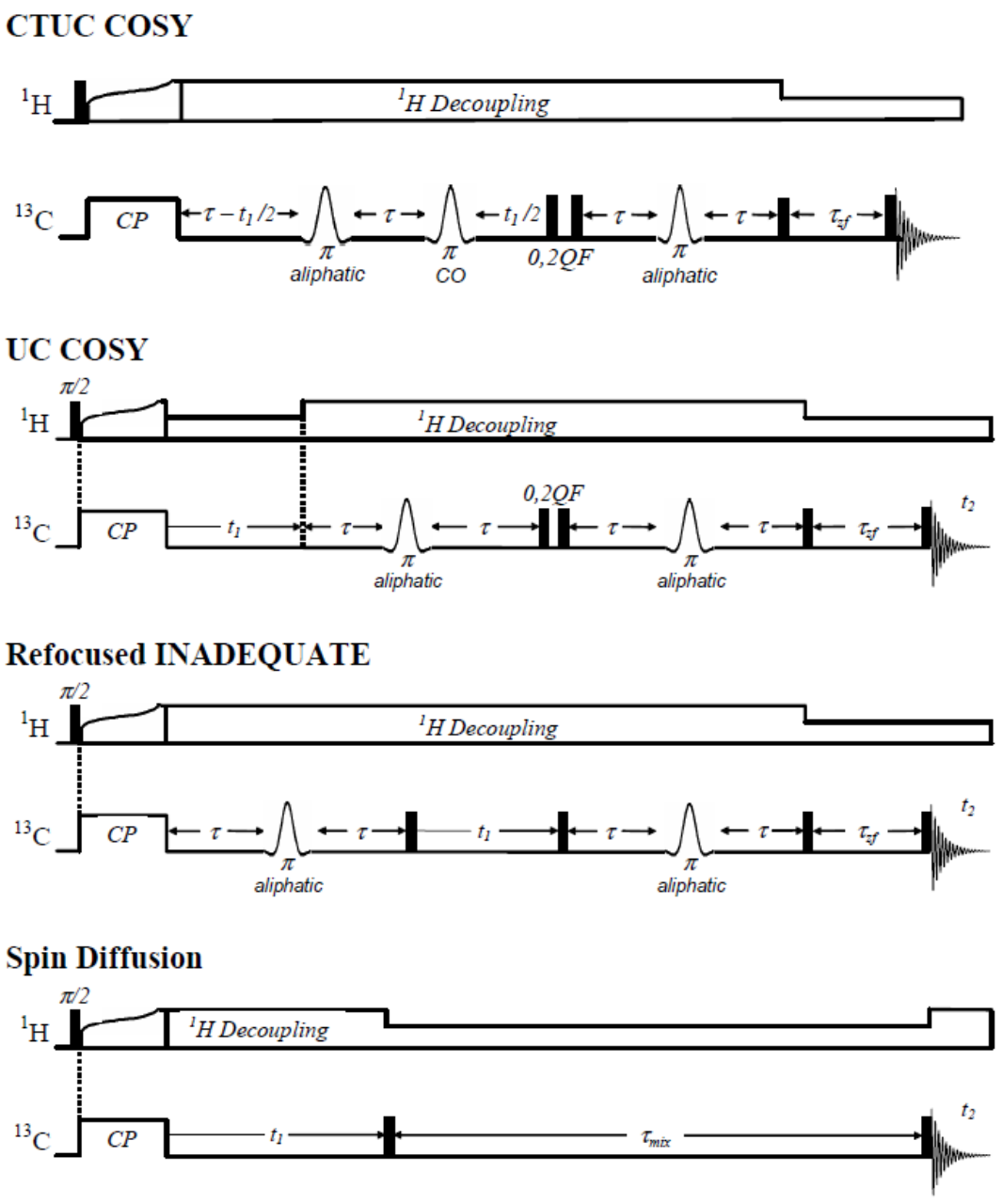

Figure 2.11 Pulse sequences for DARR and the aliphatic selective CTUC COSY, UC COSY, and refocused INADEQUATE

In pulse sequences in Figure 2.11, thin vertical lines indicate π/2 pulses, wide vertical lines indicate π pulses, and selective π pulses are shown as amplitude modulated waveforms. 80 kHz ^{13}C pulses were used throughout for the hard pulses along with 150 kHz SPINAL64 ^{1}H decoupling during the τ and constant-time intervals and 100 kHz decupling during the z-filter (τ_{zf}, typically 16 ms) and acquisition (t_2). For the selective π pulses, 180 μs and 420 μs r-SNOB pulses were used for selective aliphatic and carbonyl pulses, respectively. These were centered in the respective spectral regions and rotor synchronized as described in Ref 9. The rotor-synchronized refocusing delay τ was set to 5 ms for the COSY and INADEQUATE experiments and a 5 ms mixing time was used in DARR. Data were acquired on a 9.4 T Bruker DSX spectrometer (^{1}H frequency 400.13 MHz) equipped with a double resonance 2.5 mm MAS probe spinning at a MAS rate of 25 kHz (COSY and INADEQUATE) and 9 kHz (DARR). 125 complex-valued t_1 points and 256 complex t_2 points were acquired with a spectral width of 12.5 kHz in each dimension for the COSY and INADEQUTE experiments. 128 scans per t_1 increment were co-added with a relaxation delay of 2 s. Proton driven spin diffusion using DARR at 9 kHz MAS was acquired with 250 complex-valued t_1 points and 512 complex t_2 points with a spectral width of 25 kHz in both dimensions; 64 scans per t_1 increment were co-added with a relaxation delay of 2 s. All spectra were linear predicted once in the

indirect dimension and zero filled to 4096 points in both dimensions before Fourier transformation.

For all experiments, the data were acquired under identical conditions, i.e., identical spectral resolution (in both dimensions), total acquisition time, rf powers, decoupling, and MAS rate (except as already noted for DARR). As well, all spectra were processed identically, with data linear predicted once in the indirect dimension and zero filled to 4096 points in both dimensions before Fourier transformation. The corresponding carbonyl-aliphatic regions of the spectra are shown on Figure 2.12.

Great care was taken to ensure that the contours were drawn fairly. In particular, the lowest contour on each spectrum was drawn so that the line widths in the direct, F2, dimension were equivalent, as expected under free evolution with the same experimental conditions. In each case the contour multiplier was set to 1.30 and the number of contours drawn was 20. 1D slices are shown on Figure 2.13 for easier comparison. Here, the absolute intensities are used as the experiments were acquired and processed the same way.

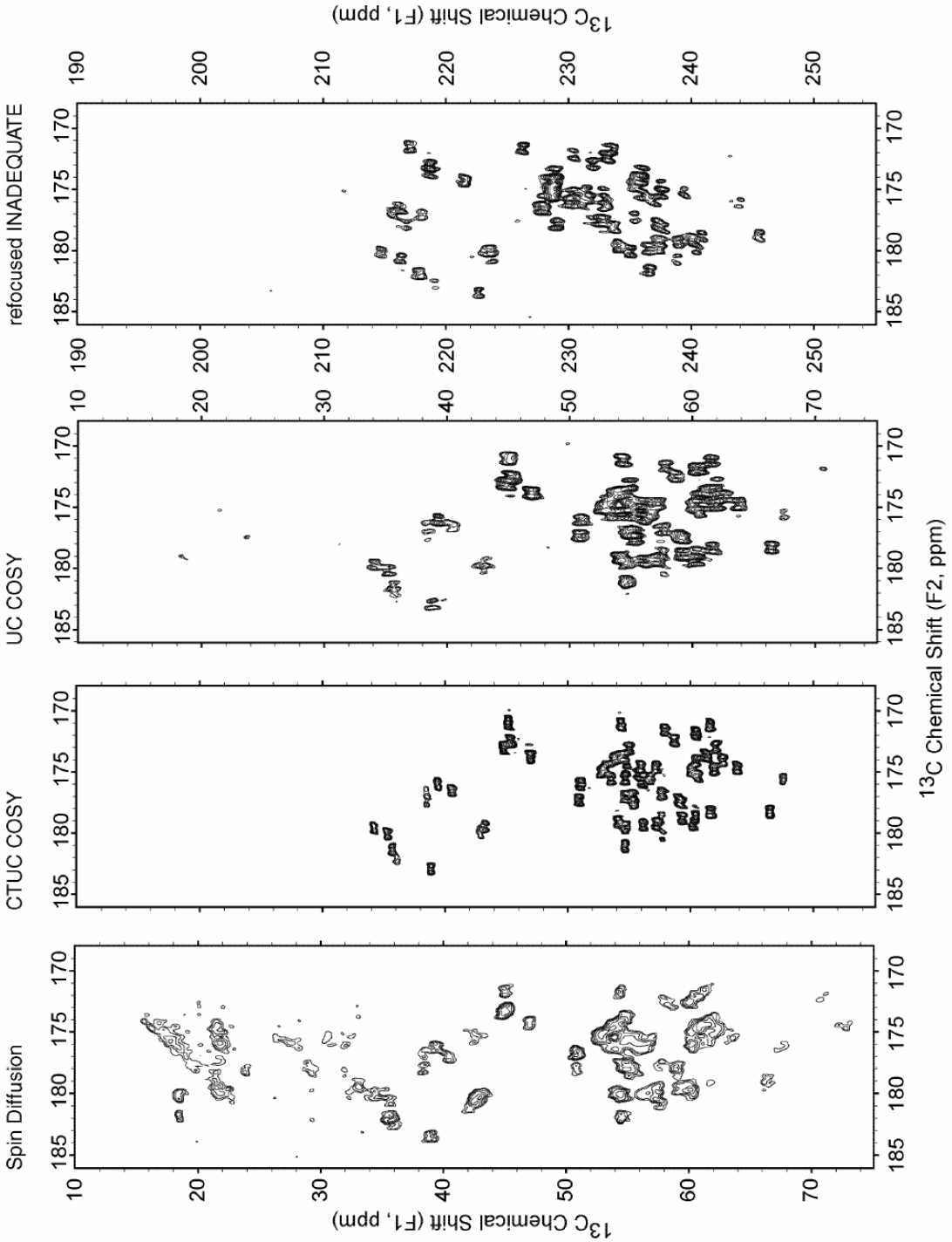

Figure 2.12 CTUC COSY comparing to other methods in carbonyl-aliphatic region

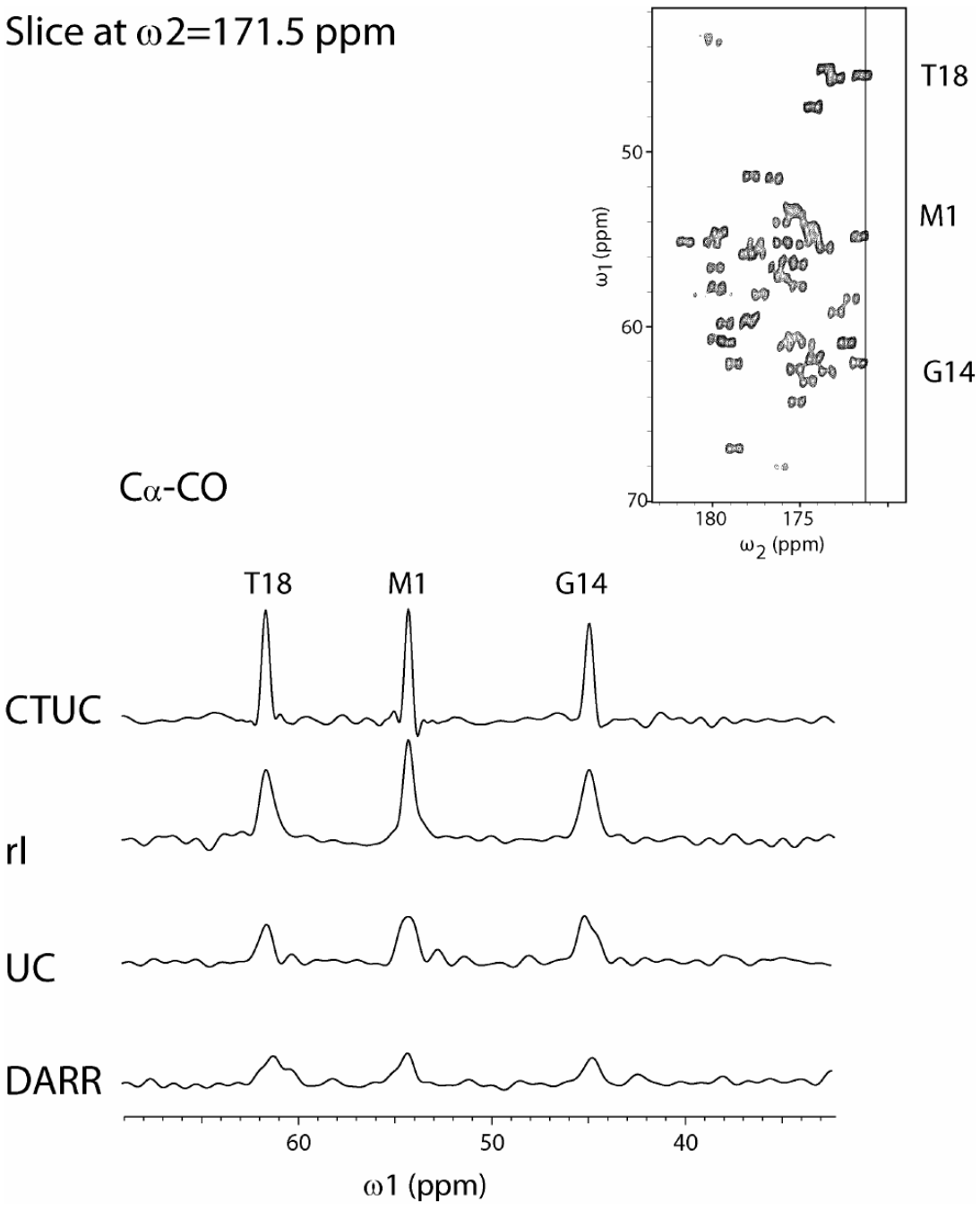

Figure 2.13 1D slides along the indirect dimensional of T18, M1 and G14

The aliphatic regions were acquired using the aliphatic-selective sequences shown in Figure 2.11 and the corresponding spectra are shown in Figure 2.14.

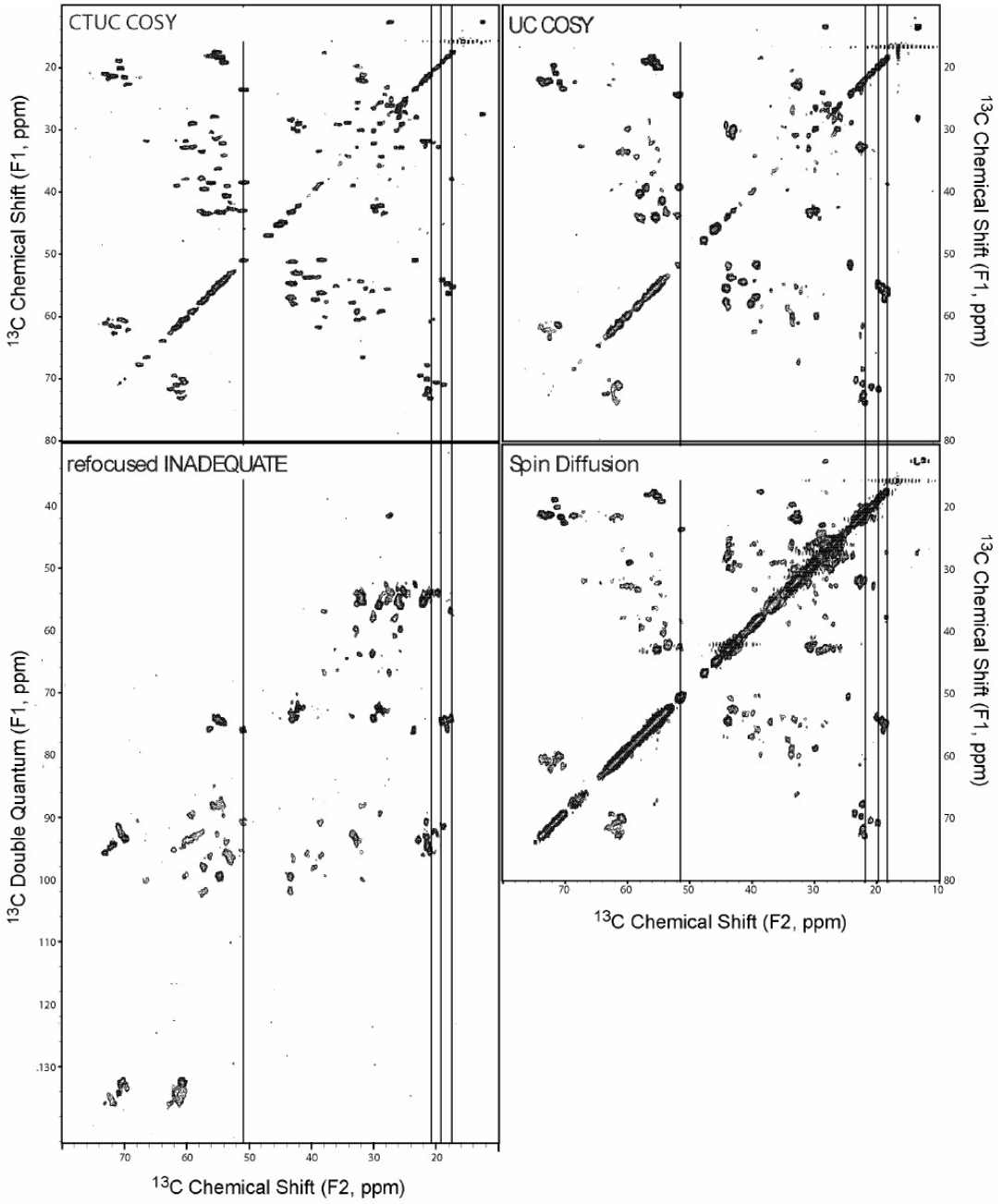

Figure 2.14 CTUC COSY comparing to other method in aliphatic region

Although we use analogous selective pulses for the preparation/transfer periods of the refocused INADEQUATE and UC COSY, we do not decouple the carbonyls during t_1. In principle, this could be accomplished using the approach of Straus and Ernst[12]. A number of 1D slices are shown on Figure 2.15-2.18 for easier comparison in the aliphatic region. Here, the absolute intensities are again used, as the experiments were acquired and processed the same way. In all cases we see the expected increase in resolution for the *J* decoupled experiment. For the UC COSY (non-constant-time) and spin diffusion, contributions to the line width due to both the active coupling (30-50 Hz) and all passive couplings (an additional 30-80 Hz) are observed. We also note that due to the slower MAS rate for DARR (9 kHz), approximately 10-15 Hz of additional broadening is observed in both frequency domains. For the refocused-INADEQUATE, the evolving double quantum coherence commutes with the active coupling and is therefore not observed and does not broaden the lines. The double quantum coherence does, however, evolve under the passive couplings, which again can broaden the lines by 30-100 Hz. For a fair comparison of the refocused-INADEQUATE, we found it necessary to digitize the FID in the indirect dimension to the same digital resolution as in the single-quantum correlation experiments; otherwise, artificially broad lines were observed. Signal-to-noise ratios also scale as expected, with approximately twice the sensitivity for the CTUC COSY compared to the direct evolve UC COSY, 20%-60% better sensitivity compared to

the refocused INADEQUATE, and 2-4 times better sensitivity compared to DARR (depending on spin system, *vide supra*).

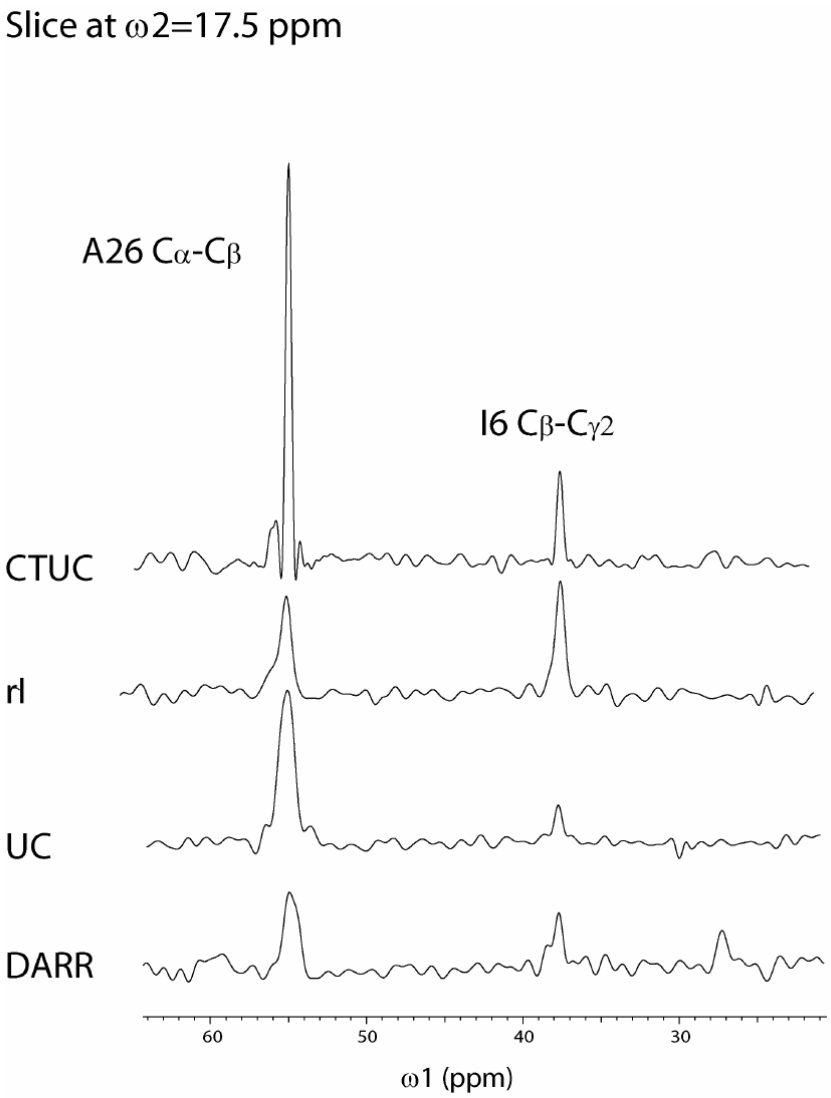

Figure 2.15 1D slices along ω_1 dimension in aliphatic region for A26 and I6

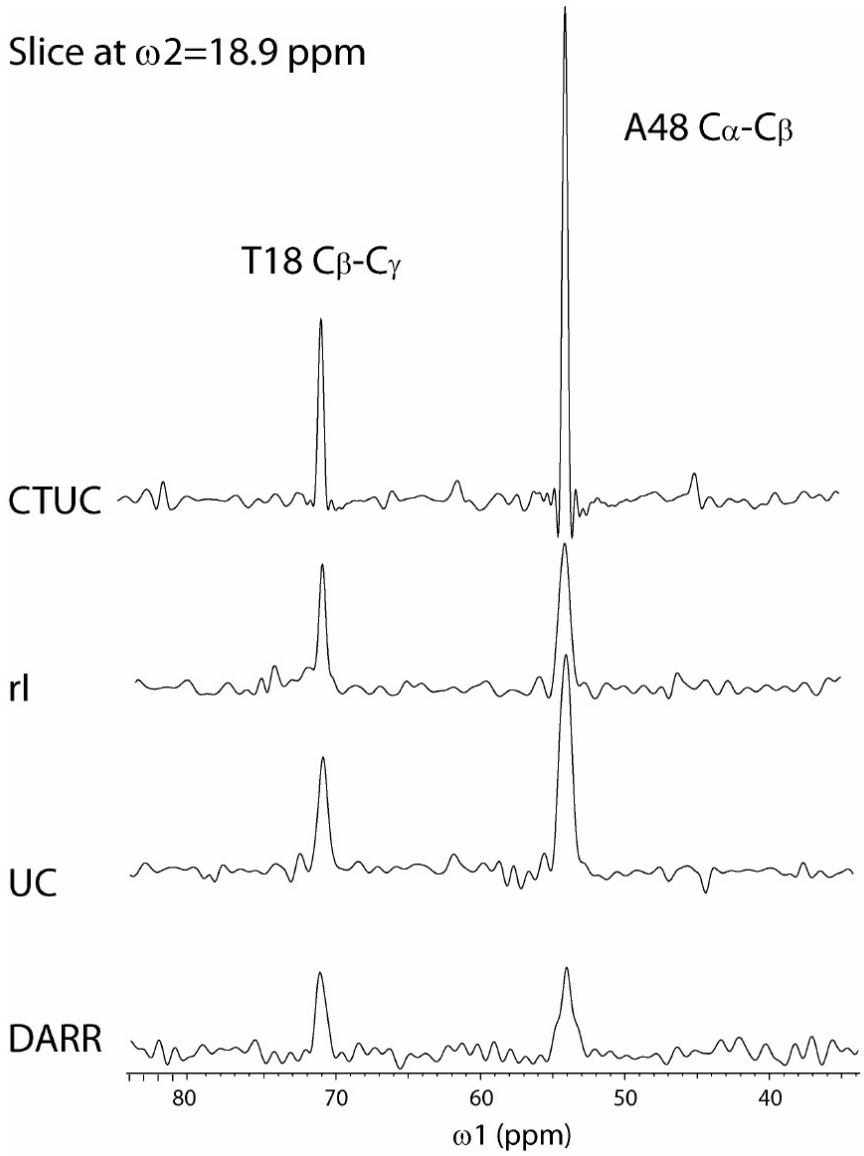

Figure 2.16 1D slices along ω_1 dimension in aliphatic region for T18 and A48

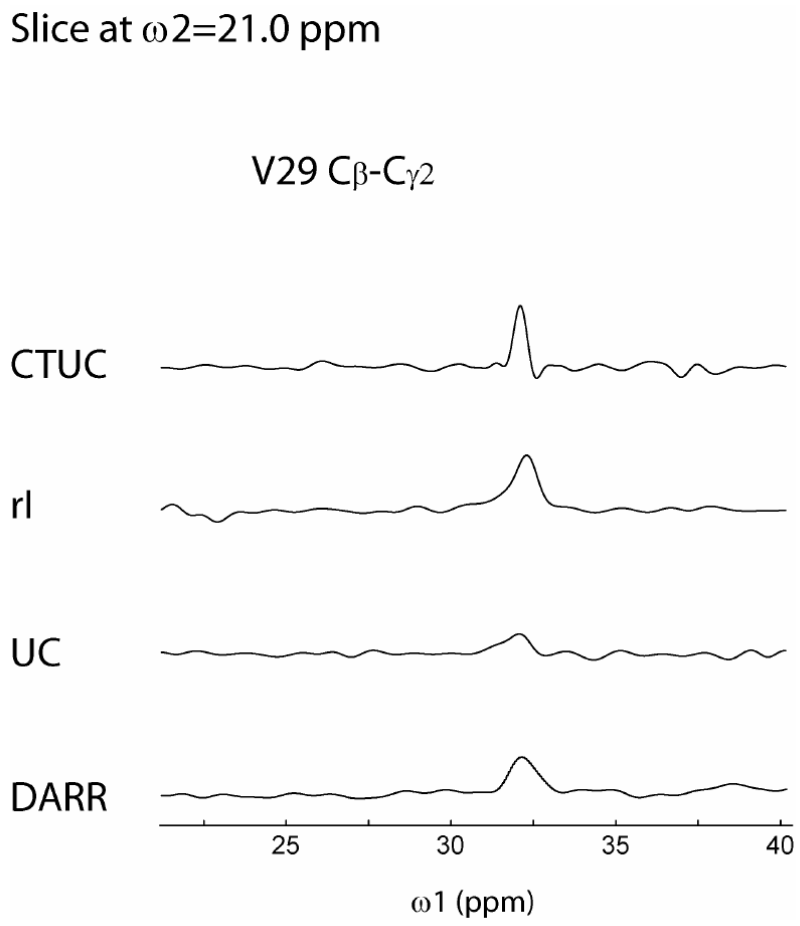

Figure 2.17 1D slices along ω_1 dimension in aliphatic region for V29

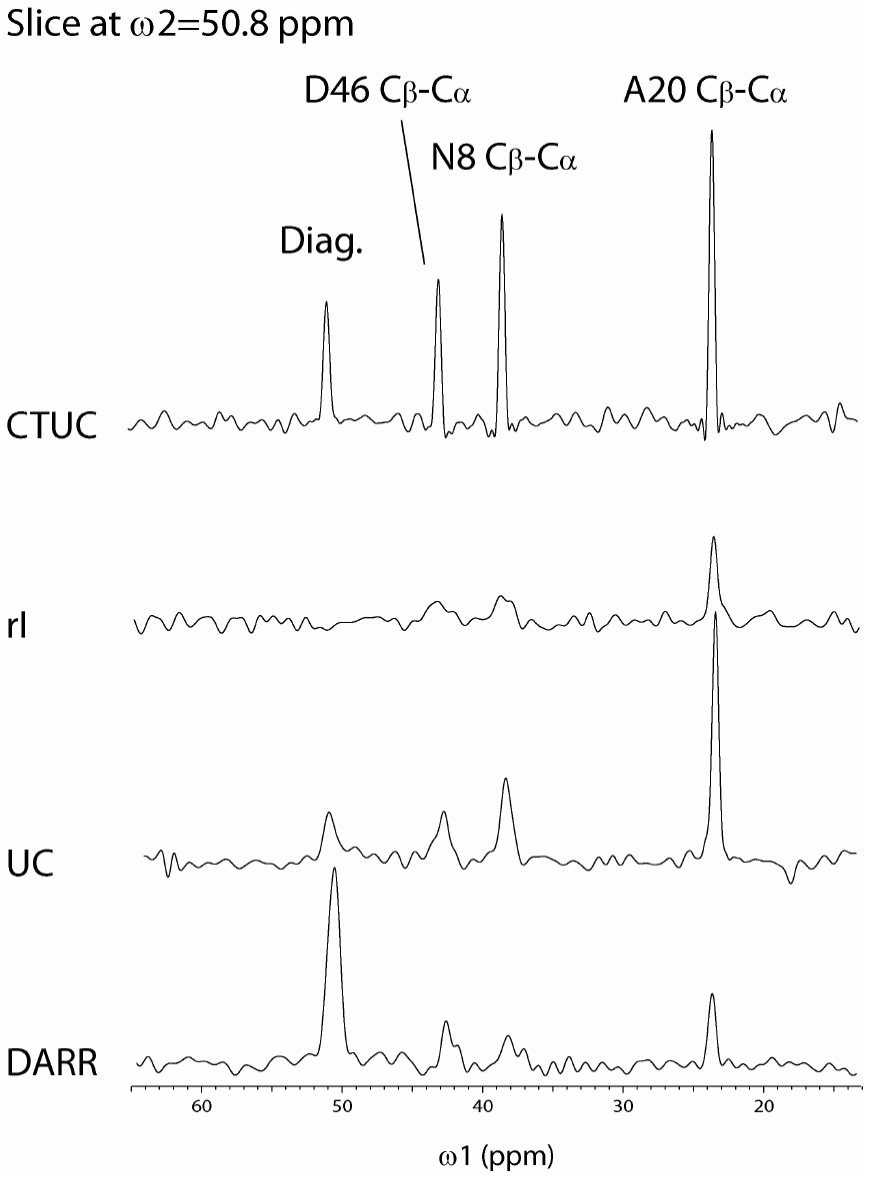

Figure 2.18 1D slices along ω_1 dimension in aliphatic region for D46, N8 and A20

2.5 CTUC COSY AT SLOWER MAS RATES

Due to the slower MAS rate for DARR (9 kHz), approximately 10-15 Hz of additional broadening is observed in both frequency domains. To help separate the contributions due to MAS rate and those due to the constant time format, we have also run the CTUC COSY at 9 kHz for comparison to DARR, as is shown below. While the resolution at 9 kHz is not as good as the resolution at 25 kHz, it is clearly better for the *J*-decoupled CTUC COSY than for Spin Diffusion.

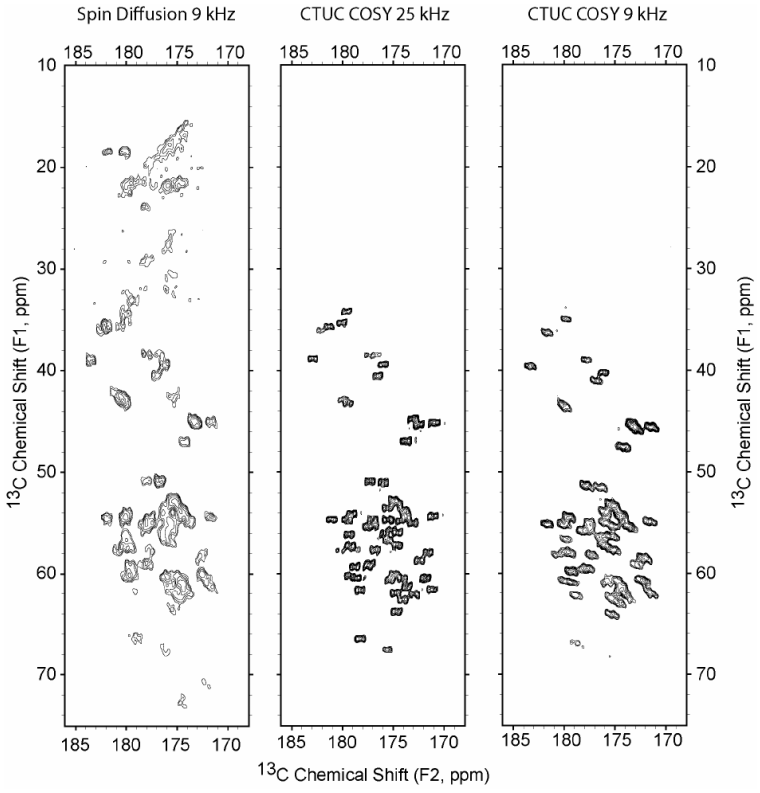

Figure 2.19 CTUC COSY AT SLOWER MAS RATES

2.6 CONCLUSION

Even as available magnetic fields for NMR continue to increase, resolution remains one of the most critical limitations in assigning and solving structures of larger biomolecules. The constant-time UC COSY offers superior resolution, by a factor of 2 to 3, compared to that of directly evolved experiments. The sensitivity is also enhanced and the sequence performs as well or better than the commonly used dipolar methods, especially for side-chain sites exhibiting molecular motion. The improved sensitivity of this scalar-coupling driven method is comparable to results found by Meier using the isotropic-mixing TOBSY sequence,[3] although the CTUC COSY offers the additional resolution advantage of a constant-time implementation. Because the indirect evolution and transfer periods can be combined into a single constant time interval, the increased resolution is not obtained at the cost of sensitivity, a distinguishing feature of COSY-type sequences compared to that of strong-coupling or INADEQUATE sequences. For GB1, this allows for multiple peaks to be resolved that are otherwise obscured.

REFERENCES

1. States, D.J.; Haberkorn, R.A.; Ruben, D.J. *J. Magn. Reson.* **1982**, *48*, 286-292

2. Pauli, J.; Baldus, M.; van Rossum, B.; de Groot, H.; Oschkinat, H. *ChemBioChem* **2001**, *2*, 272-281. Baldus, M. *Prog. Nucl. Magn. Reson. Spectrosc.* **2002**, *41*, 1-47. Hohwy, M.; Rienstra, C. M.; Griffin, R. G. *J. Chem. Phys.* **2002**, *117*, 4973-4987. Igumenova, T. I.; McDermott, A. E.; Zilm, K. W.; Martin, R. W.; Paulson, E. K.; Wand, A. J. *J. Am. Chem. Soc.* **2004**, *126*, 6720-6727. Harris, R. K.; Joyce, S. A.; Pickard, C. J.; Cadars, S.; Emsley, L. *Phys. Chem. Chem. Phys.* **2006**, *8*, 137-143.

3. Franks, W. T.; Zhou, D. H.; Wylie, B. J.; Money, B. G.; Graesser, D. T.; Frericks, H. L.; Sahota, G.; Rienstra, C. M. *J. Am. Chem. Soc.* **2005**, *127*, 12291-12305.

4. Ernst, M.; Detken, A.; Bockmann, A.; Meier, B. H. *J. Am. Chem. Soc.* **2003**, *125*, 15807-15810.

5. Bockmann, A.; Juy, M.; Bettler, E.; Emsley, L.; Galinier, A.; Penin, F.; Lesage, A. *J. Biomol. NMR* **2005**, *32*, 195-207.

6. Bax, A.; Freeman, R. *J. Magn. Reson.* **1981**, *44*, 542-561

7. Mueller, L. J.; Elliott, D. W.; Kim, K. C.; Reed, C. A.; Boyd, P. D. W. *J. Am. Chem. Soc.* **2002**, *124*, 9360-9361. Mueller, L. J.; Elliott, D. W.; Leskowitz, G. M.; Struppe, J.; Olsen, R. A.; Kim, K. C.; Reed, C. A. *J. Magn. Reson.* **2004**, *168*, 327-335

8. De Paepe, G.; Lesage, A.; Emsley, L. *J. Chem. Phys.* **2003**, *119*, 4833-4841.

9. Fayon, F.; Massiot, D.; Levitt, M. H.; Titman, J. J.; Gregory, D. H.; Duma, L.; Emsley, L.; Brown, S. P. *J. Chem. Phys.* **2005**, *122*, 194313-194314.

10. Fung, B. M.; Khitrin, A. K.; Ermolaev, K. *J. Magn. Reson.* **2000**, *142*, 97-101.

11. Li, Y.; Wylie, B. J.; Rienstra, C. M. *J. Magn. Reson.* **2006**, *179*, 206-216.

12. Straus and Ernst, *Chem. Phys. Lett.* **1996**, 262:709

13. Mueller, L.J. *J. Magn. Reson.* **2004**, *168*, 327-335

CHAPTER III

J-BASED 2D HETERONUCLEAR CORRELATION IN SOLID-STATE PROTEINS

ABSTRACT

Scalar-based two-dimensional heteronuclear experiments are presented for NCO and NCA chemical shift correlation in the solid state. In conjunction with homonuclear CACO correlation, these experiments form a useful set for tracing connectivities and assigning backbone resonances in solid-state proteins. The applicability of this approach is demonstrated on two proteins, the β1 immunoglobulin binding domain of protein G at 9.4 T and reassembled thioredoxin at 14.1 T, using different decoupling conditions and MAS frequencies. These constant-time J-based correlation experiments exhibit increased resolution in the indirect dimension owing to homonuclear and heteronuclear decoupling, and because the indirect evolution and transfer periods are combined into a single constant time interval, this increased resolution is not obtained at the cost of sensitivity. These experiments are also shown to be compatible with in-phase anti-phase (IPAP) selection, giving increased resolution in the directly detected dimension.

3.1 INTRODUCTION

Solid-state NMR spectroscopy has developed as a unique tool for chemistry and biology owing to its ability to provide detailed structural information for molecules lacking macroscopic order. For example, fibrils,[1–3] macromolecular assemblies,[4–6] and membrane proteins[7–12] have been successfully studied in recent years by this approach. A necessary starting point in all NMR studies is resonance assignments, which in solids are typically made by analyzing cross-peak patterns in spectra obtained using through-space, dipolar-driven correlation spectroscopy.[13–19] As an alternative method of assignment, scalar-coupling-based correlation spectroscopy has now been demonstrated in several contexts for biological solids.[20–30] Through-bond, scalar-coupling driven correlation schemes offer several important features that are complementary to through-space methods. In particular, scalar couplings are insensitive to global molecular motion, which often compromises sensitivity in dipolar methods. Scalar methods also provide a means to delineate through-bond and through-space connectivity, a critical step for establishing unambiguous sequential assignments.

In chapter II, it was shown that through-bond correlation in solids can be implemented efficiently in a ‘constant time’ pulse sequence element, with the indirect evolution and coherence transfer periods combined into a single time interval. This

method substantially increases spectral resolution by decoupling scalar interactions in the indirect dimension.[31] In constant-time 2D ^{13}C–^{13}C experiments, [28] sensitivity was found to be comparable to or better than that of dipolar methods, in part owing to the relatively large homonuclear scalar couplings (~35–55 Hz) responsible for the coherence transfer. In previous studies, the focus was primarily on the β1 immunoglobulin binding domain of protein G (GB1), which is especially thermostable and therefore able to withstand fast magic-angle spinning (MAS) and high power decoupling to achieve optimal relaxation behavior. Here, the implementation of heteronuclear 2D correlation experiments using purely scalar (J_{NC}) based transfers for NCA and NCO correlation is investigated and combined with CACO correlation[28] for the assignment of backbone resonances in solid-state proteins. More extensive studies of a second protein, thioredoxin (TRX), are also included under experimentally moderate conditions of MAS and decoupling. These illustrate the wide range of parameters over which these experiments can be applied. Finally, these experiments are shown to be compatible with in-phase anti-phase (IPAP) selection, giving increased resolution in the directly detected dimension. Overall, scalar-based correlation schemes are found to be broadly applicable, substantially increase spectral resolution without compromising sensitivity, and provide valuable information content including both intraresidue and interresidue correlations.

3.2 EXPERIMENTAL

3.2.1 2D NMR experiments

2D NMR experiments were performed using the pulse sequences in Figure 3.1 and 3.6 (described in detail in section) at 9.4 T on a Bruker DSX spectrometer (^{1}H frequency 400 MHz) and at 14.1 T on a Varian InfinityPlus spectrometer (^{1}H frequency 600 MHz). The 9.4 T Bruker DSX spectrometer was equipped with a triple-resonance 2.5 mm MAS probe and experiments were performed with an MAS rate of 25 kHz. Hard π/2 and π pulses at 80 kHz for ^{13}C and 50 kHz for ^{15}N pulses were used throughout, along with 150 kHz SPINAL64[32] ^{1}H decoupling during the constant time intervals and 100 kHz SPINAL64 decoupling during the 16 ms z-filter and acquisition (t_2). Selective 180 and 420 μs r-SNOB pulses were used for the alpha and carbonyl π pulses, respectively, and were rotor-synchronized as described in Ref. 33. In all experiments, the carbon carrier frequency was centered between the alpha and carbonyl regions and selective pulses were implemented using a phase modulation. Pure phase spectra were obtained using the method of States[34] by incrementing the phase of the spin-lock pulse on ^{13}C or ^{15}N. Minimal phase cycles are indicated in Figure 3.1; further phase cycling of the π pulses and proton excitation pulse is optional, and may be of benefit with conditions of rapid ^{13}C T_1 relaxation and/or lower B_1 field homogeneity. Experiment-specific parameters are

described in the figure captions. The 600 MHz Varian IinfinityPlus spectrometer was fitted with a triple-resonance 3.2 mm T3 probe and the MAS rate was typically 14.705 kHz in the experiments presented here. TPPM decoupling on ^{1}H was used with nutation frequencies of 90, 83, and 50 kHz during the *J*-evolution, acquisition, and z-filter periods, respectively. The carrier was again centered between the alpha and carbonyl regions and 170 and 374 μs selective r-SNOB pulses were used for selective pulses, respectively. Pure phase spectra were obtained using the TPPI detection in the indirect dimension.[35]

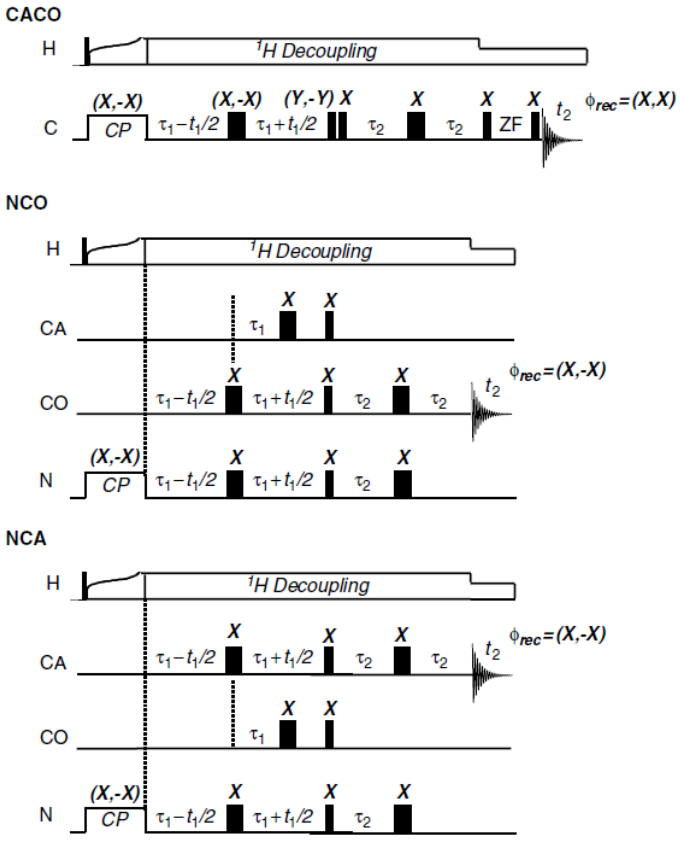

Figure 3.1 Constant-time *J*-MAS CACO, NCO, and NCA 2D heteronuclear correlation experiments

In these pulse sequences, thin vertical lines indicate π/2 pulses and wide vertical lines indicate π pulses that are either selective (single carbon channel) or broad-banded (shown as simultaneous CA and CO pulses). The indirect evolution increments, π refocusing periods, and z-filter (zf) are all rotor-synchronized.

3.2.2 T_2' Measurements

T_2' was measured over a range of MAS rates and proton decoupling powers using a simple τ - π (selective)- τ dephasing period following CP from ^{1}H. The echo intensity decay was then fitted to an exponential function in τ, typically using 6–10 τ values. In each case, decoupling was optimized for maximum T_2' on the alpha carbon and then used without further optimization for the carbonyl and nitrogen measurements. For the selective alpha and carbonyl pulses, 3.2 ms and 420 μs r-SNOB pulses were used, respectively. The 3.2 ms alpha pulse was found to be necessary to provide consistent echo line shapes without distortion from couplings to the beta carbons. In all cases, the average relaxation rate for the spectral window of interest was measured, rather than for individual sites, in order to report the overall characteristic of the protein. These were well fitted to a single exponential rate, indicating a relatively small range of decay rates at individual sites throughout the protein. Therefore we did not attempt to measure site-specific relaxation rates in this study.

3.2.3 Sample Preparation

Overexpression and purification of isotopically enriched thioredoxin have been reported previously.[36,37] The preparation of the differentially enriched thioredoxin 1–73(U–^{13}C,^{15}N)/74–108(U–^{15}N) was conducted similar to the procedure for preparation of the 1–73(U–^{15}N)/74–108(U–^{13}C,^{15}N) thioredoxin reassembly except that the N-terminal fragment containing residues 1–73 was uniformly (U–^{13}C,^{15}N) enriched and reconstituted with the complementary C–terminal (U–^{15}N) enriched fragment containing residues 74–108. The sample for solid-state NMR spectroscopy was prepared by controlled precipitation of the differentially enriched reassembly with polyethylene glycol (PEG)-4000, using the protocols reported by Marulanda and Polenova.[36, 37] The PEG precipitate was centrifuged, the supernatant removed, and the resulting sample transferred into a 3.2 mm Varian rotor. The sample was sealed using upper spacers and top spinners, according to the standard procedures. The final amount of the hydrated, precipitated thioredoxin samples packed in the NMR rotors was 11 mg.

The 56 residue β1 immunoglobulin binding domain of protein G was prepared uniformly ^{13}C, ^{15}N-enriched through overexpression and purification as reported by Franks and Rienstra .[16]

3.3 RESULTS AND DISCUSSION

3.3.1 Applications of NCO, NCA and CACO Experiments in GB1

The approach makes use of the 2D *J*-based MAS experiments shown in Figure 3.1. These experiments are inspired by their solution-state counterparts, particularly as implemented by Bertini and coworkers for protonless correlation in paramagnetic proteins in solution.[38, 39] The spin dynamics for the coherence transfer steps are similar in each of these three experiments. During the first constant-time period, antiphase terms develop under the scalar coupling interaction. This can be either the homonuclear (CACO) or heteronuclear (NCA and NCO) coupling. The transverse component of the anti-phase term is then transferred from the source spin to the destination spin by hard $\pi/2$ pulses, and rephases during the second constant-time interval to transverse coherence solely on the destination spin. The chemical shift is encoded in the first dimension by incrementing the π pulse position. The additional π pulse on CO and CA in the NCA and NCO experiments, respectively, ensures that additional passive couplings remain refocused as the π pulses are moved off center. (A corresponding ^{15}N π pulse could be added to the CACO correlation should this be found advantageous.) This pathway is summarized below for an ideal two-spin system:

$$I_x \xrightarrow{(\tau - t_1/2) - \pi - (\tau + t_1/2)} \cos(\omega_1 t_1) 2I_y S_z \xrightarrow{\pi/2(I_x + S_x)} \cos(\omega_1 t_1) 2I_z S_y$$
$$\xrightarrow{\tau - \pi - \tau} \cos(\omega_1 t_1) S_x$$

As in the liquid state, the combined constant-time evolution and mixing period improves resolution through homonuclear and heteronucler decoupling in the indirect dimension. At the same time, since the coherence transfer and single-quantum evolution are combined in one constant time period, the increased resolution is not obtained at the cost of sensitivity.

Figure 3.2 shows the application of the *J*–MAS CACO, NCO, and NCA to uniformly ^{13}C, ^{15}N-enriched GB1. This combination of experiments establishes correlations along the protein backbone, one part of which is traced out. Because of the homonuclear and heteronucler decoupling in the indirect dimension, we find significantly improved resolution, with a reduction in line widths in the indirect dimension to 30–40 Hz for both carbon and nitrogen. The resolution in the CACO and NCO experiments is adequate to identify most of the individual resonances, although the NCA resolution is somewhat compromised owing to the presence of both CO and CB couplings in the directly detected dimension. It is important to note that additional two-bond correlations arise from the NCA transfers; these peaks are also seen in solution. While the two-bond correlations may result in additional spectral congestion, they are quite useful in corroborating the resonance assignments. As in solution-state NMR, these two

dimensional sequences can be used as the building blocks for three-dimensional experiments with correspondingly greater resolution (see chapter IV).[30]

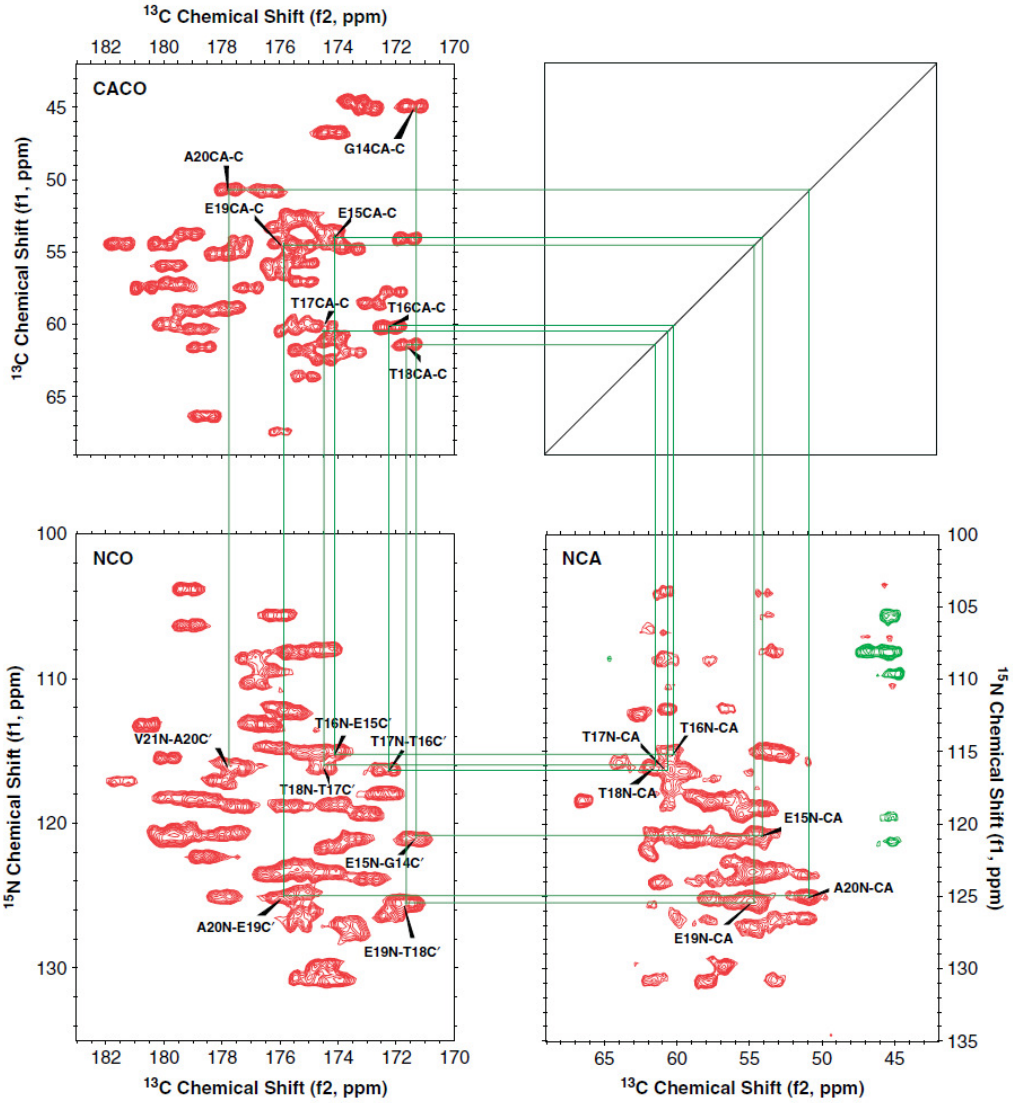

Figure 3.2 *J*-MAS CACO, NCO, and NCA experiments for GB1 at 9.4 T, illustrating the backbone assignments

Experiment-specific parameters for CACO: $\tau_1 = \tau_2 = 4.8$ ms; 8 scans per t_1 increment; 1024 complex points with a dwell of 40 μs (spectral width 25 kHz, total acquisition time 40.96 ms) in t_2; 230 complex points with a dwell of 40 μs (spectral width 25 kHz, total acquisition time 9.2 ms) in t_1; recycle delay of 2 s for a total experiment time of 2.2 h. Acquisition parameters for NCO: $\tau_1 = \tau_2 = 11.2$ ms, 4 scans per t_1 increment; 1024 complex points with a dwell of 40 μs (spectral width 25 kHz, total acquisition time 40.96 ms) in t_2; 128 complex points with a dwell of 160 μs (spectral width 6.25 kHz, total acquisition time 20.48 ms) in t_1. Recycle delay: 4 s; total experiment time: 1.2 h.

Acquisition parameters for NCA: $\tau_1 = 9.6$ ms, $\tau_2 = 12.8$ ms; 16 scans per t_1 increment, 1024 complex points with a dwell of 40 μs (spectral width 25 kHz, total acquisition time 40.96 ms) in t_2; 119 complex points with a dwell of 160 μs (spectral width 6.25 kHz, total acquisition time 19.04 ms) in t_1. Recycle delay: 4 s; total experiment time: 4.5 h. All three spectra were zero-filled to 2048 points it t_2 and 512 points in t_1 and processed with 10 Hz line broadening in the directly detected t_2 dimension, and no apodization in the indirect t_1 dimension.

3.3.2 Modulation of Spin Dynamic

For most residues, the NCA correlation peaks have the opposite sign as that for glycine. This is due to an additional modulation of the of the CA coherence by CB spins during the second τ - π - τ mixing period. Indeed, in the choice of the mixing times in these experiments, one must consider the number of active and passive couplings present along the protein backbone. Typical couplings along the backbone are illustrated in Figure 3.3.

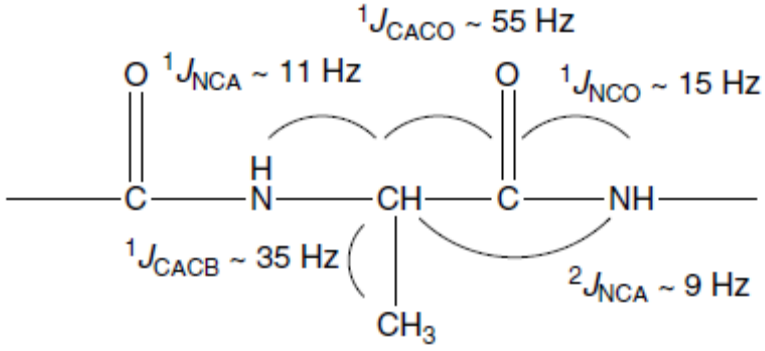

Figure 3.3 Homonuclear and heteronuclear spin coupling networks along the protein backbone.[40]

In general, the spin dynamics follows a straightforward response, with the efficiency of transfer during a single τ - π - τ period exhibiting a sinusoidal dependence determined by the coupling for the desired transfer through the active coupling and a cosinusoidal dependence for each additional (and typically unwanted) passive coupling:

$$S_{12} = \exp(-2\tau / T_2^{'}) \sin(2\pi J_{12}\tau) \prod_{n_1} \cos(2\pi J_{1n_1}\tau) \quad (3.1)$$

Here, S_{12} is the efficiency for transverse magnetization beginning on spin 1 (e.g. I_{1x}) to become anti-phase magnetization through the active coupling with spin 2 (e.g. $I_{1y}S_{2z}$), while also being passively coupled to as many as n1 additional spins. This same expression is valid for the reverse process as well, in which the anti-phase magnetization on spin 1 rephases, but we note that in general $S12 \neq S21$ and that the overall theoretical transfer efficiency for the entire sequence is the product over both mixing steps. As the passive spins often lead to a lower than ideal transfer efficiency, they are removed by selective pulses whenever possible. This is, of course, practical only when good frequency discrimination is present, such as between CO and CA, but usually not between CA and CB, and certainly not for distinguishing the 1- and 2-bond NCA couplings. In Figure 3.4, we have mapped out the modulation of the $t_1 = 0$ spectrum for the J-MAS CACO, NCO, and NCA as a function of the τ values in Figure 3.1 and compare them with the expected response from Eqn. 3.1.

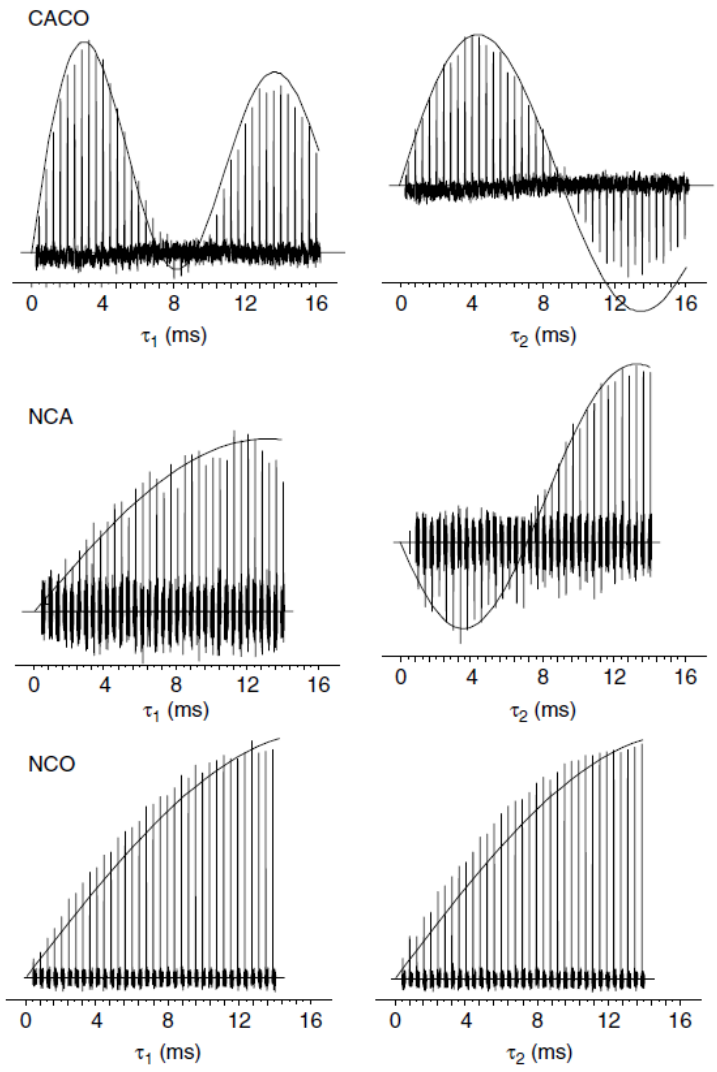

Figure 3.4 The $t_1 = 0$ spectrum in the *J*-MAS experiments modulated by the homomuclear and heteronuclear couplings as a function of the two τ values in the CACO, NCA, and NCO experiments from Figure 3.1. Data points are shown as compressed spectra, while the solid curves represent the theoretically expected response based on Eqn. 3.1 and the spin coupling networks in Figure 3.3. Specifically, for

CACO: $S(I_x^{CA} \rightarrow I_y^{CA} I_z^{CO}) = \exp(-2\tau_1 / T_{2,CA}^{'}) \sin(2\pi J_{CACO} \tau_1) \cos(2\pi J_{CACB} \tau_1)$, and

$S(I_z^{CA} I_y^{CO} \rightarrow I_y^{CO}) = \exp(-2\tau_2 / T_{2,CO}^{'}) \sin(2\pi J_{CACO} \tau_2)$. For NCA:

$S(I_x^{N} \rightarrow I_y^{N} I_z^{CA}) = \exp(-2\tau_1 / T_{2,N}^{'}) \sin(2\pi {}^1J_{NCA} \tau_1) \cos(2\pi {}^2J_{NCA} \tau_1)$, and

$S(I_z^{N} I_x^{CA} \rightarrow I_y^{CA}) = \exp(-2\tau_2 / T_{2,CA}^{'}) \sin(2\pi {}^1J_{NCA} \tau_2) \cos(2\pi {}^2J_{NCA} \tau_2) \cos(2\pi J_{CACB} \tau_2)$. For NCO: $S(I_x^{N} \rightarrow I_y^{N} I_z^{CO}) = \exp(-2\tau_1 / T_{2,N}^{'}) \sin(2\pi J_{NCO} \tau_1)$, and

$S(I_z^{N} I_x^{CO} \rightarrow I_y^{CO}) = \exp(-2\tau_2 / T_{2,CO}^{'}) \sin(2\pi J_{NCO} \tau_2)$

3.3.3 Practical Aspects of Experiments

First, the z-filter element is important in terms of maintaining the pure absorption phase of the lines for the CACO experiments. Emsley's group has recently reviewed several methods for implementing z-filters in solids.[41] In general, this period must be long enough to dephase transverse coherences, but short enough to minimize spin diffusion. We find that by decreasing the decoupling to 80–100 kHz and using relatively long delays we can mitigate spin diffusion while efficiently dephasing the transverse components. It may be possible to decrease this delay somewhat by using rotary resonance fields on the ^{1}H channel, as others have found for fast (~40 kHz) MAS conditions.[42] The situation is easier for the NCA and NCO experiments, as a final $\pi/2$ purge pulse on the nitrogen channel could be implemented prior to acquisition to transfer any remaining anti-phase terms into unobservable multiple quantum coherence. Given the small size of the NC coupling, however, line shape distortions due to the antiphase dispersive terms were not observed and this pulse was omitted.

Second, how well these experiments work depends strongly on the echo lifetimes (often denoted as $T_2^{'}$). The GB1 experiments were carried out under the 25 kHz MAS and 150 kHz proton decoupling, conditions in which $T_2^{'}$ is maximized[43] and residual dipolar couplings suppressed. Under these conditions, we find strong backbone correlations

consistently throughout the spectra, with transfer efficiencies of 65% for CACO, 71% for NCO, and 25% for NCA, making them comparable to dipolar-driven correlations using SPECIFIC-CP14,[45] (for NC transfers) and DARR[46, 47] (for CC spin diffusion transfers). The NCA transfer is less efficient because of the smaller scalar coupling and more rapid dephasing. For comparison, we have summarized in Table 3.1 values for T_2' over a range of MAS rates and proton decoupling powers for GB1 at 9.4 T. Although we acquired the GB1 data under 25 kHz MAS and 150 kHz proton decoupling, there are a number of experimental conditions with reduced MAS rates and decoupling powers in which the relaxation rates are still quite favorable. For example, 18 kHz MAS and 125 kHz decoupling (routine for 3.2 mm probes) have very good relaxation properties, essentially the same as the 25 kHz MAS and 150 kHz decoupling we used, while 9 kHz MAS and 100 kHz decoupling (routine for 4 mm probes) is still quite respectable. Indeed, under more routine experimental conditions, such as 14.7 kHz MAS and 90 kHz decoupling used for TRX in Figure 3.5, we find that sensitivity of the 2D experiments is nevertheless adequate for acquisition of high-quality spectra, although the efficiency has fallen to 20% for CACO, 24% for NCO, and 8% for NCA. More importantly, even under these moderate decoupling conditions the resolution is significantly improved by the elimination of the heteronuclear and homonuclear couplings. Table 3.2 summarizes the T_2' values for TRX under these experimental conditions.

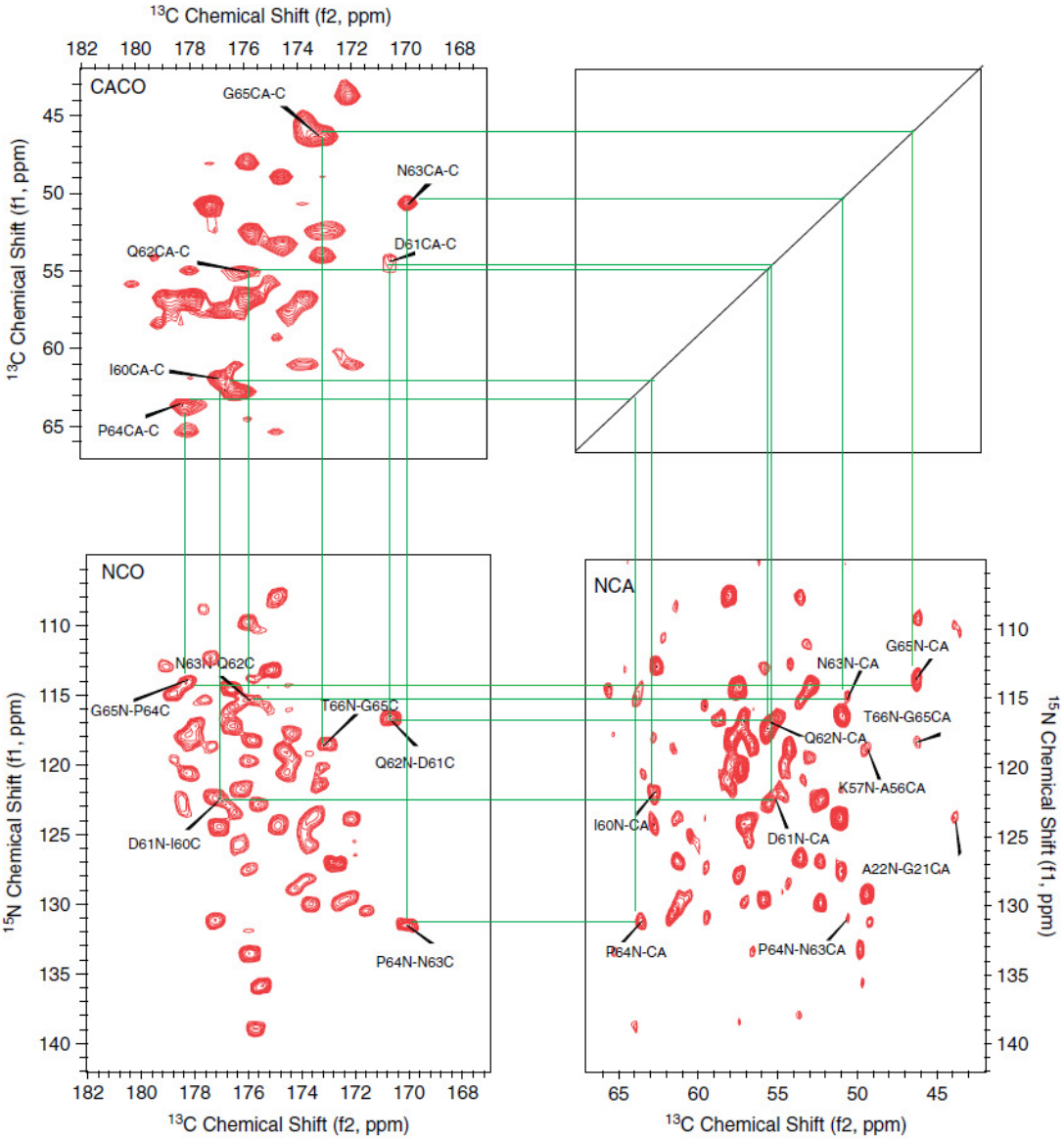

Figure 3.5 J-MAS CACO, NCO, and NCA experiments for TRX at 14.1 T, illustrating the backbone assignments. Experiment-specific parameters for CACO: τ_1 = 5.1 ms; τ_2 =

2.9 ms; 32 scans per t_1 increment; 1111 complex points with a dwell of 18 μs (spectral width 55.555 kHz, total acquisition time 20 ms) in t_2; 339 real points with a dwell of 15 μs (spectral width 33.333 kHz, total acquisition time 10.2 ms) in t_1; recycle delay of 2 s for a total experiment time of 6.1 h. Acquisition parameters for NCO: $\tau_1 = \tau_2 = 12$ ms, 146 scans per t_1 increment; 833 complex points with a dwell of 18 μs (spectral width 55.555 kHz, total acquisition time 15 ms) in t_2; 175 real points with a dwell of 68 μs (spectral width 7.353 kHz, total acquisition time 11.9 ms) in t_1. Recycle delay: 2 s; total experiment time: 14.4 h. Acquisition parameters for NCA: $\tau_1 = 12.2$ ms, $\tau_2 = 2.0$ ms; 230 scans per t_1 increment, 833 complex points with a dwell of 18 μs (spectral width 55.555 kHz, total acquisition time 15 ms) in t_2; 179 real points with a dwell of 68 μs (spectral width 7.353 kHz, total acquisition time 12.2 ms) in t_1. Recycle delay: 2 s; total experiment time: 23.2 h. All three spectra were zero-filled to 2048 points in both dimensions and processed with 60° shifted sinebell in both dimensions, and mirror-image linear prediction in the t_1 dimension.

Table 3.1 $T_2^{'}$ (ms) for GB1 at 9.4 T

	MAS 9 kHz			MAS 18 kHz			MAS 25 kHz		
^{1}H Dec. (kHz)	N	CO	CA	N	CO	CA	N	CO	CA
75	29	22	13	28	30	9	24	28	8
100	55	33	20	68	62	25	43	44	16
125	51	36	21	96	69	33	90	83	32
150	76	40	22	101	84	30	104	96	36

Table 3.2 $T_2^{'}$ (ms) for TRX at 14.1 T

	MAS 14.7 kHz		
^{1}H Dec. (kHz)	N	CO	CA
70	23	14	6
80	35	16	7
90	33	17	7
100	32	17	7

3.3.4 IPAP Selection

Although the resolution in the NCO and CACO experiments is high enough to observe nearly all the expected correlations for GB1 and TRX, increased resolution would allow these experiments to be effective on even larger proteins. Several methods have now been demonstrated in solids for increasing resolution in the directly observed dimension. Following the previous study by Emsley and Bertini,[52] we have implemented the IPAP method for NCO and CACO correlation using the pulse sequences shown in Figure 3.6. In the IPAP experiments, both in-phase and anti-phase spectra are separately acquired in the direct dimension, and then added together to choose one of the major doublet components. As the large (355 Hz) CACO coupling is nearly resolved when observing final magnetization on CO in both the CACO and NCO 2D experiments, this coupling is a natural choice to use in the IPAP protocol. For the anti-phase CACO sequence shown in Figure 3.6, the anti-phase absorptive cross-peak is accompanied by an in-phase dispersive diagonal. The diagonal peak can be removed using soft $\pi/2$ pulses on CO to form a selective z-filter.[52] In practice, we found this to be unnecessary, as the diagonal is so far removed from the spectral region of interest that it produces no detectable interference in CACO correlation. For the NCO sequence, residual in-phase components on CO could contribute to the final cross-peak signal if the timings are not properly set. We did not find this to be a significant problem, however, perhaps due to the

uniformity of J_{CACO} couplings in most proteins. If it were found to be a problem, a z-filter could again be constructed to remove the in-phase (dispersive) component using selective $\pi/2$ pulses on the CO channel. Figure 3.7 illustrates the IPAP procedure for GB1, showing both the IPAP 2D spectra and the resulting IPAP combination.

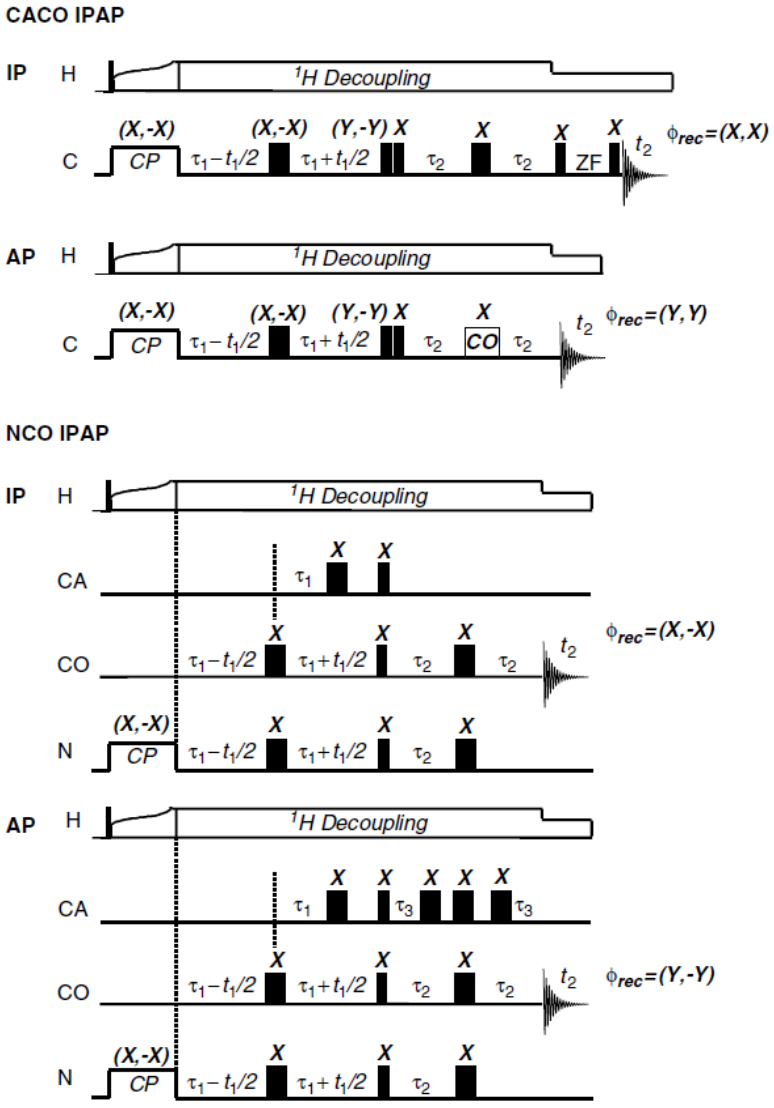

Figure 3.6 In-phase (IP) and anti-phase (AP) constant-time J-MAS CACO and NCO 2D correlation experiments. In these pulse sequences, thin vertical lines indicate π/2 pulses and wide vertical lines indicate π pulses that are either selective (single carbon channel) or broadbanded (shown as simultaneous CA and CO pulses). The indirect evolution increments, π refocusing periods, and z-filter (zf) are all rotor-synchronized.

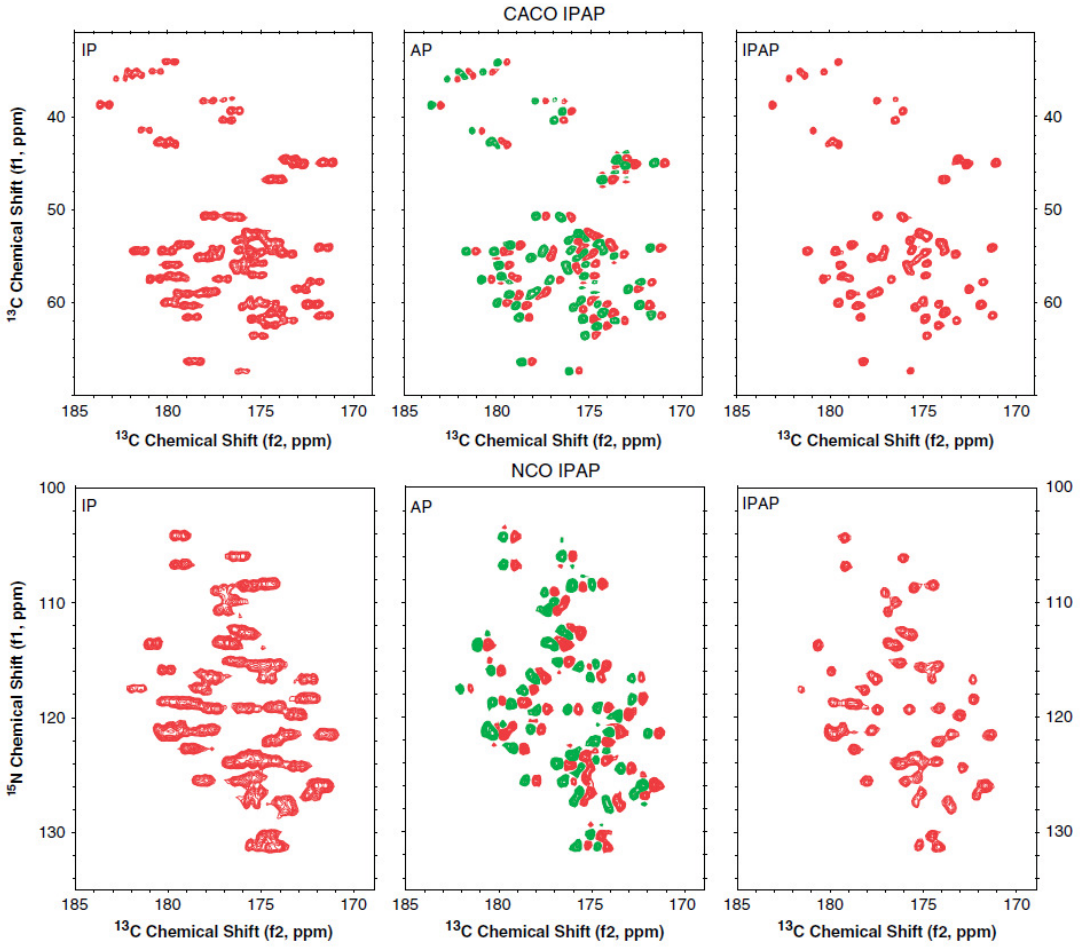

Figure 3.7 IPAP combinations for the J-MAS CACO and NCO experiments for GB1 at 9.4 T. Experimental acquisition and processing parameters are identical to those in Figure 3.2, with the addition of τ = 3.2 ms for the NCO AP correlation.

3.3.5 Spin-State-Selection

As described above, IPAP selection needs acquire in-phase and anti-phase spectra separately and then add them together to choose one of the major doublet components, which means one has to perform at least 2 scans to achieve the goal.

We've been trying to incorporate the idea of spin state selection[48-51] to select one of the doublet in just one scan and achieve twice the sensitivity. Work in this direction is in progress.

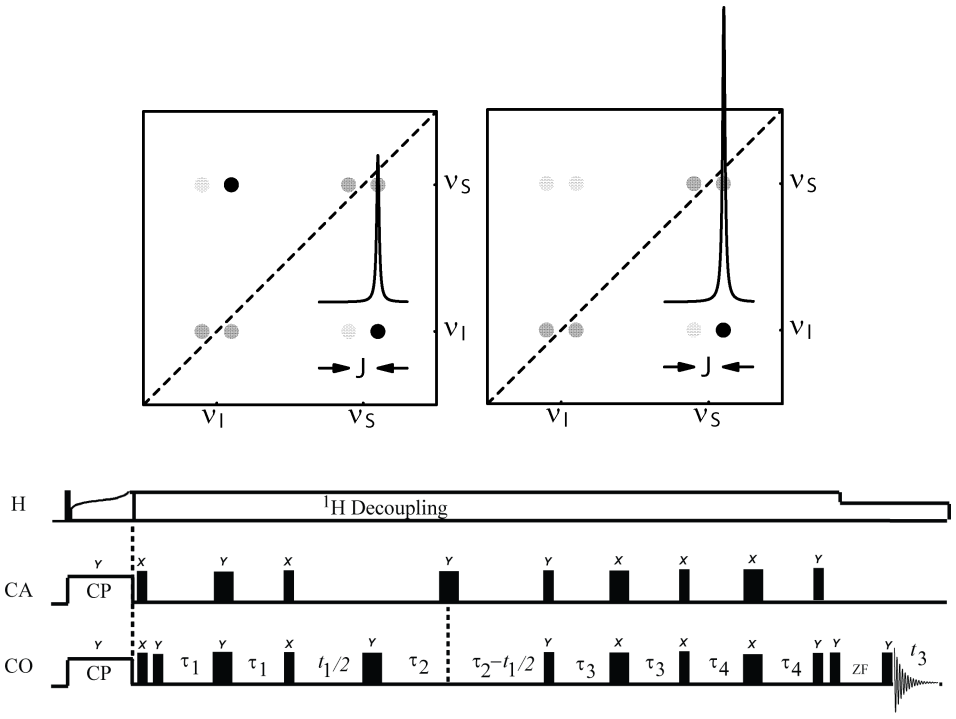

Figure 3.8 Pulse sequence and modulation spectrum for CTUCCOSY combined with Spin-state-selection

3.4 CONCLUSIONS

Despite being orders-of-magnitude smaller than the dipolar interaction, scalar couplings provide a robust and efficient mechanism for coherence exchange and correlation spectroscopy in solid-state proteins. Together, the two dimensional *J*-MAS CACO, NCO, and NCA correlation experiments form a set that can be used to trace out and assign backbone resonances. These scalar-based constant time experiments exhibit increased resolution through homonuclear and heteronuclear decoupling in the indirect dimension and are compatible with IPAP selection in the direct dimension for further increases in resolution. These results help demonstrate that scalar-based methods are sufficiently well developed to serve as a complementary tool to dipolar methods in solid-state NMR, which should be particularly useful under fast MAS conditions or in the presence of molecular motion, when the sensitivity of dipolar methods is greatly compromised.

REFERENCES

1. Jaroniec, C.P.; MacPhee, C.E.; Bajaj, V.S.; McMahon, M.T.; Dobson, C.M.; Griffin, R.G. *Proc. Natl. Acad. Sci.*, U.S.A., **2004**, *101*, 711.

2. Tycko, R. *Q. Rev. Biophys.*, **2006**, *39*, 1.

3. Tycko, R. *Methods Enzymol.*, **2006**, *413*, 103.

4. Goldbourt, A.; Gross, B.J.; Day, L.A.; McDermott, A.E. *J. Am. Chem. Soc.*, **2007**, *129*, 2338.

5. Paik, Y.; Yang, C.; Metaferia, B.; Tang, S.B.; Bane, S.; Ravindra, R.; Shanker, N.; Alcaraz, A.A.; Johnson, S.A.; Schaefer J. *J. Am. Chem. Soc.*, **2007**, *129*, 361.

6. Baldus, M. *Curr. Opin. Struct. Biol.*, **2006**, *16*, 618.

7. Park, S.H.; Prytulla, S.; De Angelis, A.A.; Brown, J.M.; Kiefe,r H.; Opella, S.J. *J. Am. Chem. Soc.*, **2006**, *128*, 7402.

8. Etzkorn, M.; Martell, S.; Andronesi, O.C.; Seidel, K.; Engelhard, M.; Baldus, M. *Angew. Chem. Int. Ed.*, **2007**, *46*, 459.

9. Kobayashi, M.; Matsuki, Y.; Akutsu, H. J. *Biomol. NMR* , **2006**, *36*, 279.

10. Hong, M. *Structure*, **2006**, *14*, 1731.

11. Frericks, H.L.; Zhou, D.H.; Yap, L.L.; Gennis, R.B.; Rienstra, C.M. *J. Biomol. NMR*, **2006**, *36*, 55.

12. Lange, A.; Giller, K.; Hornig, S.; Martin-Eauclaire, M.F.; Pongs, O.; Becker, S.; Baldus, M. *Nature*, **2006**, *440*, 959.

13. Pauli, J.; Baldus, M.; van Rossum, B.; de Groot, H.; Oschkinat, H. *Chembiochem*, **2001**, *2*, 272.

14. Baldus, M. *Prog. Nucl. Magn. Reson. Spectrosc.*, **2002**, *41*, 1.

15. Igumenova, T.I.; McDermott, A.E.; Zilm, K.W.; Martin, R.W.; Paulson, E.K.; Wand, A.J. *J. Am. Chem. Soc.*, **2004**, *126*, 6720.

16. Franks, W.T.; Zhou, D.H.; Wylie, B.J.; Money, B.G.; Graesser, D.T.; Frericks, H.L.; Sahota, G.; Rienstra, C.M. *J. Am. Chem. Soc.*, **2005**, *127*, 12291.

17. Ernst, M.; Detken, A.; Bockmann, A.; Meier, B.H. *J. Am. Chem. Soc.*, **2003**, *125*, 15807.

18. McDermott, A.E. *Curr. Opin. Struct. Biol.*, **2004**, *14*, 554.

19. Hughes, C.E.; Baldus, M. *Annu. Rep. NMR Spectrosc.*, **2005**, *55*, 121.

20. Baldus, M.; Meier, B.H. *J. Magn. Reson. A*, **1996**, *121*, 65.

21. Hardy, E.H.; Verel, R.; Meier, B.H. *J. Magn. Reson.*, **2001**, *148*, 459.

22. Lesage, A.; Emsley, L. J. *Magn. Reson.* , **2001**, *148*, 449.

23. Lesage, A.; Bardet, M.; Emsley, L. *J. Am. Chem. Soc.*, **1999**, *121*, 10987.

24. Mueller, L.J.; Elliott, D.W.; Leskowitz, G.M.; Struppe, J.; Olsen, R.A.; Kim, K.C.; Reed, C.A. *J. Magn. Reson.*, **2004**, *168*, 327.

25. Elena, B.; Lesage, A.; Steuernagel, S.; Bockmann, A.; Emsley, L. *J. Am. Chem. Soc.*, **2005**, *127*, 17296.

26. Bockmann, A.; Juy, M.; Bettler, E.; Emsley, L.; Galinier, A.; Penin, F.; Lesage, A. J. *Biomol. NMR*, **2005**, *32*, 195.

27. Olsen, R.A.; Struppe, J.; Elliott, D.W.; Thomas, R.J.; Mueller, L.J. *J. Am. Chem. Soc.*, **2003**, *125*, 11784.

28. Chen, L.L.; Olsen, R.A.; Elliott, D.W.; Boettcher, J.M.; Zhou, D.H.; Rienstra C.M.; Mueller, L.J. *J. Am. Chem. Soc.*, **2006**, *128*, 9992.

29. Pintacuda, G.; Giraud, N.; Pierattelli, R.; Bockmann, A.; Bertini, I.; Emsley, L. *Angew. Chem.*, *Int. Ed.*, **2007**, *46*, 1079.

30. Chen, L.; Kaiser, J.M.; Polenova, T.; Yang, J.; Rienstra, C.M.; Mueller, L.J. *J. Am. Chem. Soc.*, **2007**, *129*, 10650.

31. Straus, S.K.; Bremi, T.; Ernst, R.R. *Chem. Phys. Lett.*, **1996**, *262*, 709.

32. Fung, B.M.; Khitrin, A.K.; Ermolaev, K. *J. Magn. Reson.*, **2000**, *142*, 97.

33. Li, Y.; Wylie, B.J.; Rienstra, C.M. *J. Magn. Reson.*, **2006**, *179*, 206.

34. States, D.J.; Haberkorn, R.A.; Ruben, D.J. *J. Magn. Reson.*, **1982**, *48*, 286.

35. Marion, D.; Wuthrich, K. *Biochem. Biophys. Res. Commun.*, **1983**, *113*, 967.

36. Marulanda, D.; Tasayco, M.L.; Cataldi, M.; Arriaran, V.; Polenova, T. *J. Phys. Chem. B*, **2005**, *109*, 18135.

37. Marulanda, D.; Tasayco, M.L.; McDermott, A.; Cataldi, M.; Arriaran, V.; Polenova, T. *J. Am. Chem. Soc.*, **2004**, *126*, 16608.

38. Bertini, I.; Duma, L.; Felli, I.C.; Fey, M.; Luchinat, C.; Pierattelli, R.; Vasos, P.R. *Angew. Chem.*, *Int. Ed.*, **2004**, *43*, 2257.

39. Bermel, W.; Bertini, I.; Felli, I.C.; Kummerle, R.; Pierattelli, R. *J. Magn. Reson.*, **2006**, *178*, 56.

40. Cavanagh, J.; Fairbrother, W.J.; Palmer, A.G. III; Skelton, N.J. *Protein NMR Spectroscopy Principles and Practice.*, Academic Press: San Diego, **1996**.

41. Cadars, S.; Sein, J.; Duma, L.; Lesage, A.; Pham, T.N.; Baltisberger, J.H.; Brown, S.P.; Emsley, L. *J. Magn. Reson.*, **2007**, 188, 24.

42. Zhou, D.H.; Shah, G.; Cormos, M.; Mullen, C.; Sandoz, D.; Rienstra, C.M. *J. Am. Chem. Soc.*, **2007**, *129*, 11791.

43. De Paepe, G.; Lesage, A.; Emsley, L. *J. Chem. Phys.*, **2003**, *119*, 4833.

44. Fayon, F.; Massiot, D.; Levitt, M.H.; Titman, J.J.; Gregory, D.H.; Duma, L.; Emsley, L.; Brown, S.P. *J. Chem. Phys.*, **2005**, *122*, 194313/1.

45. Baldus, M.; Petkova, A.T.; Herzfeld, J.; Griffin, R.G. *Mol. Phys.*, **1998**, *95*, 1197.

46. Takegoshi, K.; Nakamura, S.; Terao, T. *Chem. Phys. Lett.*, **2001**, *344*, 631.

47. Morcombe, C.R.; Gaponenko, V.; Byrd, R.A.; Zilm, K.W. *J. Am. Chem. Soc.*, **2004**, *126*, 7196.

48. Verel, R.; van Beek, J.D.; Meier, B.H. *J. Magn. Reson.*, **1999**, *140*, 300.

49. Duma, L.; Hediger, S.; Lesage, A.; Emsley, L. *J. Magn. Reson.*, **2003**, *164*, 187.

50. Duma, L.; Hediger, S.; Brutscher, B.; Bockmann, A.; Emsley, L. *J. Am. Chem. Soc.*, **2003**, *125*, 11816.

51. Verel, R.; Manolikas, T.; Siemer, A.B.; Meier, B.H. *J. Magn. Reson.*, **2007**, *184*, 322.

52. Bermel, W.; Bertini, I.; Duma, L.; Felli, I.C.; Emsley, L.; Pierattelli, R.; Vasos, P.R. *Angew. Chem., Int. Ed.*, **2005**, *44*, 3089.

53. Duma L., Hediger S. and Emsley L., *Journal of Magnetic Resonance*, **2003**, *164*, 187-195.

CHAPTER IV

J-BASED 3D HETERONUCLEAR CORRELATION SPECTROSCOPY

ABSTRACT:

3D NCACO, NCOCA, and CANCO scalar-coupling driven correlation experiments are presented for protein backbone assignments in the solid-state. These *J*-MAS experiments show superior resolution in the indirect dimensions through the elimination of heteronuclear and homonuclear couplings and enhanced sensitivity, which allow us to trace out the entire protein backbone for GB1. The results demonstrate that scalar-based methods are sufficiently well-developed to serve as a complementary tool to dipolar methods, which will be especially useful for assignment of large proteins, where resonance overlap presents a major challenge to solid-state NMR.

4.1 INTRODUCTION

Solid-state NMR spectroscopy is emerging as a mainstream tool in structural biology due to its unique capability to yield atomic-level information in macroscopically

disordered systems, such as fibrils[1,2] , macromolecular assemblies,[3-5] and membrane proteins.[6-11] Resonance assignments are an essential first step of structural studies, and in all studies to date, these have employed through-space, dipolar-driven correlation spectroscopy.[12, 13] Scalar-coupling driven correlation in solids has been reported by several groups,[14-20] including the through-bond homonuclear ^{13}C-^{13}C and heteronuclear ^{13}C- ^{15}N correlation spectroscopy illustrated in chapter III which can be implemented in a highly efficient manner for the assignment of protein resonances with solid-state NMR.[21] In this chapter, heteronuclear 3D correlation experiments will be introduced, which can similarly be implemented using purely scalar-based transfers for the assignment of backbone resonances. One of the 3D experiments, NCOCA in GB1, is shown in Figure 4.1. Again substantially increased spectral resolution was found without compromising sensitivity, which is comparable to, or better than, that of dipolar methods. The approach was illustrated on two proteins, the β1 immunoglobulin binding domain of protein G (GB1) and reassembled thioredoxin (TRX).

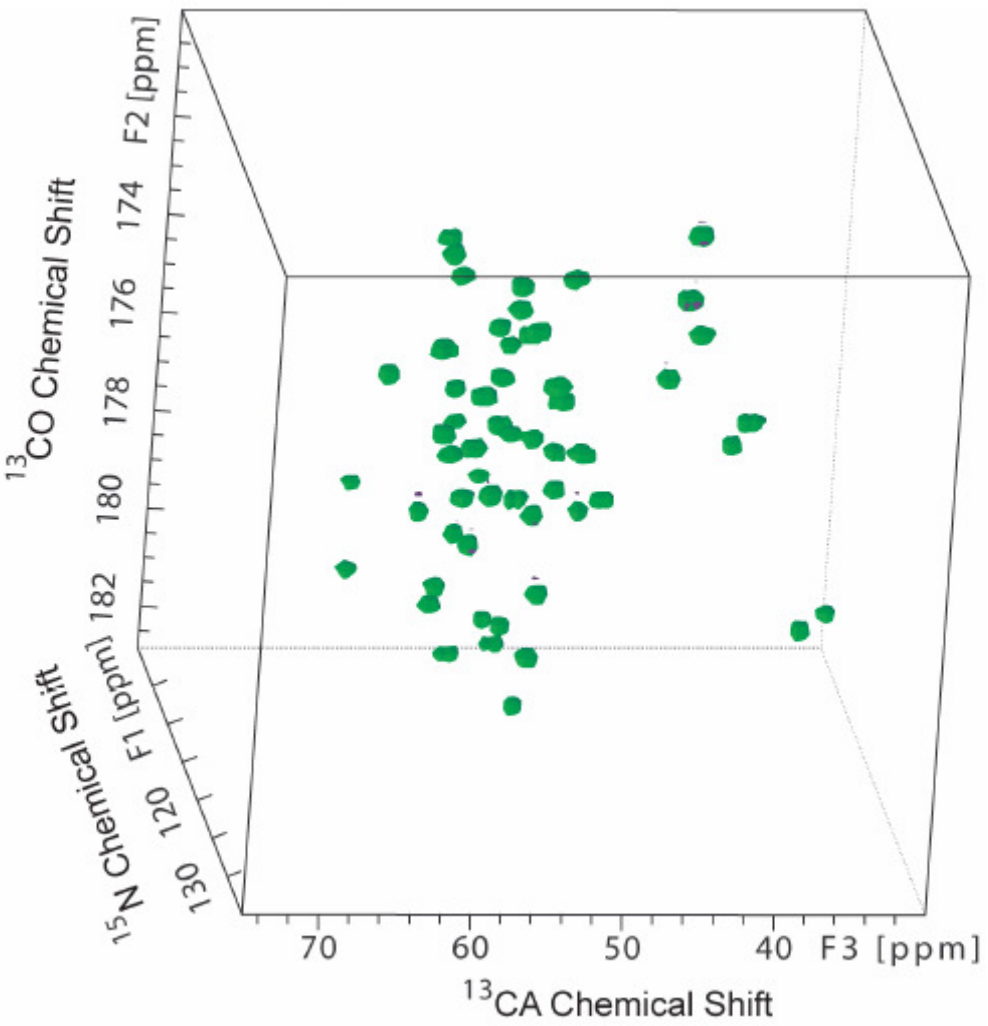

Figure 4.1 3D NCOCA experiments on GB1

4.2 EXPERIMENTAL

4.2.1 Complete Phase Cycles and Off-Resonance Compensation for 3D J-MAS Experiments

The approach makes use of the 3D *J*-based MAS experiments shown in Figure 4.2. These experiments are inspired by their solution-state counterparts, particularly as implemented by Bertini and co-workers.[22, 23] In the MAS versions, the indirect evolution periods are rotor synchronized along with the τ refocusing periods. As in liquid-state, the combined constant-time evolution and mixing period improves resolution through homonuclear and heteronucler decoupling in the indirect dimension, giving increased sensitivity when the scalar couplings are partially or fully resolved.

(a) J-MAS NCACO (and NCOCA)

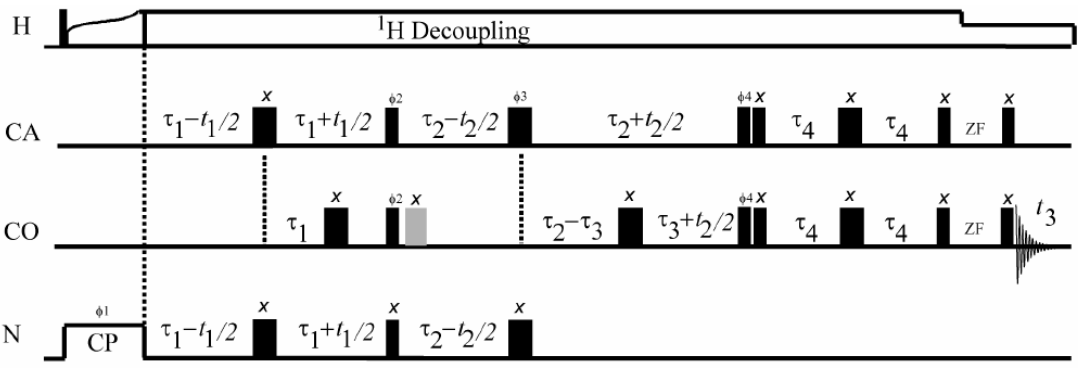

Phase	Cycle
ϕ_1	0, 2
ϕ_2	0, 0, 2, 2
ϕ_3	0, 0, 2, 2
ϕ_4	1, 1, 3, 3
ϕ_{rec}	0, 2, 0, 2

(b) J-MAS CANCO

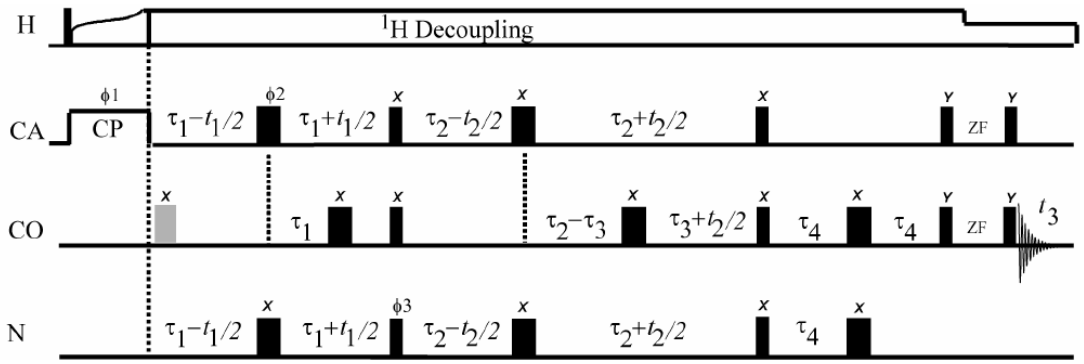

Phase	Cycle
ϕ_1	0
ϕ_2	0, 1, 2, 3
ϕ_3	0
ϕ_{rec}	0, 2, 0, 2

Figure 4.2 Constant-time *J*-MAS NCACO, NCOCA, and CANCO 3D heteronuclear correlation experiments.

In these pulse sequences, thin vertical lines indicate π/2 pulses and wide vertical lines indicate π pulses that are either selective (single carbon channel) or broad-banded (shown as simultaneous CA and CO pulses). The NCOCA experiment is obtained by flipping the CA and CO channels shown in part (a). The indirect evolution increments, τ refocusing periods, and z-filter (zf) are all rotor synchronized.

Although we did not find off-resonance effects to be significant under our experimental conditions, they could in general lead to phase errors in the indirect dimensions. In such cases, an additional π pulse on the passive spin (shown as the grey, shaded pulse) can be incorporated to refocus off-resonance effects.

A minimal phase cycle is needed. The ^{15}N spin lock is cycled for +/- 1 and the three ^{13}C pulses (φ2, φ3, φ4) are independently phase cycled together for zero and double quantum selection. In the table below the phase of the rf is given as integer multiples of 90 ° (i.e., 0 = "x", 1 = "y", 2 = "-x", 3= "-y") and the list repeats once the end of the line has been reached. 3D pure phase spectra are obtained using the method of States[8] by incrementing φ1 by 90°and φ2 by 90° for t_1 and t_2, respectively.

4.2.2 Applications

Figure 4.3 shows the application of the *J*-MAS NCOCA, NCACO, and CANCO to uniformly-^{13}C, ^{15}N-enriched GB1. This combination of experiments allows an

unambiguous assignment of the full protein backbone, one part of which is traced out in the figure. As in solution, both one- and two-bond correlations are observed in the NCA transfers, with the one-bond transfer being more intense. Under 25 kHz magic angle spinning (MAS) and 150 kHz proton decoupling (conditions where T_2' is maximized[25] and residual dipolar couplings suppressed[26]), we find strong backbone correlations consistently throughout the spectra, with sensitivity comparable to dipolar-driven correlation using SPECIFIC CP (for NC transfers) and DARR (for CC spin diffusion transfers), albeit at necessarily lower MAS rates. Most dramatically, we find significantly improved resolution, with a reduction in line widths in the indirect dimension to 30-40 Hz for both carbon and nitrogen. Even under more routine experimental conditions, such as 14.7 kHz MAS and 90 kHz decoupling used for TRX and GB1 in Figures 4.5 and 4.6, we find that sensitivity of the 3D experiments is nevertheless adequate for acquisition of high-quality spectra. More importantly, even under these moderate decoupling conditions the resolution is significantly improved compared with the dipolar experiments by the elimination of the heteronuclear and homonuclear couplings.

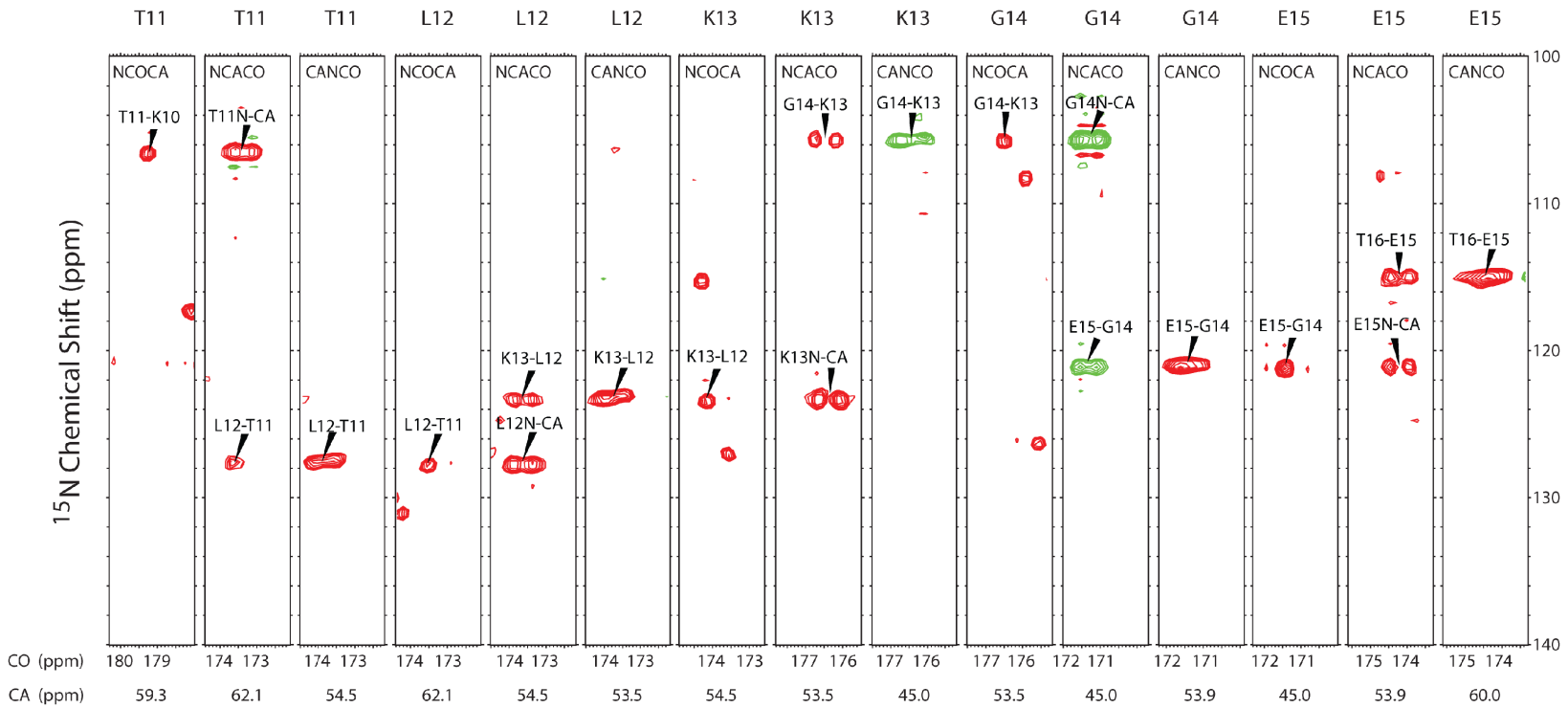

Figure 4.3 The backbone walk in uniformly-^{13}C,^{15}N-enriched GB1[30] using the *J*-MAS NCACO, NCOCA, and CANCO experiments

Data were acquired on a 9.4 T Bruker DSX spectrometer (^{1}H frequency 400.13 MHz) equipped with a triple resonance 2.5 mm MAS probe spinning at a MAS rate of 25 kHz. 80 kHz ^{13}C and 50 kHz ^{15}N pulses were used throughout for the hard pulses along with 150 kHz SPINAL64 ^{1}H decoupling[27, 28] during the constant-time intervals and 100 kHz decupling during the 16 ms z-filter and acquisition (t_3). r-SNOB pulses of 180 and 420 μs were used for the selective $\pi/2$- and carbonyl-π pulses, respectively, and were rotor synchronized as described in ref 29. In all experiments, the carbon carrier was centered in the C^α region and the selective carbonyl pulses were implemented using a phase modulation. Experiment specific parameters for NCACO: τ_1 = 9.6 ms, τ_2 = 12.8 ms, τ_3 = τ_4 = 4.4 ms; 4 scans, 1024 complex points in t_3 (total acquisition time 34.1 ms), 128 complex points in t_2 (total acquisition time 20.48 ms), and 38 complex points in t_1 (total acquisition time 18.24 ms); recycle delay of 3 s for a total experiment time of 65 h. Acquisition parameters for NCOCA: τ_1 = τ_2 = 11.2 ms, τ_3 = 5.2 ms, and τ_4 = 3.2 ms; 4 scans, 512 complex points in t_3 (total acquisition time 20.5 ms), 45 complex points in t_2 (total acquisition time 21.6 ms), and 45 complex points in t_1 (total acquisition time 21.6 ms). Recycle delay, 4 s; total experiment time, 36 h. Acquisition parameters for CANCO: τ_1 = 12.8 ms, τ_2 = τ_3 = 13.2 ms, and τ_4 = 11.6 ms; 2 scans, 1024 complex points in t_3 (total acquisition time 17.1 ms), 38 complex points in t_2 (total acquisition time 18.24 ms), and 128 complex points in t_1 (total acquisition time 20.48 ms). Recycle delay. 4 s; total

experiment time. 45 h. All three spectra were processed with 10 Hz line broadening in the directly detected t_3 dimension and no apodization in the indirect t_1 and t_2 dimensions.

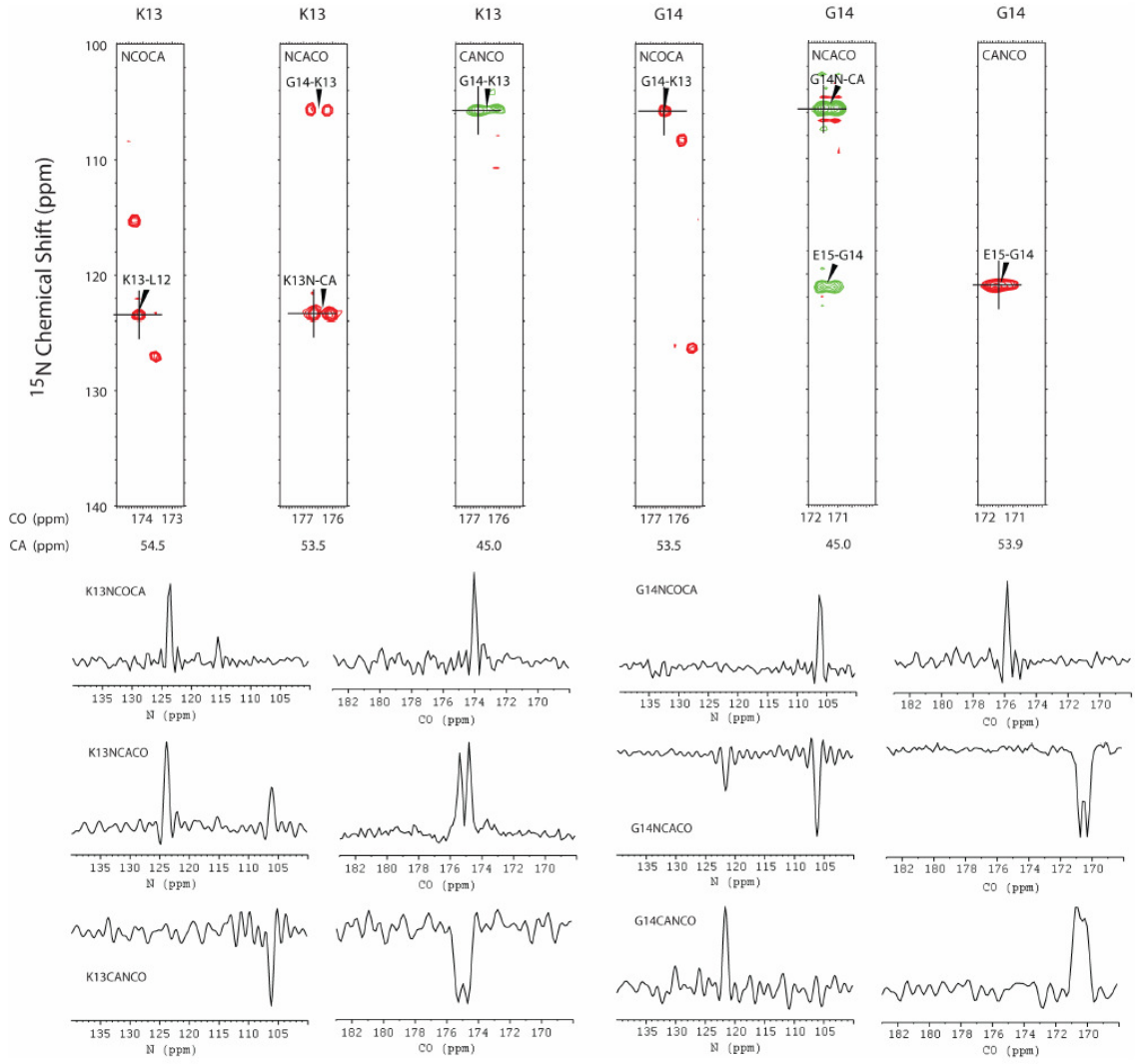

Figure 4.4 1D slices are shown for several of the strip plots from Figure 4.2.

The majority of these slices show signal-to-noise ratios over 20:1. Taking 4:1 as the limit where it is still possible to consistently discriminate peaks from noise, we anticipate that assigning proteins up to 5 times larger than the 6 kDa GB1 should be feasible even at

9.4 T, while moving to higher field will extend this even further. In practice, the upper end of this range may require additional signal averaging, but should still be accessible within reasonable experimental times.

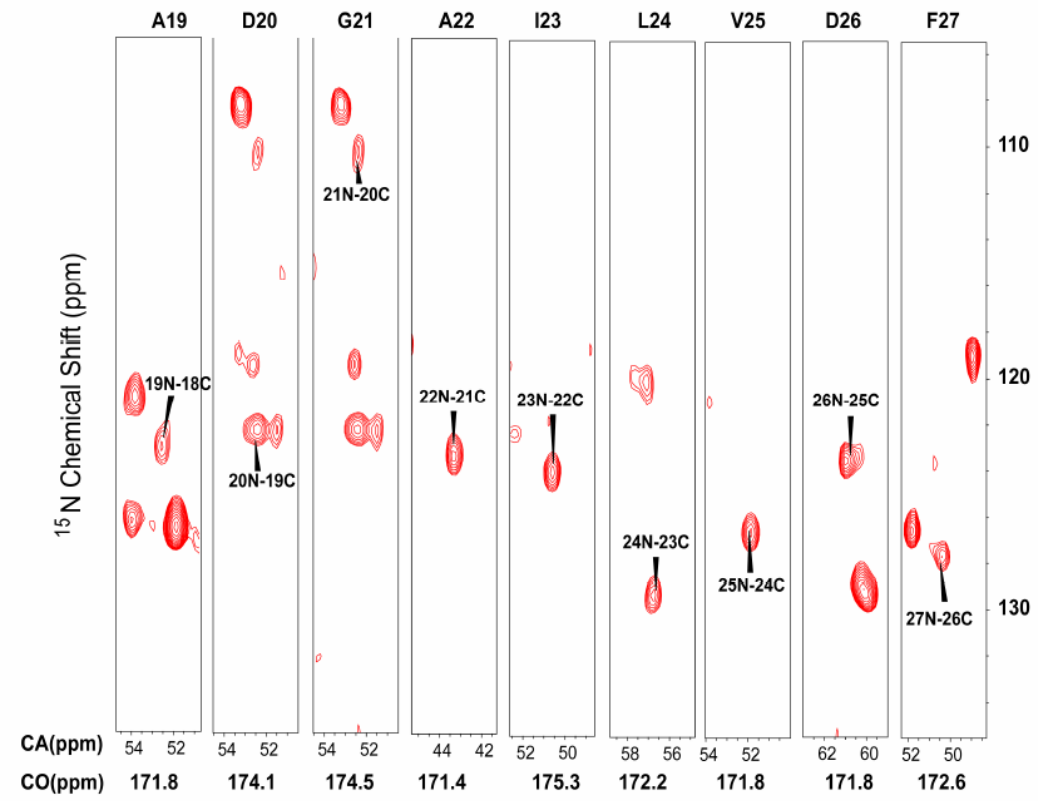

Figure 4.5 Strip plot of the 3D NCOCA spectrum of reassembled thioredoxin.

The spectra were acquired at 14.1 T on a Varian InfinityPlus spectrometer outfitted with the triple-resonance 3.2 mm T3 probe. Acquisition parameters: 128 scans, 833 complex points in t_3 (total acquisition time 16 ms), 40 real points in t_1 and t_2 (total acquisition time 11.9 ms). Recycle delay: 2 s; total experiment time: 5 days. Phase

sensitive detection in t_1 and t_2 using TPPI. MAS frequency of 14.705 kHz. 90, 83 and 50 kHz ^{1}H TPPM decoupling was employed during the *J*-evolution, the acquisition and the z-filter periods, respectively. $\tau_1 = \tau_2 = 11.5$ ms; $\tau_3 = \tau_4 = 2.7$ ms. 170 and 374 μs selective r-SNOB pulses were used for the carbonyl and aliphatic regions, respectively. The spectra were processed with cosine apodization in t_1 and t_3 dimension, and with 60-degree shifted sinebell apodization in t_2 dimension; linear prediction to twice the number of points was applied in the t_1 and t_2 dimensions.

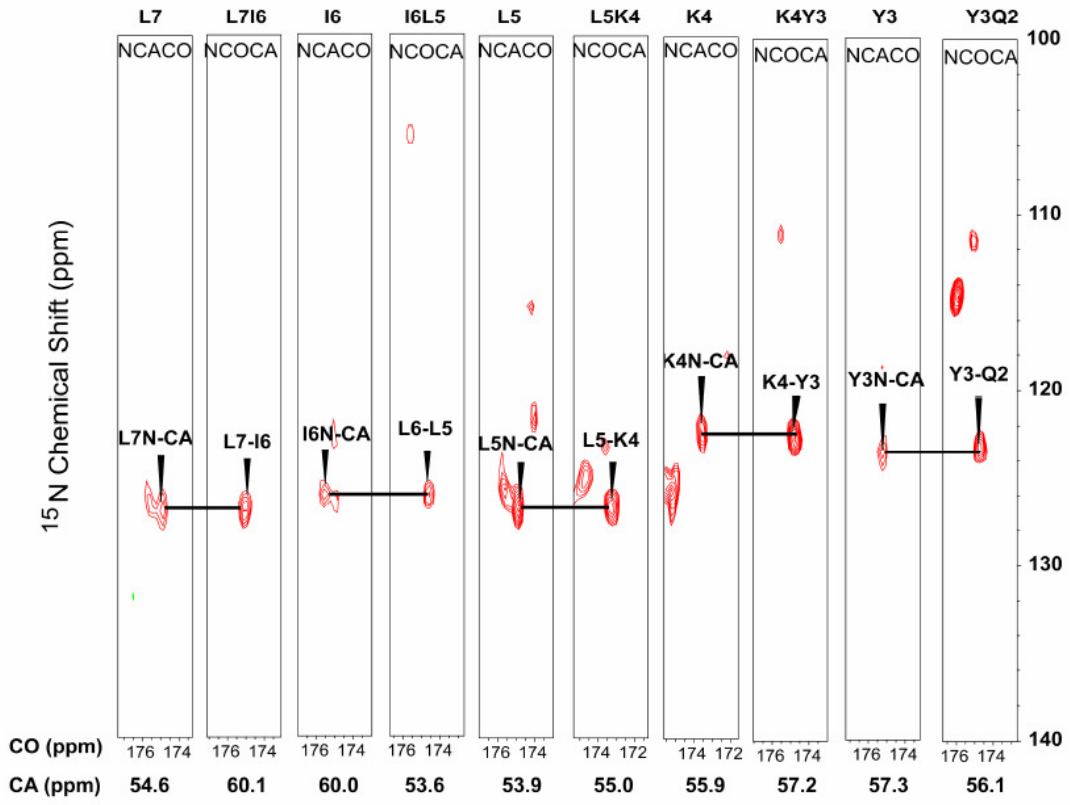

Figure 4.6 Strip plot of the 3D NCOCA and NCACO spectra of GB1.

The spectra were acquired at 14.1 T on a Varian InfinityPlus spectrometer outfitted with the tripleresonance 3.2 mm T3 probe. Acquisition parameters (NCACO): 172 scans, 833 complex points in t_3 (total acquisition time 16 ms), 25 and 19 real points in t_1 and t_2 respectively (total acquisition time in t_1 and t_2 3.4 and 1.48 ms respectively). Recycle delay: 2 s; total experiment time: 45.3 hours. Acquisition parameters (NCOCA): 48 scans, 833 complex points in t_3 (total acquisition time 16 ms), 38 real points in t_1 and t_2 (total acquisition time in t_1 and t_2 5.2 ms). Recycle delay: 2 s; total experiment time: 40.3hours. The following parameters apply to both experiments. Phase sensitive detection in t_1 and t_2 using TPPI. MAS frequency of 14.705 kHz. 90, 83 and 50 kHz 1H TPPM decoupling was employed during the *J*-evolution, the acquisition and the z-filter periods, respectively. For NCOCA, $\tau_1 = \tau_2 = 11.5$ ms; $\tau_3 = \tau_4 = 2.7$ ms. For NCACO, $\tau_1 = 11.2$ ms; $\tau_2 = 4.4$ ms; $\tau_3 = \tau_4 = 2.7$ ms. For NCOCA, 170 and 374 μs selective rSNOB pulses were used for the carbonyl and aliphatic regions, respectively. For NCACO, 442 and 374 μs selective r-SNOB pulses were used for the carbonyl and aliphatic regions, respectively. The spectra were processed with cosine apodization in t_1 and t_3 dimension, and with 60-degree shifted sinebell apodization in t_2 dimension; linear prediction to twice the number of points was applied in the t_1 and t_2 dimensions.

4.3 T_2' VS. MAS RATE AND DECOUPLING POWER

How well the *J*-MAS experiments work depends strongly on relaxation rates during the echo transfer periods (often denoted T_2'). T_2' values were measured over a range of MAS rates and proton decoupling powers for GB1 at 9.4 T using a simple τ - π (selective) - τ dephasing period, and were summarized in Table 4.1. The echo intensity fall-off was then fit to an exponential decay in τ (typically using 6-7 time points). In each case, SPINAL 64 decoupling was used and optimized for maximum T_2' on the alpha carbon and then used without further optimization for the carbonyl and nitrogen decays. 3.2 msec and 420 μsec r-SNOB pulses were used for the selective alpha and carbonyl pulses, respectively. The 3.2 msec alpha pulse was found to be necessary to provide consistent echo line shapes without distortion from beta couplings. In all cases, it is not the echo decay rates for individual sites measured, but rather it is an average rate for the spectral window. There are a number of experimental conditions with reduced MAS rates and decoupling powers where the relaxation rates are still quite favorable. For example, 18 kHz MAS and 125 kHz decoupling (routine for 3.2 mm probes) has very good relaxation properties, essentially the same as the 25 kHz MAS and 150 kHz decoupling we used, while 9 kHz MAS and 100 kHz decoupling (routine for 4 mm probes) is still quite respectable.

Table 4.1 T_2' vs. MAS Rate and Decoupling Power

T_2' (ms) at MAS 9 kHz

^1H Dec.	N	CO	CA
75	29	22	13
100	55	33	20
125	51	36	21
150	76	40	22

T_2' (ms) at MAS 18 kHz

^1H Dec.	N	CO	CA
75	28	30	9
100	68	62	25
125	96	69	33
150	101	84	30

T_2' (ms) at MAS 25 kHz

^1H Dec.	N	CO	CA
75	24	28	8
100	43	44	16
125	90	83	32
150	104	96	36

4.4 CONCLUSION

On the basis of the experimentally measured T_2' relaxation rates of 104 ms for backbone ^{15}N, 96 ms for ^{13}CO, and 36 ms for ^{13}CA, we estimate theoretically that over half of the intensity loss in these experiments is still due to relaxation at our experimental conditions of 25 kHz MAS and 150 kHz ^{1}H decoupling. Yet these experiments are competitive with dipolar methods in terms of overall sensitivity, and at even faster MAS rates and/or with deuteration[27, 28] (where more efficient decoupling becomes possible at lower power), we anticipate further improvements in both sensitivity and resolution. We note that dipolar and scalar experiments offer complementary information; homonuclear dipolar mixing conditions can be adjusted to yield additional sequential correlations to validate the resonance assignments, while certain cross-peaks that are attenuated in the dipolar experiments because of motion are present in the scalar correlations. The results demonstrate that scalar-based methods are sufficiently well-developed to serve as a complementary tool to dipolar methods such as DARR mentioned before, which will be especially useful for assignment of large proteins, where resonance overlap presents a major challenge to solid-state NMR. On the basis of our sensitivity, we anticipate that assignment of proteins in the range of 30-40 kDa should be feasible with current technology, even at 9.4 T, while moving to higher fields will extend this range even further.

REFERENCES

1. Jaroniec, C. P.; MacPhee, C. E.; Bajaj, V. S.; McMahon, M. T.; Dobson, C. M.; Griffin, R. G. *Proc. Natl. Acad. Sci. U.S.A.* **2004**, *101*, 711-716.

2. Tycko, R. *Q. Rev. Biophys.* **2006**, *39*, 1-55. Tycko, R. *Method Enzymol.* **2006**, *413*, 103-122.

3. Goldbourt, A.; Gross, B. J.; Day, L. A.; McDermott, A. E. *J. Am. Chem. Soc.* **2007**, *129*, 2338-2344.

4. Paik, Y.; Yang, C.; Metaferia, B.; Tang, S. B.; Bane, S.; Ravindra, R.; Shanker, N.; Alcaraz, A. A.; Johnson, S. A.; Schaefer, J.; O'Connor, R. D.; Cegelski, L.; Snyder, J. P.; Kingston, D. G. I. *J. Am. Chem. Soc.* **2007**, *129*, 361-370.

5. Baldus, M. *Curr. Opin. Struct. Biol.* **2006**, *16*, 618-623.

6. Park, S. H.; Prytulla, S.; De Angelis, A. A.; Brown, J. M.; Kiefer, H.; Opella, S. J. *J. Am. Chem. Soc.* **2006**, *128*, 7402-7403.

7. Etzkorn, M.; Martell, S.; Andronesi, O. C.; Seidel, K.; Engelhard, M.; Baldus, M. *Angew. Chem., Int. Ed.* **2007**, *46*, 459-462.

8. Kobayashi, M.; Matsuki, Y.; Yumen, I.; Fujiwara, T.; Akutsu, H. *J. Biomol. NMR* **2006**, *36*, 279-293.

9. Hong, M. *Structure* **2006**, *14*, 1731-1740.

10. Frericks, H. L.; Zhou, D. H.; Yap, L. L.; Gennis, R. B.; Rienstra, C. M. *J. Biomol. NMR* **2006**, *36*, 55-71.

11. Lange, A.; Giller, K.; Hornig, S.; Martin-Eauclaire, M. F.; Pongs, O.; Becker, S.; Baldus, M. *Nature* **2006**, *440*, 959-962.

12. McDermott, A. E. *Curr. Opin. Struct. Biol.* **2004**, *14*, 554-561.

13. Hughes, C. E.; Baldus, M. *Annu. Rep. NMR Spectrosc.* **2005**, *55*, 121-158.

14. Baldus, M.; Meier, B. H. *J. Magn. Reson., Ser. A* **1996**, *121*, 65-69.

15. Hardy, E. H.; Verel, R.; Meier, B. H. *J. Magn. Reson.* **2001**, *148*, 459-464.

16. Lesage, A.; Emsley, L. *J. Magn. Reson.* **2001**, *148*, 449-454.

17. Lesage, A.; Bardet, M.; Emsley, L. *J. Am. Chem. Soc.* **1999**, *121*, 10987-10993.

18. Elena, B.; Lesage, A.; Steuernagel, S.; Bockmann, A.; Emsley, L. *J. Am. Chem. Soc.* **2005**, *127*, 17296-17302.

19. Bockmann, A.; Juy, M.; Bettler, E.; Emsley, L.; Galinier, A.; Penin, F.; Lesage, A. *J. Biomol. NMR* **2005**, *32*, 195-207.

20. Olsen, R. A.; Struppe, J.; Elliott, D. W.; Thomas, R. J.; Mueller, L. J. *J. Am. Chem. Soc.* **2003**, *125*, 11784-11785.

21. Chen, L. L.; Olsen, R. A.; Elliott, D. W.; Boettcher, J. M.; Zhou, D. H.; Rienstra, C. M.; Mueller, L. J. *J. Am. Chem. Soc.* **2006**, *128*, 9992-9993.

22. Bertini, I.; Duma, L.; Felli, I. C.; Fey, M.; Luchinat, C.; Pierattelli, R.; Vasos, P. R. *Angew. Chem., Int Ed.* **2004**, *43*, 2257-2259.

23. Bermel, W.; Bertini, I.; Felli, I. C.; Kummerle, R.; Pierattelli, R. *J. Magn. Reson.* **2006**, *178*, 56-64.

24. D. J.; Haberkorn, R. A.; Ruben, D. J. *J. Magn. Reson.***1982**, *48*, 286-292

25. De Paepe, G.; Lesage, A.; Emsley, L. *J. Chem. Phys.* **2003**, *119*, 4833-4841.

26. Fayon, F.; Massiot, D.; Levitt, M. H.; Titman, J. J.; Gregory, D. H.; Duma, L.; Emsley, L.; Brown, S. P. *J. Chem. Phys.* **2005**, *122*, 194313.

27. Morcombe, C. R.; Paulson, E. K.; Gaponenko, V.; Byrd, R. A.; Zilm, K. W. *J. Biomol. NMR* **2005**, *31*, 217-230.

28. Hologne, M.; Chevelkov, V.; Reif, B. *Prog. Nucl. Magn. Reson. Spectrosc.* **2006**, *48*, 211-232.

29. Fung, B. M.; Khitrin, A. K.; Ermolaev, K. *J. Magn. Reson.* **2000**, *142*, 97-101.

30. Li, Y.; Wylie, B. J.; Rienstra, C. M. *J. Magn. Reson.* **2006**, *179*, 206-216.

31. Franks, W. T.; Zhou, D. H.; Wylie, B. J.; Money, B. G.; Graesser, D. T.; Frericks, H. L.; Sahota, G.; Rienstra, C. M. *J. Am. Chem. Soc.* **2005**, *127*, 12291-12305.

CHAPTER V

CONCLUSION

CTUC COSY, a new scalar-coupling-driven correlation method is introduced which is robust for chemical shift correlation in solids by combining the indirect evolution and transfer periods into a single constant time interval. Both theory and experiment point to distinct advantages of this protocol which was originally motivated by the challenge of obtaining through-bond connectivities in dynamic solids, where global molecular motion renders dipolar-driven correlation methods ineffective, and where liquid-state methodologies proved inapplicable. In this work, it was shown that this new J-MAS method provides substantially increased spectral resolution without compromising sensitivity, which we find to be comparable to or better than the sensitivity of dipolar methods. In the β1 immunoglobulin binding domain of protein G (GB1), this allows us to resolve peaks that are otherwise unresolved and to make assignments in the absence of multi-bond transfers.

The two-dimensional *J*-MAS homonuclear and heteronuclear correlation experiments are very robust and can be used to trace out and assign backbone resonances. These scalar-based constant time experiments are compatible with IPAP and Spin-State-Selection in the direct dimension for further increases in resolution. These

results help demonstrate that scalar-based methods are sufficiently well developed to serve as a complementary tool to dipolar methods, which will be especially useful for the assignment of large proteins, where resonance overlap presents a major challenge to solid-state NMR.

Three-dimensional experiments work well, but might be improved even further with hybrid $D - J$ method or deuteration to improve T_2, which will allow assignments for even large systems like Trptophan Synthase[1], a 140 kDa heterodimer.

By spinning fast and decoupling well, we can take full advantage of coherent dynamics, just as they do in liquid-state NMR. This opens up remarkable tools for optimizing sensitivity and resolution for solid-state systems. Work in this direction is in progress.

REFERENCES

1. Huang X., Holden H.M., Raushel F.M., *Annu. Rev. Biochem.*, **2001**, *70***,** 149.

APPENDIX

A1. PULSE CODES

A1.1 Pulse codes of CTUC COSY for CACO correlation

```
;rcp2.cttruc3.cpd
;set edscon PHASPR 1 to 1.7 usec
;DQF chemical shift correlation with constant time
;lingling chen/05/20/2005

#include <Avance.incl>


"d11=30m"
"p27=p28-0.2"
"p25=p26-0.2"
"d0=3u"
"l3=(td1/2)"


define delay dtau1
"dtau1=((1s/cnst31)*l5    - 6u)"
define delay dtau3
"dtau3=((1s/cnst31)*l7    - 6u)"
define delay dtauz
"dtauz=((1s/cnst31)*l8-p5-3u)"
define delay dtau5
"dtau5=(dtau1-l3*in10)"
"d10=dtau1"



1 ze
2 d1 do:f2
3 d11 do:f2 pl21:f2
```

```
4 dtau5 pl21:f2
   dtau1
   d10
   (p1 ph1):f2
   3u pl23:f2
   (p3:sp1 ph2):f1 (p3:sp3 ph3):f2

   3u cpds3:f2 pl26:f2

   d0

   dtau1 pl15:f1
   (p5 ph5):f1
   (p5 ph5):f1

   d10
   6u
   (p5 ph6):f1
   3u
   (p5 ph9):f1

   6u
   dtau3
   (p5 ph10):f1
   (p5 ph10):f1
   dtau3
   6u

;DEC power lowered to pl28 during ZF on 11 May 2004
   (p5 ph15):f1
   dtauz cpds2:f2 pl28:f2
   100u ;pl28:f2
   3u ;
   (p5 ph16):f1

   go=2 ph31
   3m do:f2
   d1 wr #0 if #0 ip2 zd
   d11
```

```
   lo to 3 times 2
   d11 id0
   d11 dd10
   lo to 4 times l3
exit

ph1=1 1 1 1
ph3=0
ph2=0 2
ph4=1 3
ph5=0 2 1 3 2 0 3 1
ph7=1 3
ph6=1 3

ph9=0
ph11=0
ph10=1

ph15=0
ph16=2

ph31=0 0 2 2

;pl21 : (1H) f2 chanrsnel 90 pulse
;pl23 : (1H) f2 channel CP pulse
;pl15 : (X) f1 Pi/2 mixing pulses
;pl28: (1H) f2 channel - power level for TPPM observe decoupling
;p1 : f2 channel -    90 degree high power pulse
;p3: f1(f2) channel - contact pulse
;p5: (X) f1 channel Pi/2 mixing pulses
;p28:    1H TPPM pulse about a 160 degree pulse at pl28
;cpdprg2:    tppm cpd program
;sp1:    peak power level
;spoffs1:    0
;spnam1:    name of the shape file
;d1 : relaxation delay; 1-5 * T1
;d11 : delay for disk I/O                                    [30 msec]
;cnst31 : MAS spinning speed
;NS : 1 * n
```

;DS : none
;d0 : incremented delay (2D) [3 usec]
;l3 : loop for phase sensitive 2D using States-TPPI method: l3 = td1/2
;l5 : number of rotor periods for J refocusing T1(2)
;l7 : number of rotor periods for J refocusing T3(4)
;l8 : number of rotor periods for z-filter
;in0 : 1/(1 * SW) = 2 * DW
;nd0 : 1
;td1 : number of experiments
;MC2 : States-TPPI

A1.2 Pulse codes of CTUC COSY for Aliphatic correlation

```
;rcp2.cttru3sp5.cpd
;set edscon PHASPR 1 to 1.7 usec
;DQF chemical shift correlation with constant time
;lingling chen/05/20/2005

#include <Avance.incl>


"d11=30m"
"p27=p28-0.2"
"p25=p26-0.2"
"d0=3u"
"l3=(td1/2)"


define delay dtau1
"dtau1=((1s/cnst31)*l5)"
define delay dtau3
"dtau3=((1s/cnst31)*l7)"
define delay dtauz
"dtauz=((1s/cnst31)*l8-p5-3u)"
define delay dtau5
"dtau5=(dtau1-l3*in10)"
"d10=dtau1"

define delay dtau10
"dtau10=((1s/cnst31)*(l10+0.5))"
"p10 = dtau10"
define delay dtau11
"dtau11=((1s/cnst31)*(l11+0.5))"
"p11 = dtau11"

define delay dtau2
"dtau2=(dtau1-dtau11)"
```

```
1 ze
2 d1 do:f2
3 d11 do:f2 pl21:f2
4 d11 do:f2 pl21:f2
   dtau5
   dtau1
   d10
   (p1 ph1):f2
   3u pl23:f2
   (p3:sp1 ph2):f1 (p3:sp3 ph3):f2

   d0 cpds3:f2 pl26:f2
   (p11:sp11 ph20):f1
   dtau2 pl15:f1

   (p10:sp10 ph5):f1

   d10 pl15:f1

   (p5 ph6):f1
   3u
   (p5 ph9):f1

   dtau3
   (p10:sp10 ph10):f1
   dtau3 pl15:f1

;DEC power lowered to pl28 during ZF on 11 May 2004
   (p5 ph15):f1
   dtauz cpds2:f2 pl28:f2
   100u ;pl28:f2
   3u ;
   (p5 ph16):f1

   go=2 ph31
   3m do:f2
   d1 wr #0 if #0 ip2 zd
```

```
   d11
   lo to 3 times 2
   d11 id0
   d11 dd10
   lo to 4 times l3
exit

ph1=1 1 1 1 1 1 1 1 3 3 3 3 3 3 3 3
ph3=0
ph2=0 2
ph4=1 3
ph5=0 2 1 3 2 0 3 1
ph7=1 3
ph6=1 3

ph9=0
ph11=0
ph10={{1}*16}^1^2^3

ph15=0
ph16=2

ph20=0

ph31={0 0 2 2 0 0 2 2 2 2 0 0 2 2 0 0}^2

;pl21 : (1H) f2 chanrsnel 90 pulse
;pl23 : (1H) f2 channel CP pulse
;pl15 : (X) f1 Pi/2 mixing pulses
;pl28: (1H) f2 channel - power level for TPPM observe decoupling
;p1 : f2 channel -    90 degree high power pulse
;p3: f1(f2) channel - contact pulse
;p5: (X) f1 channel Pi/2 mixing pulses
;p28:    1H TPPM pulse about a 160 degree pulse at pl28
;cpdprg2:    tppm cpd program
;sp1:    peak power level
;spoffs1:    0
;spnam1:    name of the shape file
;d1 : relaxation delay; 1-5 * T1
```

```
;d11 : delay for disk I/O                                    [30 msec]
;cnst31 : MAS spinning speed
;NS : 1 * n
;DS : none
;d0 : incremented delay (2D)                                 [3 usec]
;l3 : loop for phase sensitive 2D using States-TPPI method: l3 = td1/2
;l5 : number of rotor periods for J refocusing T1(2)
;l7 : number of rotor periods for J refocusing T3(4)
;l8 : number of rotor periods for z-filter
;l10 : ali - number of rotor periods for selective ali
;l11 : CO - number of rotor periods for selective CO
;sp10:    ali pi
;spoffs10:    0
;spnam10:    name of the shape file
;sp11:    CO pi
;spoffs11:    10500
;spnam11:    name of the shape file
;in0 : 1/(1 * SW) = 2 * DW
;nd0 : 1
;td1 : number of experiments
;MC2 : States-TPPI
```

A1.3 Pulse codes of CTUC COSY for NCO(NCA) correlation

```
;rcp2.ctNC_b.cpd
;set edscon PHASPR 1 to 1.7 usec
;DQF chemical shift correlation with constant time
;lingling chen/05/20/2005

#include <Avance.incl>


"d11=30m"
"p27=p28-0.2"
"p25=p26-0.2"
"d0=3u"
"p10=p6+p6"
"l3=(td1/2)"

define delay dtau1
"dtau1=((1s/cnst31)*l5 - p5 - 6u)"
define delay dtau3
"dtau3=((1s/cnst31)*l6 )"
"d10=dtau1"

define delay dtau11
"dtau11=((1s/cnst31)*(l11+0.5))"
"p11 = dtau11"
define delay dtau12
"dtau12=((1s/cnst31)*(l12+0.5))"
"p12 = dtau12"

define delay dtau2
"dtau2=(dtau1-dtau12)"

define delay dtau20
"dtau20=0.5*(dtau11-p10)"

define delay dtau5
```

```
"dtau5=(dtau1-l3*in10)"


1 ze
2 d1 do:f2
3 d11 do:f2 pl21:f2
4 d11 do:f2 pl21:f2
   dtau5
   dtau1
   d10
   d0

   (p1 ph1):f2
   3u
   (p3:sp1 ph2):f3 (p3:sp3 ph3):f2

   3u cpds3:f2 pl26:f2 pl15:f1 pl30:f3

   d0
   (p12:sp12 ph20):f1
   dtau2 pl15:f1

   (p11:sp11 ph15):f1 (dtau20 p10 ph5):f3
   d10
   6u pl15:f1
   (p5 ph6):f1
   3u
   (p6 ph9):f3
   dtau3
   (p11:sp11 ph16):f1 (dtau20 p10 ph15):f3
   dtau3

   go=2 ph31 cpds2:f2 pl28:f2
   3m do:f2
   d1 wr #0 if #0 ip2 zd
   d11
   lo to 3 times 2
   d11 id0
   d11 dd10
```

```
   lo to 4 times l3
exit

;dq/zq fileter

ph1=1
ph3=0
ph2=0 2
ph4=1
ph5=0
ph7=1
ph6=1

ph9=0
ph11=0
ph10=1

ph15=0
ph16=1

ph20=0

ph31=0 2


;pl21 : (1H) f2 chanrsnel 90 pulse
;pl23 : (1H) f2 channel CP pulse
;pl15 : (X) f1 Pi/2 mixing pulses
;pl26: (1H) indirect decoupling
;pl28: (1H) observe decoupling
;p1 : f2 channel -    90 degree high power pulse
;p3: f1(f2) channel - contact pulse
;p5: (X) f1 channel Pi/2 mixing pulses
;p6: (X) f1 channel Pi/2 mixing pulses
;p28:    1H TPPM pulse about a 160 degree pulse at pl28
;cpdprg2:    1H direct cpd program
;cpdprg3:    1H indirectcpd program
;sp1:    peak power level
;spoffs1:    0
```

;spnam1: name of the shape file
;sp11: selective active pi
;spoffs11: 0
;spnam11: name of the shape file
;sp12: selective passive pi
;spoffs12: 0
;spnam12: name of the shape file
;d1 : relaxation delay; 1-5 * T1
;d11 : delay for disk I/O [30 msec]
;cnst31 : MAS spinning speed
;NS : 1 * n
;DS : none
;d0 : incremented delay (2D) [3 usec]
;l3 : loop for phase sensitive 2D using States-TPPI method: l3 = td1/2
;l5 : number of rotor periods for J refocusing T1(2)
;l6 : number of rotor periods for J refocusing T3(4)
;l8 : number of rotor periods for z-filter
;l11 : selective pulse active
;l12 : selective pulse passive
;in0 : 1/(1 * SW) = 2 * DW
;nd0 : 1
;td1 : number of experiments
;MC2 : States-TPPI

A1.4 Pulse codes of CTUC COSY for 3D NCACO(NCOCA) correlation

```
;rcp2.ctNCC.cpd

#include <Avance.incl>


"d21=30m"
"p27=p28-0.2"
"p25=p26-0.2"
"d0=3u"
"d10=3u"
"p10=p6+p6"

"l3=(td1/2)"
"l4=(td2/2)"

define delay dtau1
"dtau1=((1s/cnst31)*l5 - p5 - 6u)"
define delay dtau3
"dtau3=((1s/cnst31)*l6 )"
define delay dtau5
"dtau5=((1s/cnst31)*l7 )"
define delay dtau7
"dtau7=((1s/cnst31)*l8 )"


define delay dtau15
"dtau15=(dtau1-l3*in11)"

define delay dtau16
"dtau16=(dtau3-l4*in12)"


define delay dtau35
"dtau35=(dtau3-dtau5 )"
```

```
define delay dtauz
"dtauz=((1s/cnst31)*l9-p5-3u)"

"d11=dtau1"
"d12=dtau3"

define delay dtau11
"dtau11=((1s/cnst31)*(l11+0.5))"
"p11 = dtau11"
define delay dtau12
"dtau12=((1s/cnst31)*(l12+0.5))"
"p12 = dtau12"

define delay dtau2
"dtau2=(dtau1-dtau12)"
define delay dtau6
"dtau6=(dtau5-dtau12)"

define delay dtau20
"dtau20=0.5*(dtau11-p10)"


1 ze

   dtau1
   dtau3
   dtau11
   dtau12
   dtau2
   dtau20



2 d1 do:f2
3 d21
4 d21
5 d21 do:f2
6 d21 do:f2 pl21:f2
```

```
   dtau15
   dtau16
   d0
   d11
   d10
   d12

;  CP

   (p1 ph1):f2
   3u
   (p3:sp1 ph2):f3 (p3:sp3 ph3):f2

;  t1

   3u cpds3:f2 pl26:f2 pl15:f1 pl30:f3

   d0
   (p12:sp12 ph20):f1
   dtau2 pl15:f1

   (p11:sp11 ph15):f1 (dtau20 p10 ph5):f3
   d11
   6u pl15:f1
   (p5 ph6):f1
   3u
   (p6 ph9):f3

;  t1 rephase t2 evolve

   d10
   dtau6
   (p12:sp12 ph20):f1
   dtau35
   (p11:sp11 ph8):f1 (dtau20 p10 ph5):f3
   d12    pl15:f1

;  t2 rephase
```

```
    (p5 ph17):f1
    3u
    (p5 ph18):f1

    dtau7
    (p5 ph20):f1
    (p5 ph20):f1
    dtau7


;   zf

    (p5 ph25):f1
    dtauz cpds2:f2 pl28:f2
    100u ;pl28:f2
    3u ;
    (p5 ph26):f1



;   t3

    go=2 ph31 cpds2:f2 pl28:f2
    3m do:f2
    d1 wr #0 if #0 ip2 zd
    d21
    lo to 5 times 2
    d21 id0
    d21 dd11
    lo to 6 times l3
    d21 rd0
    d21 rd11
    d21 ip6
    lo to 3 times 2
    d21 id10
    d21 dd12
    lo to 4 times l4
```

exit

;dq/zq fileter

ph1=1
ph3=0
ph2=0 2
ph4=1
ph5=0 0
ph7=1
ph6=0 0; 2 2
ph8=0 0 ;2 2

ph9=0
ph11=0
ph10=1

ph15=0
ph16=1
ph17=1 1 ;3 3
ph18=0

ph20=0

ph25=0
ph26=2

ph31=0 2 ;0 2

;pl21 : (1H) f2 chanrsnel 90 pulse
;pl23 : (1H) f2 channel CP pulse
;pl15 : (X) f1 Pi/2 mixing pulses
;pl26: (1H) indirect decoupling
;pl28: (1H) observe decoupling
;p1 : f2 channel - 90 degree high power pulse
;p3: f1(f2) channel - contact pulse
;p5: (X) f1 channel Pi/2 mixing pulses

;p6: (X) f3 channel Pi/2 mixing pulses
;p28: 1H TPPM pulse about a 160 degree pulse at pl28
;cpdprg2: 1H direct cpd program
;cpdprg3: 1H indirectcpd program
;sp1: peak power level
;spoffs1: 0
;spnam1: name of the shape file
;sp11: selective active pi
;spoffs11: 0
;spnam11: name of the shape file
;sp12: selective passive pi
;spoffs12: 0
;spnam12: name of the shape file
;d1 : relaxation delay; 1-5 * T1
;d21 : delay for disk I/O [30 msec]
;cnst31 : MAS spinning speed
;NS : 1 * n
;DS : none
;d0 : incremented delay (2D) [3 usec]
;l3 : loop for phase sensitive 2D using States-TPPI method: l3 = td1/2
;l5 : rotor periods tau1 (NC-1)
;l6 : rotor periods tau3 (NC-2)
;l7 : rotor periods tau5 (CC-1)
;l8 : rotor periods tau7 (CC-2)
;l9 : number of rotor periods for z-filter
;l11 : selective pulse active
;l12 : selective pulse passive
;in0 : 1/(1 * SW) = 2 * DW
;nd0 : 1
;td1 : number of experiments
;MC2 : States-TPPI

A1.5 Pulse codes of CTUC COSY for 3D CANCO correlation

```
;rcp2.ctCNC.cpd

#include <Avance.incl>

"d21=30m"
"p27=p28-0.2"
"p25=p26-0.2"
"d0=3u"
"d10=3u"
"p10=p6+p6"
"p9=p5+p5"

"l3=(td1/2)"
"l4=(td2/2)"

define delay dtau1
"dtau1=((1s/cnst31)*l5 - 6u)"
define delay dtau3
"dtau3=((1s/cnst31)*l6 – 3u)"
define delay dtau7
"dtau7=((1s/cnst31)*l8 )"


define delay dtau15
"dtau15=(dtau1-l3*in11)"

define delay dtau16
"dtau16=(dtau3-l4*in12)"

define delay dtauz
"dtauz=((1s/cnst31)*l9-p5-3u)"

"d11=dtau1"
"d12=dtau3"
```

```
define delay dtau11
"dtau11=((1s/cnst31)*(l11+0.5))"
"p11 = dtau11"
define delay dtau12
"dtau12=((1s/cnst31)*(l12+0.5))"
"p12 = dtau12"

define delay dtau2
"dtau2=(dtau1-dtau12)"

define delay dtau20
"dtau20=0.5*(dtau11-p10)"
define delay dtau21
"dtau21=0.5*(dtau12-p10)"


1 ze

   dtau1
   dtau3
   dtau11
   dtau12
   dtau2
   dtau20



2 d1 do:f2
3 d21
4 d21
5 d21 do:f2
6 d21 do:f2 pl21:f2

   dtau15
   dtau16
   d0
   d11
   d10
   d12
```

```
;   CP

    (p1 ph1):f2
    3u
    (p3:sp1 ph2):f1 (p3:sp3 ph3):f2

;   t1

    3u cpds3:f2 pl26:f2

    d0 pl30:f3
    (p12:sp12 ph20):f1
    dtau2 pl15:f1

    (p11:sp11 ph15):f1 (dtau20 p10 ph5):f3
    d11
    6u pl15:f1
    (p5 ph9):f1 (p6 ph6):f3

;   t1 rephase t2 evolve

    d10
    dtau3
    (p9 ph8):f1 (p10 ph5):f3
    d12    pl15:f1
    3u

;   t2 rephase

    (p5 ph17):f1 (p6 ph18):f3

    dtau7
    (p12:sp12 ph20):f1 (dtau21 p10 ph5):f3
    dtau7 pl15:f1


;   zf
```

```
    (p5 ph25):f1
    dtauz cpds2:f2 pl28:f2
    100u ;pl28:f2
    3u ;
    (p5 ph26):f1



;    t3

    go=2 ph31 cpds2:f2 pl28:f2
    3m do:f2
    d1 wr #0 if #0 ip2 zd
    d21
    lo to 5 times 2
    d21 id0
    d21 dd11
    lo to 6 times l3
    d21 rd0
    d21 rd11
    d21 ip6
    lo to 3 times 2
    d21 id10
    d21 dd12
    lo to 4 times l4


exit

;dq/zq fileter

ph1=1
ph3=0
ph2=0
ph4=1
ph5=0 0
ph7=1
ph6=0
ph8=0 0
```

```
ph9=0
ph11=0
ph10=1

ph15=0 1
ph16=1
ph17=0
ph18=0

ph20=0

ph25=1
ph26=3

ph31=0 2



;pl21 : (1H) f2 chanrsnel 90 pulse
;pl23 : (1H) f2 channel CP pulse
;pl15 : (X) f1 Pi/2 mixing pulses
;pl26: (1H) indirect decoupling
;pl28: (1H) observe decoupling
;p1 : f2 channel -    90 degree high power pulse
;p3: f1(f2) channel - contact pulse
;p5: (X) f1 channel Pi/2 mixing pulses
;p6: (X) f3 channel Pi/2 mixing pulses
;p28:    1H TPPM pulse about a 160 degree pulse at pl28
;cpdprg2:    1H direct cpd program
;cpdprg3:    1H indirectcpd program
;sp1:    peak power level
;spoffs1:    0
;spnam1:    name of the shape file
;sp11:    selective active pi
;spoffs11:    0
;spnam11:    name of the shape file
;sp12:    selective passive pi
;spoffs12:    0
```

;spnam12: name of the shape file
;d1 : relaxation delay; 1-5 * T1
;d21 : delay for disk I/O [30 msec]
;cnst31 : MAS spinning speed
;NS : 1 * n
;DS : none
;d0 : incremented delay (2D) [3 usec]
;l3 : loop for phase sensitive 2D using States-TPPI method: l3 = td1/2
;l5 : rotor periods tau1 (NC-1)
;l6 : rotor periods tau3 (NC-2)
;l7 : rotor periods tau5 (CC-1)
;l8 : rotor periods tau7 (CC-2)
;l9 : number of rotor periods for z-filter
;l11 : selective pulse active
;l12 : selective pulse passive
;in0 : 1/(1 * SW) = 2 * DW
;nd0 : 1
;td1 : number of experiments
;MC2 : States-TPPI